TECHNICKÁ UNIVERZITA V LIBERCI
TECHNICAL UNIVERSITY OF LIBEREC

Fakulta textilní
Faculty of Textile Engineering

Katedra textilních technologií
Department of Textile Technologies

Disertačni práce
Ph.D. Dissertation

Anizotropie tahových vlastností tkaniny v plátnové vazbě
Anisotropy in Tensile Properties of Plain Weave Fabric

2009

Vypracoval: Mehdi Kamali Dolatabadi, M.Sc.
Worked out by: Mehdi Kamali Dolatabadi, M.Sc.

Školitel: Prof. Ing. Radko Kovař, CSc.
Supervisor: Prof. Ing. Radko Kovař, CSc.

IN THE NAME OF GOD

THE BENEFICENT AND THE MERCIFUL

ABSTRACT

Anisotropy in tensile properties of plain weave fabric was subjected to research in this study. For this purpose, on the basis of elliptical yarn cross-section and curves a geometry model was suggested for fabric structure before deformation. This model was extended to evaluate fabric deformation in bias direction. Afterward, on the source of yarn deformation another mechanical-geometrical model was put in forward. Yarns crimp interchange, yarns flattening and bending rigidity of yarns was contemplated in this model. The authority of both models was investigated by imposing tensile stress on polypropylene and cotton fabrics in different directions. To evaluate exterior geometry of fabric during deformation an image processing method was explained and applied. Furthermore, modified jaws were employed to reduce stress concentration on sample's corners. It was found that the first model is valid to evaluate fabric geometry before deformation and during deformation in bias direction. In addition, it was revealed that the mechanical-geometrical model is applicable to predict force tensile-displacement and internal geometry of a fabric when it is subjected to stress in arbitrary direction.

ABSTRAKT (IN CZECH)

Předložená disertační práce se zabývá výzkumem v oblasti anizotropie tahových deformačních vlastností tkanin. Z tohoto důvodu byl navržen model relaxované tkaniny, vycházející z eliptického průřezu nitě. Tento model byl po úpravě použit i pro popis tkaniny, deformované šikmým zatížením. Poté byl na základě deformace nitě navržen další model, který počítá i se záměnou amplitudy vazné vlny mezi osnovou a útkem, se zploštěním nitě a s její ohybovou tuhostí. Oba modely byly ověřovány zatěžováním polypropylenových a bavlněných tkanin v různých směrech. Pro hodnocení vnější geometrie tkaniny v průběhu deformace byly používány prostředky obrazové analýzy. Dále byly použity čelisti dynamometru, speciálně modifikované pro omezení vlivu koncentrace napětí v rozích vzorku na výsledek měření. Bylo zjištěno, že první model je vhodný pro tkaniny před deformací a při deformaci v šikmých směrech. Rovněž bylo zjištěno, že mechanicko-geometrický model je použitelný pro predikci vztahu mezi napětím a deformací a vnitřní geometrie tkaniny při zatěžování v libovolném směru.

Dedicated to

my beloved wife,

Maryam Mohammadi, who is a constant source of encouragement

and

my darling daughter,

Setayesh Kamali, the greatest joy in my life.

ACKNOWLEDGMENTS

It is a pleasure to thank the many people who made this thesis possible.

I would like to express my deep and sincere gratitude to my Ph.D. supervisor, Prof. Ing. Radko Kovař, CSc., with his enthusiasm and his great efforts to explain things clearly and simply. Throughout my thesis-writing period, he provided encouragement, sound advice, good teaching, good company, and lots of good ideas. I would have been lost without him.

I am deeply grateful to Prof. Ing. Jiří Militký CSc., head of the Textile Faculty, Technical University of Liberec, for his important support throughout this work.

I owe my most sincere gratitude to Doc. Dr. Ing. Dana Křemenáková, who gave me the opportunity to work in the Department of Textile Technology.

I wish to express my warm and sincere thanks to Prof. Ing. Bohuslav Neckář DrSc. His wide knowledge and his logical way of thinking have been of great value for me.

I warmly thank Prof. Ing. Sayed Ibrahim CSc., for his valuable advice and friendly help.

I am deeply gratitude to Ing. Jana Drašarová Ph.D., for proving samples. Her extensive discussions around yarn cross-section have been very helpful for this study.

I would like to appreciate Dr. A. Alamdar and Ing. Monika Vyšanská Ph.D., for their detailed review and constructive criticism during the preparation of this thesis.

Lastly, and most importantly, I wish to thank my parents, Kobra P. Mashhadi and Hasan Kamali D. They supported me, taught me, and loved me.

Liberec, Czech Republic, 2009

Mehdi Kamali D.

Table of contents

RESULTS AND DISCUSSION

CONCLUSION

APPENDIXES

LIST OF TABLES

List of figures

Preface

This dissertation is submitted to the Faculty of Textile in partial fulfillment of the requirements for the degree of Doctor of Philosophy at the Technical University of Liberec, Czech Republic. It is prepared in seven chapters.

Chapter one contains of scopes of this dissertation.

On the basis of our existing knowledge, summary of issued literatures around of this topic is presented in chapter two.

To assess behavior of woven fabric in bias and arbitrary directions, two models are developed in chapter three.

Methods and materials used in this study are described in chapter four. Several concepts to measure bending rigidity of yarn and tensile strength of fabric in arbitrary direction are offered in this chapter.

Chapter five demonstrates the obtained results. Then, comparison between experimental and theoretical values is discussed.

Overall conclusions of this dissertation are presented in chapter six.

Appendixes are included of solving differential equations, proofing of validity of derived equations, and results of some empirical works in this study.

1 Introduction

1.1 Introduction

Nowadays, applications of fiber assemblies are hastily growing in industry. Within textile structures, the plain weave fabric is more concerned due to individually yarn configuration and maximum yarns interlacing in comparison with other textile structures. The most attention in woven fabric investigations is focused on properties of woven fabric in principal directions. However, to achieve individual properties of woven fabric end use, understanding the behavior of woven fabric in off-axis is fundamental key. Garment industry, composite performance, parachutes, airbags, etc. are some applications which the woven fabric are subjected to stress not only in principal directions but also in other directions. Accordingly, anisotropy in tensile properties of woven fabric is addressed in this study.

1.2 Aims

Behavior of woven fabric under tensile stress is extremely anisotropic due to complex fabric configuration, yarns interaction and yarn deformation. Multifaceted deformations include of crimp-interchange, consolidation, extension and flattening are anticipated for yarns inside of fabric structure under tensile stress. To challenge anisotropy in tensile properties of plain weave fabric following two distinct aims are considered.

1.2.1 Fabric geometry before deformation and after bias deformation

The priority in studies of fabric under tensile stress belongs to fabric geometry due to high dependence of mechanical properties on fabric geometry. Accordingly, developing a 3D model for fabric geometry before deformation and during deformation in bias directions (±45°) would be the first scope of this study.

1.2.2 Tensile properties of fabric in arbitrary direction

Then, the tensile properties of woven fabric in arbitrary direction, which includes of fabric geometry and mechanical properties, would be discussed. For this purpose, a micromechanical and geometrical model of fabric deformation in arbitrary direction would be established.

2 Literature review

2 Literature review

2.1 Fabric geometry

Geometry of fabric plays a vital role to predict physical and mechanical behavior of fabric as well as weaving loom adjustment. To establish a geometrical model considering some idealization for yarn parameters and configuration is not avoidable. The history of research on fabric geometry probably refers to 1937, when Pierce expressed his famous model [1]. He established a model for fabric geometry by assuming incompressible, full flexible and circular cross-section yarns, in which the curvature of yarns are uniform and circular upon cross yarn (figure 2.1). Then, he modified it for yarns with elliptic cross-section (figure 2.2). Pierce's model justifies many specifications of woven fabric, but in some cases such as close structure of woven fabric deformation of yarns has significant affect on properties of fabric.

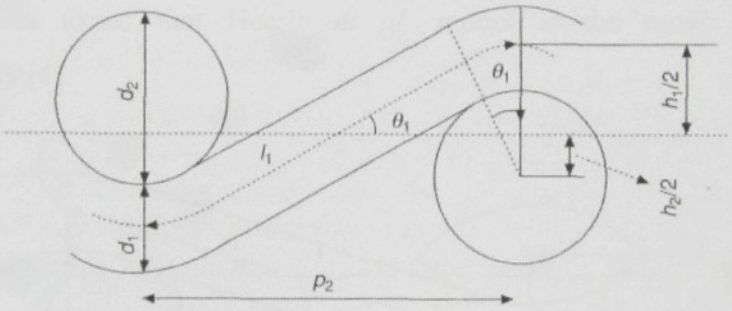

Figure 2.1- Peirce's circular cross-section geometry of plain weave fabric [4]

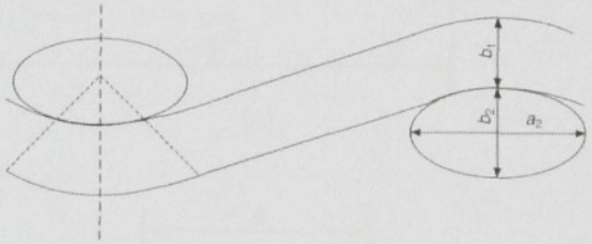

Figure 2.2- Peirce's approximate treatment of flattened yarn geometry of plain weave fabric [4]

Afterward, Kemp [2] modeled yarn cross-section that is composed of a rectangular with two semicircular ends (figure 2.3). This model justifies the jamming conditions of the structure by simple relations as well.

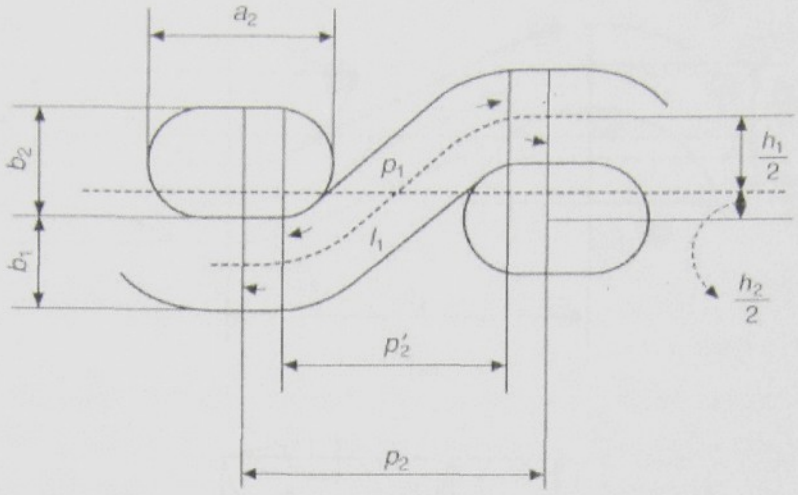

Figure 2.3- Kemp's racetrack cross-section geometry of plain weave fabric [4]

Hearle *et al.* [3] suggested a model consisting of lenticular cross-section and applying energy method for calculation fabric mechanics (figure 2.4). Among the mentioned models, it was found that Hearle *et al.* model is the most general model mathematically [4].

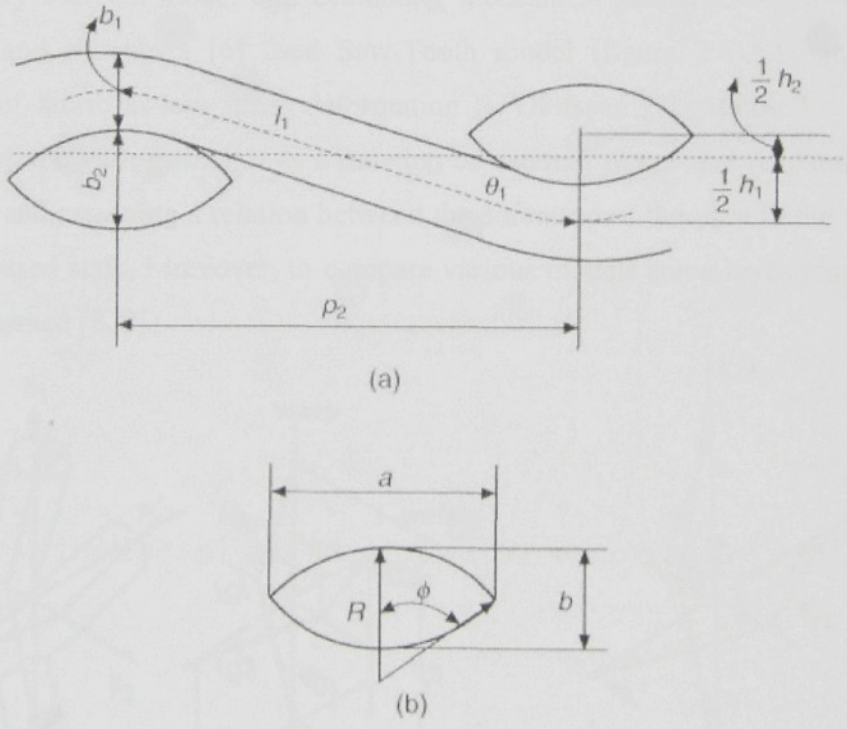

Figure 2.4- Hearle's lenticular cross-section geometry of plain weave fabric; a: unit cell of plain weave, b: yarn cross-section geometry [4]

Later, according to observations and the principles of lenticular geometry a bow shaped model was proposed by Hu J L (figure 2.5) [4].

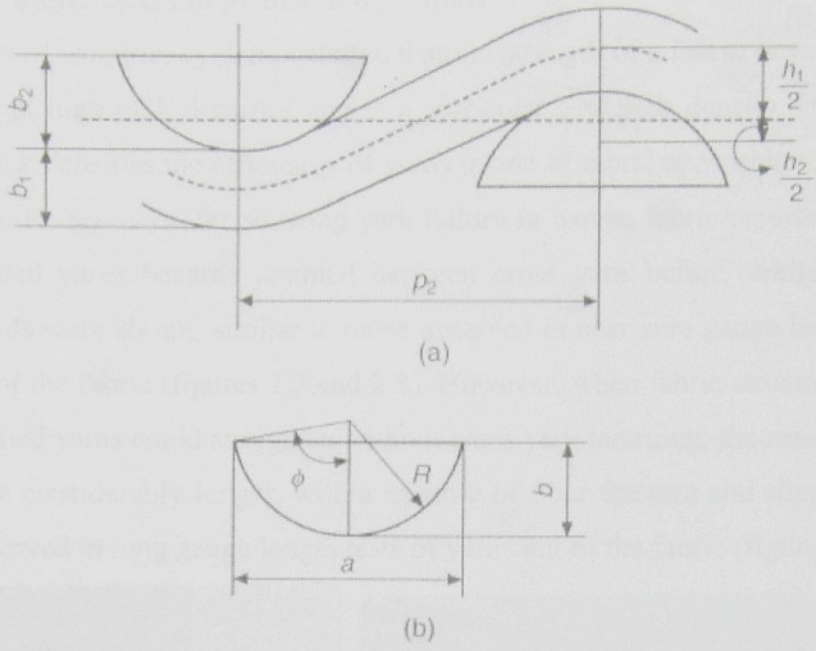

Figure 2.5- Bow shape cross-section geometry of plain weave fabric; a: unit cell of plain weave, b: yarn cross-section geometry [4]

To simplify Pierce's model and evaluating mechanical properties of woven fabric Leaf [5] and Kawabata [6] used Saw-Tooth model (figure 2.6). To interpret of behavior of fabric in low stress deformation B. Olofsson [7] proposed a model by considering the yarn geometry as a function of external forces and reaction forces in the fabric and assuming a relation between the curvature of the yarn in the fabric and in the released state. Moreover, to compare various models some investigations have been performed [8, 9].

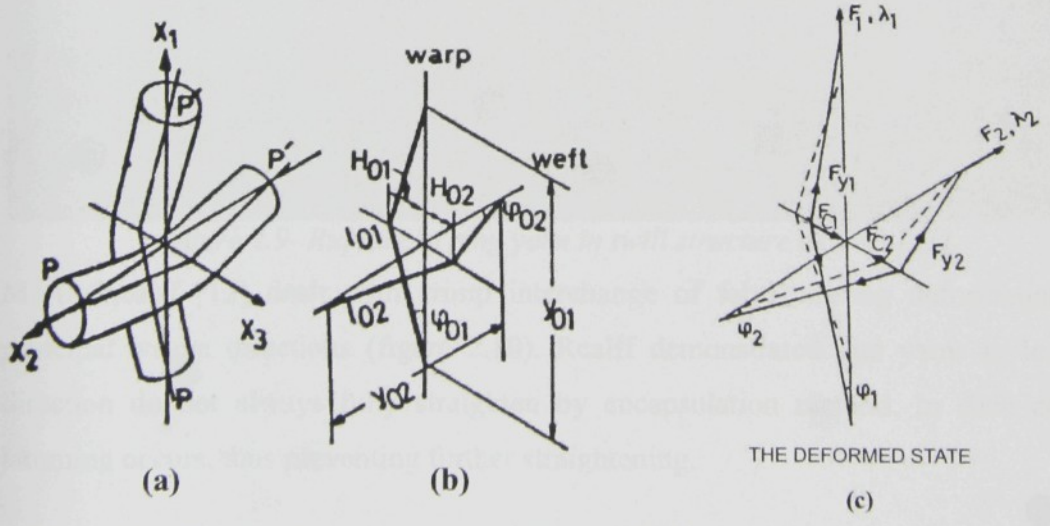

Figure 2.6- Saw-tooth cross-section geometry of plain weave fabric, relaxed (a, b) and deformed (c) state

2.2 Fabric under stress in principal directions

J.Skelton *et al.* empirically demonstrated that the strength of a fabric in warp direction is reduced at high pick densities and at a particular low pick density. However, for medium pick densities the efficiency of yarns inside of fabric approaches about 100% [10]. Moon H. Seo *et al.* for showing yarn failure in woven fabric reported that when the tensioned yarns became jammed between cross yarn before straightening, the fracture ends were abrupt, similar to those observed in near zero gauge length tests of yarns out of the fabric (figures 2.7 and 2.8). However, when fabric structure was such that tensioned yarns could straighten without cross yarn jamming, the resulting failure zones were considerably longer, with a mixture of fiber fracture and slippage similar to that observed in long gauge length tests of yarns out of the fabric (figure 2.9)[11].

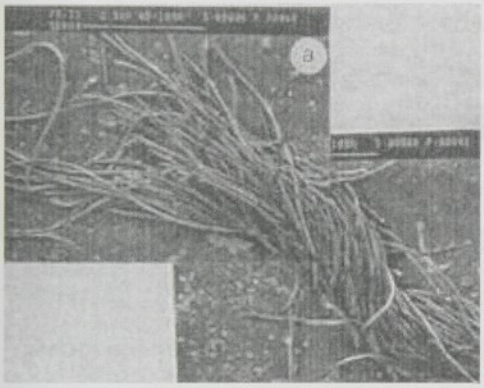

Figure 2.7- Rupture of ring yarn in twill structure as warp [11]

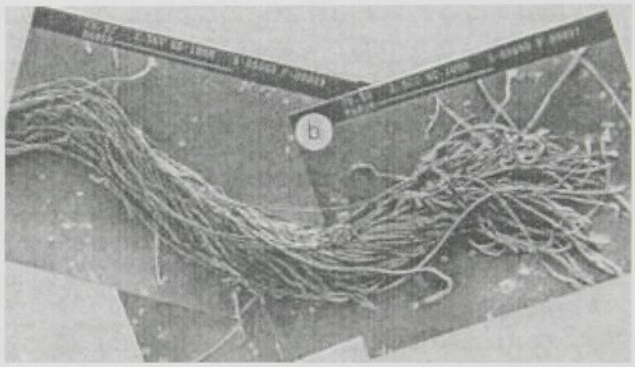

Figure 2.8- Rupture of rotor yarn in twill structure as warp [11]

Figure 2.9- Rupture of ring yarn in twill structure as weft [11]

M. L. Realff [12] dealt with crimp interchange of fabric during deformation in principal weave directions (figure 2.10). Realff demonstrated that yarns in loaded direction do not always fully straighten by encapsulation method. In such cases, jamming occurs, thus preventing further straightening.

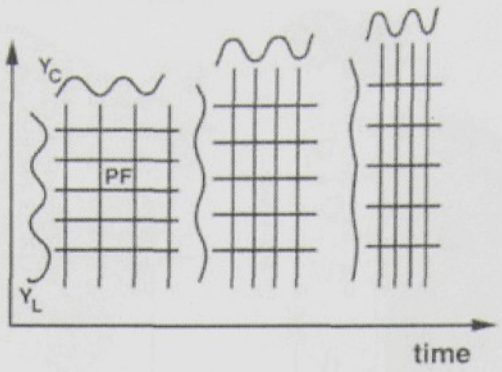

Figure 2.10- Crimp interchange when a fabric is subjected to vertical stress [12]

In other work M. L. Realff *et al.* [13] proposed a micromechanical model for predicting fabric properties by using Kawabata deformation geometry [6] and measuring consolidation and flattening of yarn properties. Ning Pan [14] dealt with predicting fabric strength under uniaxial and biaxial forces. He pointed out that the interaction forces of yarn-yarn at crossing point are consisted of two components, a pressure-independent adhesive component and a pressure-dependent frictional one. Rajesh D., Anandjiwala and G.A. Leaf [15] surveyed the trend of woven fabric under large-scale extension and recovery. They pointed out that medium to high curvature yarn bending, which is inherent in fabric's large-scale deformation, should be taken into consideration. Moreover, a modification for yarn bending rule had been proposed by accounting inter-fiber friction restraint mechanism in mentioned study. Sagar *et al.* [16] applied energy method for interlacing fiber assemblies in mesoscale. They demonstrated that the energy method is a effective way for predicting tensile response of plain weave fabric. Recently, B. Neckar *et al.* has been put forward a method to estimate jamming phenomenon and limit sett of a fabric on the basis of Pierce model when it is subjected to stress in principal weave directions (figures 2.11 and 2.12) [17].

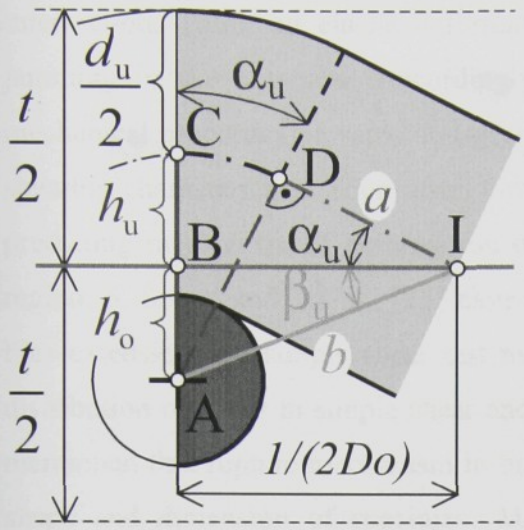

Figure 2.11- Pierce concept geometry [17]

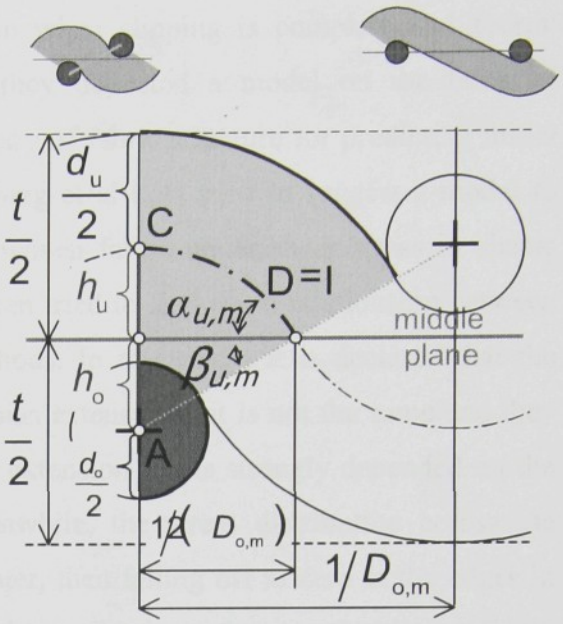

Figure 2.12- Jamming condition on the base of Pierce model [17]

2.3 Fabric under stress in arbitrary direction

To interpret the deformation of woven fabric in bias direction, the concept of Weissenberg *et. al.* [18, 19] has been contemplated by most of the researchers. On the basis of this theory it is assumed that the motion of yarns at the interlacing point is pin-jointed motion and the incompressible and inextensible warp and weft yarns in a unit cell of fabric have the constant sett. Although some Weissenberg's assumptions are acceptable in ordinary fabrics under low shear deformation, however the dimension of yarns and yarns sett are subjected to change in high shear deformation. Afterward, Lindberg *et al.* [20] dealt with shear behavior of woven fabric. They found that shear deformation takes place on the basis of two levels: initial shear without sliding and shear with sliding, and then jamming. They mentioned that shear deformation is initially resisted by friction in cross-over force and then elastic forces after jamming. Kilby [21] had been suggested a formula for calculating Young's module of fabric in arbitrary direction on the basis of Young's modules of fabric in warp and weft direction. Treloar [22] demonstrated that test sample dimension has significant effect on behavior of fabric in simple shear. He mentioned that the maximum shear strain, which can be applied without the occurrence of wrinkling, is dependent on the shape of specimen and length-width ratio. Later on, several distinct modes of deformation had been put in forward by Grosberg *et al.* [23] depending the degree of shear imposed upon the fabric. First: deformation due to rigid intersections when the shear is too small to overcome the friction. Second: yarn slippage at the

intersection. Third: an elastic deformation when slipping is complete and fourth: jamming in the structure. Accordingly they deducted a model on the basis of mechanical properties of yarns and geometry of fabric structure for predicting initial shearing characteristics. Soon after, Grosberg et al [24] tried to suggest a model to predicting mechanism of deformation of woven fabric under shear stress in elastic region. S. Spival and Treloar [25] have been tried to find some relationship between bias extension and simple shear test methods. In this study, it is declared that the distribution of stress in simple shear and bias extension test is not the same and they mentioned that rupture mechanism in bias extension test is strongly depended on the shape and dimension of specimen. Meanwhile, the stress distribution across the specimen would be a maximum at the center, then falling off to zero at the edges in bias extension test. They pointed out that the mechanism of rupture has been gliding to disassembly in edges. i.e., the frictional forces at the cross-over were not sufficient to maintain the pin-pointing at the cross-over points. Skelton [26] studied the limitation in shear deformation of a fabric. In this study it is pointed out that the limits of shear are usually defined geometrically. For a wide range of conventional fabrics the shear limit is essentially defined by side-by-side contact of one set of yarns. Afterward, Leaf and Sheta [27] demonstrated that the Young's module of a fabric under bias stress is connected with shear modulus and fabric Poisson's ratio in warp and weft. Postel et al [28] proposed an energy method to apply mechanical properties of woven fabrics. Sinoimeri and Drean [29] utilized this method for predicting shear behavior of plain weave fabric. Ning Pan *et al.* [30] tried to show anisotropy in strength of fabric. In their study the anisotropy in strength of fabric was plotted by applying harmonic cosine series on measured values of strength as pretest. Clearly, the accuracy of this method is depended on number of pretest in different directions. P. Buckenham [31] compared simple shear and bias extension test method again after S. Spival and Treloar [25]. He mentioned that the bias extension test is more appropriate for industrial use than simple shear. Prodromou and Chen [32] tried to find a relationship between shear angles and wrinkling of several layers of woven fabrics that were used for composite performances. They measured angular deformation of warp and weft as shear angles by usage a trellis frame and image processing method. Moreover, buckling or wrinkling that occurred due to compressive forces was studied in this research. Critical shear angle, so called 'locking angle', was defined as the shear angle under onset of buckling in this study.

Also, shear angle was predicted up to locking angle with pin-joint assumption and some geometrical parameters, such as, yarn width, space between yarns and friction were considered for modifying the model. T. M. McBride and Julie Chen [33] dealt with change in internal geometry during shear deformation. They offered a geometric model for unit cell of a woven fabric by considering four sinusoidal curves. In that model, it was deemed that the yarn width, yarn space and fabric height were measurable during the deformation. So, some input data for the model were to be measured beforehand. They found that thickness of the fabric did not depend on shear deformation. For small shear deformation the fiber volume fraction was found to increase directly with shear angle. J. Wang *et al.* [34] reported that in a bias extension test, the aspect ratio of the specimen significantly affects on the deformation pattern and gross stress-strain relation. In this study, the slippage is observed in carbon fabric during bias deformation. However, for glass fabric with much lower bending rigidity, no clear slippage is observed under bias stress. J. Page and J. Wang [35, 39] dealt with prediction of shear force and yarn slippage analysis by using 3D non-linear finite element method. Zhang and Fu had suggested a 2D micromechanical model for woven fabric and its application to analyze buckling of fabric under uniaxial tension [36-38]. W M Lo and J L Hu [40] tried to evaluate shear properties of fabric in all directions on the base of Kilby's model [21]. They found that there is strongly linear relationship between shear rigidity and shear hysteresis in all direction. Lomov *et al.* carried out several investigations about internal structure of fabrics and shear deformation of composite fabrics and braided fabrics. However, the fabrics, under consideration, were mostly composite material [41-44]. Osamu Kuwazuru *et al.* studied anisotropy in tensile properties of plain weave fabric in arbitrary direction numerically by new concept of Pseudo-Continuum model [45-47]. This model is constructed on the basis of three modes of deformation of fabric and Strut-Spring concept (figures 2.13-2.15).

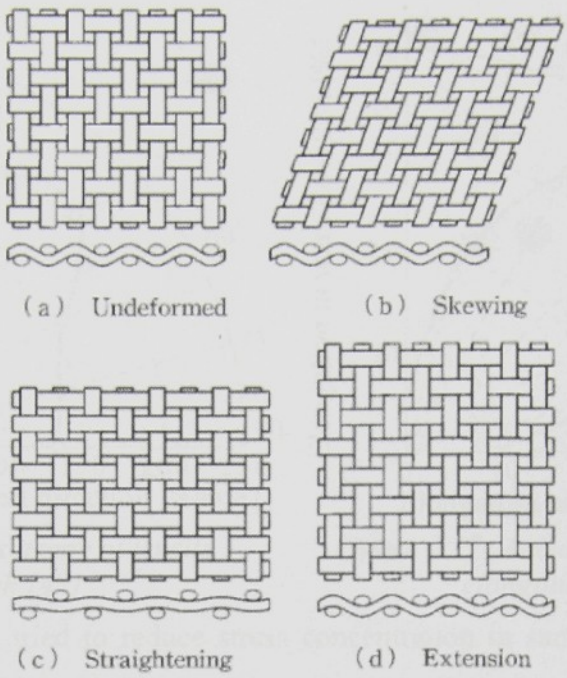

Figure 2.13- Modes of woven fabric deformation [45]

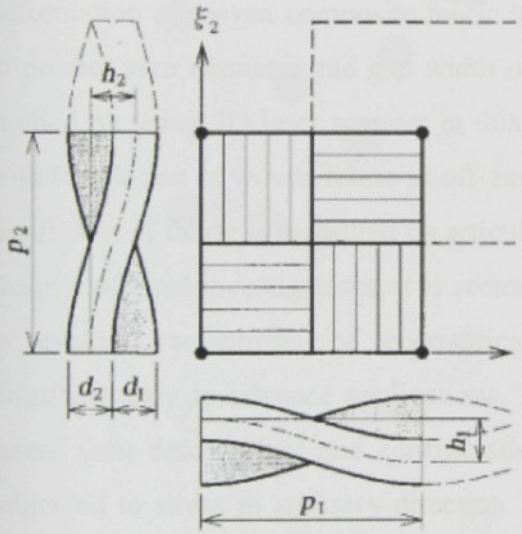

Figure 2.14- Unit cell of weave structure [45]

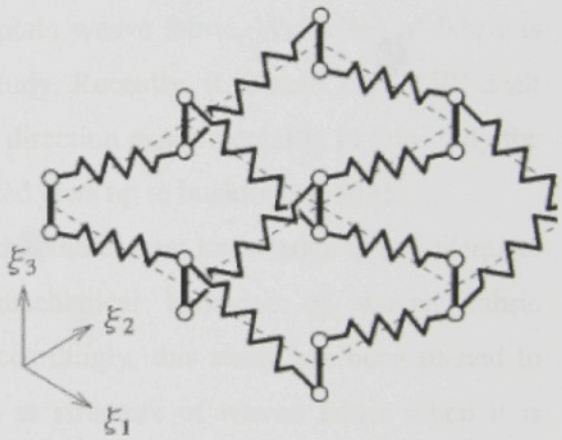

Figure 2.15- Strut-Spring model [45]

The obtained outcomes of this model in anisotropy of ultimate strength and strain by numerical solution of an imaginary fabric are presented in figures 2.16 and 2.17 respectively.

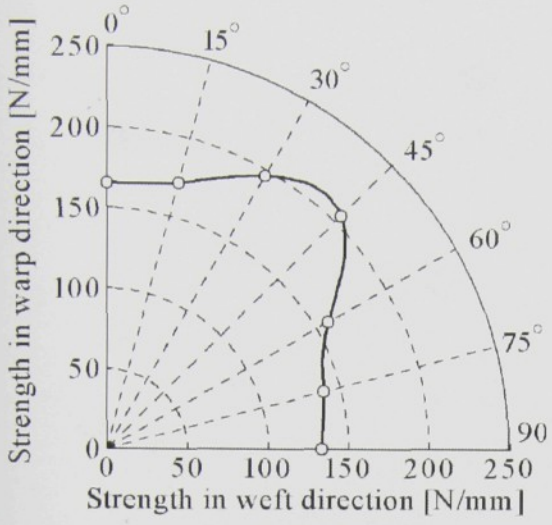

Figure 2.16- Anisotropy of tensile strength [47]

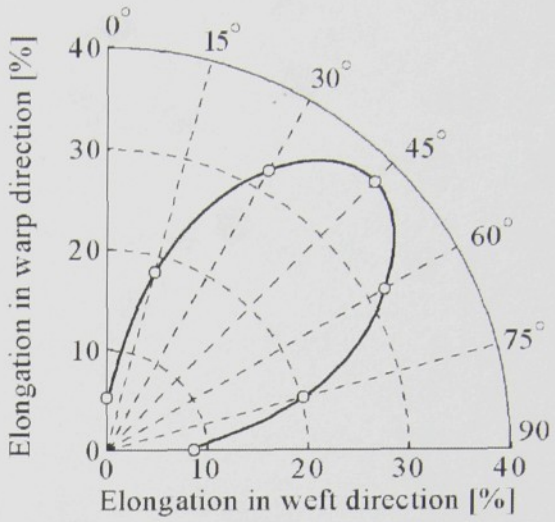

Figure 2.17- Anisotropy of breaking elongation [47]

R. Kovar *et al.* [48] tried to reduce stress concentration in sample's corners under tensile stress in different directions. An experimental study about in-plane shear deformation of woven composite fabric has been done by Zhu *et al.* [49]. They tried to predict yarn diameter and gap width of plain weave fabric. Wrinkling of fabric is studied by using 3D laser scanner in this study. Recently, R. Zouari *et al.* [50] dealt with tensile test of woven fabric in off-axes direction experimentally. In this study the tensile test of fabric is measured by articulated jaws up to buckling of fabric.

Despite of cited investigations, it is seems that the current knowledge is not adequate to evaluate anisotropy of geometrical-mechanical behavior of woven fabric simultaneously in advance applications. Accordingly, this study has been planed to assess yarn deformation and configuration in structure of woven fabric when it is subjected to stress in arbitrary direction. Concurrently, the tensile force required for certain deformation is studied in this investigation.

3 Theory

3 Theory

3.1 Geometrical Models

3.1.1 Geometry of plain weave fabric before deformation

Cross-sections in warp and weft direction are schematically illustrated in figure 3.1 and 3.2. Present model is to be on the basis of two principal assumptions; the yarns curvature axis and yarns cross-section shape are elliptic form and the minimum change in packing density is supposed after weaving process. Assumptions of this model are followed in details.

Assumptions

1. Yarn counts, yarn setts, weight of warp and weft yarns in a certain area (or yarns crimp) are defined as six general data of a fabric. Weight of warp and weft of yarns in a certain area of fabric could be calculated by measuring crimp.
2. Elliptical shape and arc is considered for yarn cross-section shape and yarn axis respectively.
3. Packing density of warp and weft yarns in contact area of yarns is very close to each other. It could be justified by equality in interaction force and contact area between yarns. Accordingly, it is supposed that warp and weft yarns have the same packing density.
4. Packing densities of yarns are increased due to spatial limitation in some structures and bending deformations of yarns during weaving process. Thus, packing density of yarns inside of a fabric can be laid between original yarn packing density and 0.8 (maximum possibility in packing density of fibrous assembly [51]). On the other hand, the inherent tendency of yarn is to fill the available space of the structure. Therefore, minimum packing density among all possibility of results can be chosen as packing density of yarns inside of fabric.

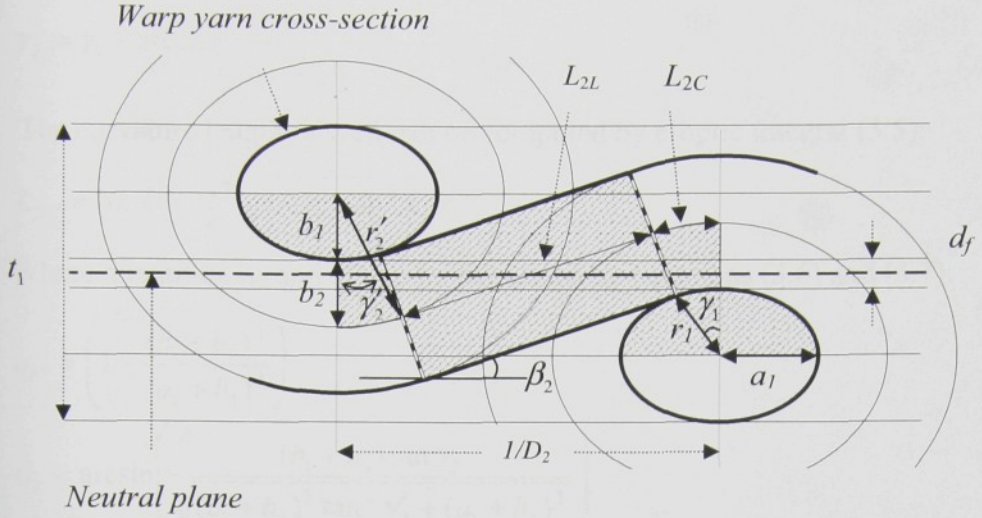

Figure 3.1- Warp cross-section

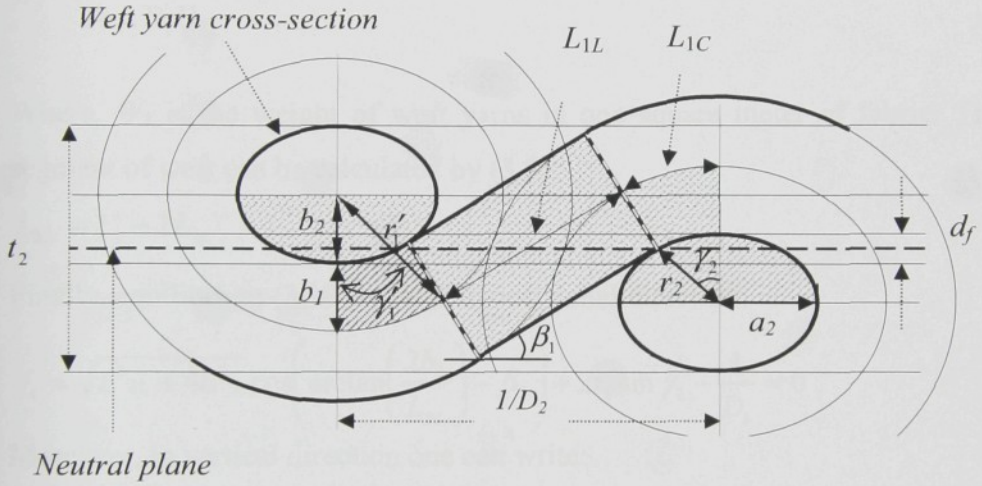

Figure 3.2- Weft cross-section

According to the schematic cross-sections, represented by figures 3.1 and 3.2, there are several relationships between internal geometry of a plain weave fabric. The following equations can be derived from figure 3.1 in the direction of warp cross-section.

$$r_1 = \frac{a_1 b_1}{\sqrt{(b_1 \sin\gamma_1)^2 + (a_1 \cos\gamma_1)^2}} \tag{3.1}$$

The inflection angle of weft is given by making a differential from elliptic equation:

$$\beta_2 = \arctan\left(\frac{b_1^{\,2} \operatorname{tag}\gamma_1}{a_1^{\,2}}\right) \tag{3.2}$$

$$r_2' = \sqrt{r_1^{\,2} + b_2^{\,2} + 2 r_1 b_2 \cos(\beta_2 - \gamma_1)} \tag{3.3}$$

$$\gamma_2' = \gamma_1 - \arccos\left(\frac{r_2'^2 + r_1^2 - b_2^2}{2r_2'r_1}\right) \tag{3.4}$$

The curvature length of weft can be computed by elliptic integral (3.5):

$$L_{2C} = (a_1 + b_2)\int_0^{\theta_2} \sqrt{1 - e_{r2}\sin^2 x}\,dx \tag{3.5}$$

Where quantities e_{r2} and θ_2 can be calculated by equations (3.6) and (3.7):

$$e_{r2} = \left(1 - \frac{(b_1 + b_2)^2}{(a_1 + b_2)^2}\right) \tag{3.6}$$

$$\theta_2 = \arcsin\left(\frac{(b_1 + b_2)\tan\gamma_2'}{\sqrt{(b_1 + b_2)^2\tan^2\gamma_2' + (a_1 + b_2)^2}}\right) \tag{3.7}$$

The total length of weft in unit cell is :

$$L_2 = \frac{10W_2}{Tex_2 D_1 D_2} \tag{3.8}$$

Where, W_2 is the weight of weft yarns in one square meter of fabric. Thus, linear segment of weft can be calculated by (3.9).

$$L_{2L} = L_2 - 2L_{2C} \tag{3.9}$$

Finally, equilibrium (3.10) is valid in horizontal direction.

$$f_1 = \sqrt{L^2{}_{2L} + 4b^2{}_2}\cos\left(\arctan\left(\frac{2b_2}{L_{2L}}\right) - \beta_2\right) + 2r_1\sin\gamma_1 - \frac{1}{D_1} = 0 \tag{3.10}$$

Moreover, in vertical direction one can write:

$$d_f = \sqrt{L^2{}_{2L} + 4b^2{}_2}\sin\left(\arctan\left(\frac{2b_2}{L_{2L}}\right) - \beta_2\right) + 2r_1\cos\gamma_1 - 2b_1 \tag{3.11}$$

Similarly, the following equations are valid in direction of weft cross-section (figure 3.2):

$$r_2 = \frac{a_2 b_2}{\sqrt{(b_2\sin\gamma_2)^2 + (a_2\cos\gamma_2)^2}} \tag{3.12}$$

$$\beta_1 = \arctan\left(\frac{b_2{}^2\tan\gamma_2}{a_2{}^2}\right) \tag{3.13}$$

$$r_1' = \sqrt{r_2{}^2 + b_1{}^2 + 2r_2 b_1\cos(\beta_1 - \gamma_2)} \tag{3.14}$$

$$\gamma_1' = \gamma_2 - \arccos\left(\frac{r_1'^2 + r_2{}^2 - b_1{}^2}{2r_1'r_2}\right) \tag{3.15}$$

$$L_{1C} = (a_2 + b_1)\int_0^{\theta_1} \sqrt{1 - e_{r1}\sin^2 x}\,dx \tag{3.16}$$

$$e_{r1} = 1 - \frac{(b_1 + b_2)^2}{(a_2 + b_1)^2} \tag{3.17}$$

$$\theta_1 = \arcsin\left(\frac{(b_1 + b_2)\tan\gamma_1'}{\sqrt{(b_1 + b_2)^2 \tan^2\gamma_1' + (a_2 + b_1)^2}} \right) \tag{3.18}$$

$$L_1 = \frac{10W_1}{Tex_1 D_1 D_2} \tag{3.19}$$

$$L_{1L} = L_1 - 2L_{1C} \tag{3.20}$$

$$f_2 = \sqrt{L_{1L}^2 + 4b_1^2}\cos\left(\arctan\left(\frac{2b_1}{L_{1L}}\right) - \beta_1 \right) + 2r_2 \sin\gamma_2 - \frac{1}{D_2} = 0 \tag{3.21}$$

$$f_3 = \sqrt{L_{1L}^2 + 4b_1^2}\sin\left(\arctan\left(\frac{2b_1}{L_{1L}}\right) - \beta_1 \right) + 2r_2 \cos\gamma_2 - 2b_2 + d_f = 0 \tag{3.22}$$

If the packing density of yarns in warp and weft are close to each other due to equality of interaction forces and almost equal pressure at this area, equation (3.25) is valid.

$$\mu_1 = \frac{Tex_1}{\pi\rho_1 a_1 b_1 10^5} \tag{3.23}$$

$$\mu_2 = \frac{Tex_2}{\pi\rho_2 a_2 b_2 10^5} \tag{3.24}$$

$$f_4 = \frac{\mu_2}{\mu_1} - 1 = \frac{a_1 b_1 \rho_1 Tex_2}{a_2 b_2 \rho_2 Tex_1} - 1 = 0 \tag{3.25}$$

Evidently, there are four equilibriums (3.10), (3.21), (3.22) & (3.25) depended on six unknown variables a_1, a_2, b_1, b_2, γ_1 and γ_2. These equilibriums can be solved by considering two arbitrary values k_1 (a_1/b_1) and k_2 (b_2/b_1). Certain yarn packing density can be obtained by each pair of k_1 and k_2. Quantities k_1, k_2 and yarn packing density, which satisfy mentioned equilibriums are graphically demonstrated in appendix (A) for two real fabrics. Accordingly, all possibilities in results are computed and on the basis of assumption 6, a series of results which is conducted to minimum packing density is picked out as an ultimate result. These arguments are arranged as a script in MATLAB program. Nevertheless, other respects can be considered in some special conditions in fabric structure.

Special conditions

a. Balanced Fabric

In a balanced fabric, distance between yarns and neutral plane of the fabric, $d_f/2$, is zero. Thus, equations (3.22) would be independent of equation (3.11) and equation

(3.11) can be accounted for evaluating. Accordingly five equilibriums on the basis of six unknown variables can be derived for balanced fabric.

b. Compact structure

Linear part of a yarn in structure of a fabric can be vanished if there is enough contraction in structure. Actually, this system of yarn could be considered as non-linear part (L_{1L} or/ and $L_{2L} = 0$). Therefore, equations (3.10), (3.11), (3.12) and (3.22) converted to equations which are independent of L_{1L} or/ and L_{2L}. Accordingly, both side of a fabric satisfy two new equations, if the amount of contraction is sufficient in warp and weft direction. In this case, one can evaluate internal geometry of a woven fabric. Otherwise, five equilibriums are considerable if only contraction take place in one side of fabric.

3.1.2 Geometry of plain weave fabric after deformation in bias direction

Bias direction is technically used when the initial angel of warp and weft direction with stress axis is ±45. When a piece of fabric is subjected to bias stress three distinct sectors will appear in arrangement of yarns in structure of fabric due to effects of jaws (figure 3.3). Hereafter, we will focus on area *III*. Evidently, jaws width can affect on fabric strain in this regard. Figure 3.4 illustrates this effect and related equation.

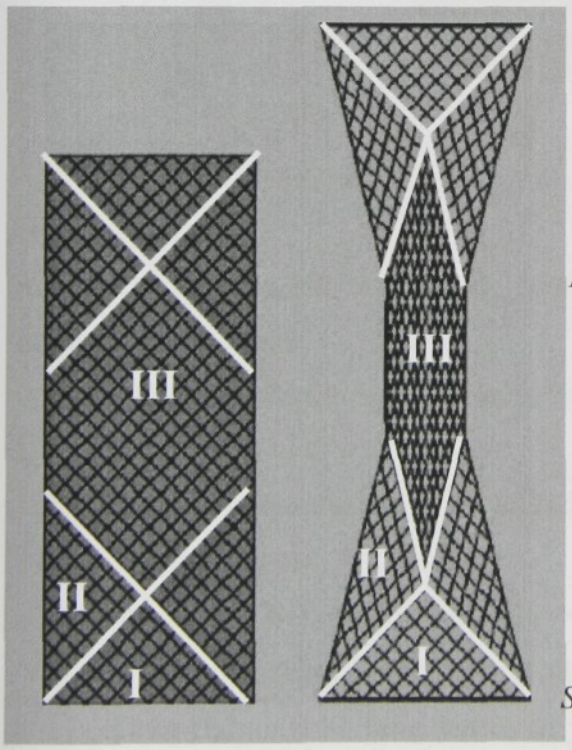

Figure 3.3- a: bias cut specimen before deformation, b: specimen under extension

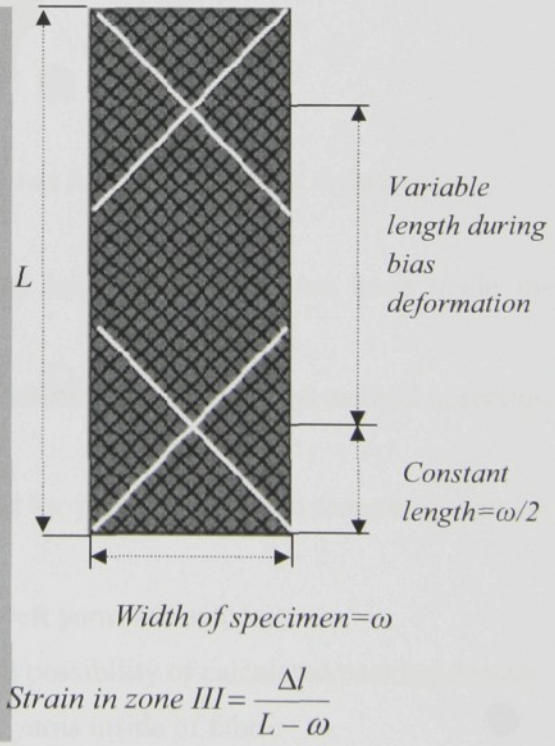

Figure 3.4- strain in zone III is depended on width of the sample.

To assess internal geometrical parameters of a plain weave fabric under deformation in bias direction, the model mentioned in section **3.1.1** is expanded. Indeed, elliptical concept for both cross-section and yarn's axis curvature is used to evaluate behavior of plain weave fabric under shear deformation. Figure 3.5 is a conceptual indication of ideal structure of woven fabric under shear deformation.

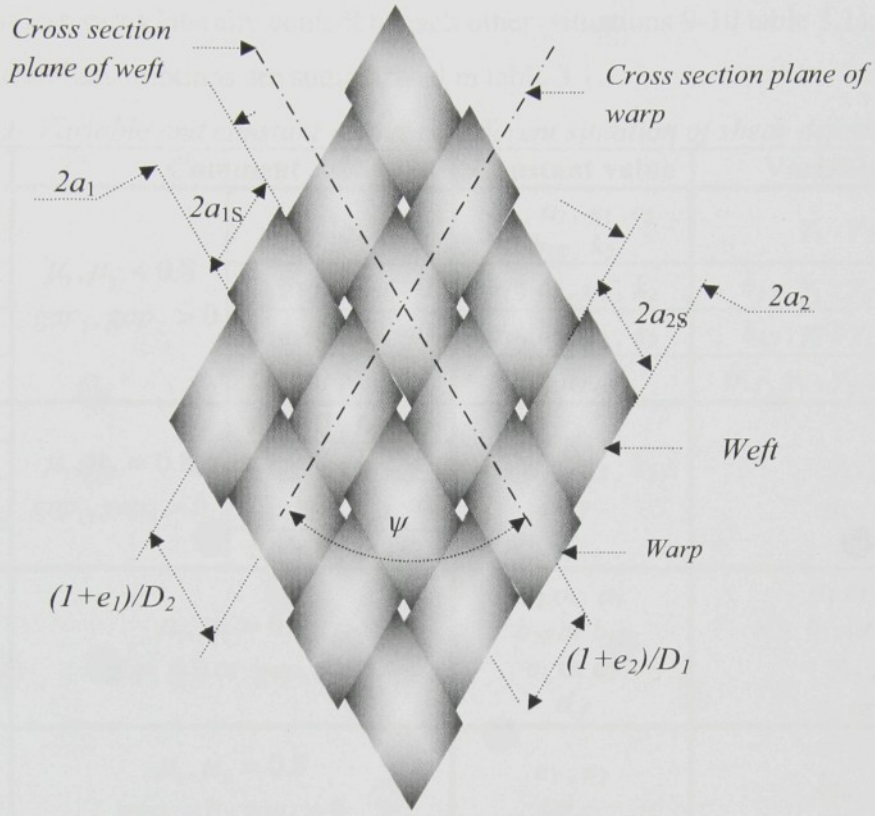

Figure 3.5- Schematic diagram of woven fabric under shear deformation

Assumptions

In order to develop the mentioned model in sheared fabric we have made the following assumptions.

1. Initial state of woven fabric can be determined by expressed method in section **3.1.1**.
2. Elliptical shape and arc is considered for yarn cross-section shape and yarn axis respectively.
3. The packing densities of warp and weft yarns are equal.
4. Minimum packing density among all possibility of calculated packing density can be chosen as packing density of yarns inside of fabric
5. Yarn setts in warp and weft are constant and equal to initial values, unless linear part of yarns in contrary system reach to zero (situations 2, 3 table 3.1).

6. Elongation of yarn is negligible while packing density of yarn is lower than the maximum value of it, namely 0.8 (situations 1-4 table 3.1).
7. Quantity d_f is constant when the packing density of yarns reaches to maximum (situations 5-10 table 3.1).
8. Major radiuses of warp and weft yarns and b_2/b_1 proportion (k_2) are constant unless yarns laterally contact to each other (situations 9-10 table 3.1).

All expressed assumptions are summarized in table 3.1.

Table 3.1- Variable and constant values in different situation of shear deformation * **

Situation	Comment		Constant value	Variable value
1	$\mu_1, \mu_2 < 0.8$ $gap_1, gap_2 > 0$	$L_{1L}, L_{2L} > 0$	a_1 , a_2, e_1 ,e_2 b_{1S} , k_2	γ_1 , γ_2 , d_f
2		$L_{1L} = 0$, $L_{2L} > 0$	a_1 , a_2, e_1 , k_2	b_{1S} , γ_1 , γ_2 , e_2 , d_f
3		$L_{1L} > 0$, $L_{2L} = 0$	a_1 , a_2, e_2 , k_2	b_{1S} , γ_1 , γ_2 , e_1 , d_f
4		$L_{1L} = 0$, $L_{2L} = 0$	a_1 , a_2, k_2	b_{1S} , γ_1 , γ_2 ,e_1, e_2, d_f
5	$\mu_1, \mu_2 = 0.8$ $gap_1, gap_2 > 0$	$L_{1L} = 0$, $L_{2L} = 0$	a_1 , a_2, b_{1S} , k_2, d_f	γ_1, γ_2 e_1 , e_2
6		$L_{1L} < 0$, $L_{2L} = 0$		
7		$L_{1L} = 0$, $L_{2L} < 0$		
8		$L_{1L} < 0$, $L_{2L} < 0$		
9	$\mu_1, \mu_2 = 0.8$ $gap_1 = 0$ or $gap_2 = 0$		a_2 or a_1 b_{2S} or b_{1S} e_1 or e_2 d_f	a_1 or a_2 b_{1S} or b_{2S} γ_1, γ_2 e_2 or e_1
10	$\mu_1, \mu_2 = 0.8$ $gap_1 = 0, gap_2 = 0$		e_1 , e_2 d_f	a_1 , a_2 b_{1S}, b_{2S} γ_1, γ_2

* *Subscripts 1 and 2 refer to warp and weft yarn. Subscript L indicates linear part of yarn and subscript S refers to shear deformation condition.*

** *Quantity b_{2S} can be calculated by $k_2 * b_{1S}$.*

In ideal structure of a plain weave fabric, the warp cross-section plane includes the central axis of a weft yarn. It is parallel to the weft yarn system, and the weft cross section plane includes the central axis of a warp yarn vice versa (figure 3.1). Obviously, major radius of warp and weft could be derived by relations (3.26) and (3.27). According to assumptions, equilibriums (3.28)-(3.31) could be inferred by substituting a_1, a_2, D_1, D_2 , b_1 and b_2 with a_{1S} , a_{2S}, $D_1/(e_2+1)$, $D_2/(e_1+1)$, b_{1S} *and* b_{2S} respectively in relations (3.1)-(3.25) of section 3.1.1. Also, gaps between yarns could be defined by respects (3.32) and (3.33).

$$a_{1S} = \frac{a_1}{\cos(\pi/2 - \psi)} \tag{3.26}$$

$$a_{2S} = \frac{a_2}{\cos(\pi/2 - \psi)} \tag{3.27}$$

$$f_1 = \sqrt{L^2{}_{2L} + 4b^2{}_{2S}}\cos\left(\arctan\left(\frac{2b_{2S}}{L_{2L}}\right) - \beta_2\right) + 2r_1\sin\gamma_1 - \frac{1+e_2}{D_1} = 0 \tag{3.28}$$

$$d_f = \sqrt{L^2{}_{2L} + 4b^2{}_{2S}}\sin\left(\arctan\left(\frac{2b_{2S}}{L_{2L}}\right) - \beta_2\right) + 2r_1\cos\gamma_1 - 2b_{1S} \tag{3.29}$$

$$f_2 = \sqrt{L^2{}_{1L} + 4b^2{}_{1S}}\cos\left(\arctan\left(\frac{2b_{1S}}{L_{1L}}\right) - \beta_1\right) + 2r_2\sin\gamma_2 - \frac{1+e_1}{D_2} = 0 \tag{3.30}$$

$$f_3 = \sqrt{L^2{}_{1L} + 4b^2{}_{1S}}\sin\left(\arctan\left(\frac{2b_{1S}}{L_{1L}}\right) - \beta_1\right) + 2r_2\cos\gamma_2 - 2b_{2S} + d_f = 0 \tag{3.31}$$

$$gap_1 = \frac{1+e_2}{D_1} - 2a_{1S} \tag{3.32}$$

$$gap_2 = \frac{1+e_1}{D_2} - 2a_{2S} \tag{3.33}$$

On the basis of assumptions, one can deal with the internal fabric geometry during deformation in bias direction different conditions.

a. Packing density is lower than maximum amount of it and gap between yarns is not vanished (situation 1-4 of table 3.1)

- **Linear part of warp and weft are none zeros value: L_{1L}, L_{2L}>0**

There are three variable, γ_1 , γ_2 and d_f , at this condition for certain warp-weft yarns angle ($\psi \leq 90$) deformation. Values a_{1S}, a_{2S} can be computed by relations (3.26) and (3.27). According to assumptions, fabric strain in warp and weft directions (e_1, e_2) are equal to zero although there is real fabric strain in bias direction due to rotation of yarns. Similarly, quantities b_{1S} and b_{2S} come through without change and they are equal to initial values b_1 and b_2. When warp-weft yarns angle begins to reduce up to certain angle, one can also calculates quantities γ_1, γ_2 and d_f by equilibriums (3.28), (3.29) and (3.31) in this condition.

- **At least linear segment in one of the warp or weft is zero: L_{1L} =0, L_{2L}>0 or L_{1L} >0, L_{2L} =0**

In this regard (L_{1L} >0, L_{2L} =0) linear segment in weft yarn is zero and in warp yarn linear segment is significant value. Equation (3.34) is valid at this condition and relation (3.29) is converted to (3.35). Eventually, equilibriums (3.30), (3.31), (3.34) and (3.35) are depended on the variables b_{1S} , γ_1, γ_2 and d_f . Then, the strain of fabric in weft direction namely; e_2 could be found by relation (3.28). It was clarified that

value b_{2S} can be gained by constant k_2 and variable b_{1S}. Concerning second condition (L_{1L} =0, L_{2L} >0), equations (3.28), (3.29), (3.36) and (3.37) could be applied. Evidently, relation (3.39) is adequate for evaluating strain of fabric in warp direction (e_1) at this condition.

$$f_4 = L_2 - 2L_{2C} = 0 \tag{3.34}$$

$$d_f = 2b_{2S}\sin(\pi/2-\beta_2) + 2r_1\cos\gamma_1 - 2b_{1S} \tag{3.35}$$

$$f_5 = L_1 - 2L_{1C} = 0 \tag{3.36}$$

$$f_3 = 2b_{1S}\sin(\pi/2-\beta_1) + 2r_2\cos\gamma_2 - 2b_{2S} + d_f = 0 \tag{3.37}$$

$$e_2 = D_1\left(2b_{2S}\cos(\pi/2-\beta_2) + 2r_1\sin\gamma_1\right) - 1 \tag{3.38}$$

$$e_1 = D_2\left(2b_{1S}\cos(\pi/2-\beta_1) + 2r_2\sin\gamma_2\right) - 1 \tag{3.39}$$

- **Linear part of warp and weft is zero: L_{1L} =0, L_{2L} =0**

According to assumptions yarn elongation is still negligible in this state therefore, the equations (3.34)-(3.37) can be used for obtaining values b_{1S} , γ_1, γ_2, d_f . Subsequently, fabric strain in warp and weft directions namely e_1 and e_2 are computed by equations (3.39) and (3.38) respectively.

b. Packing density is reached to maximum amount of it and gap between yarns is not vanished (situation 5-8 of table 3.1)

Extension in yarn length is expected in this state; accordingly, equations (3.34) and (3.36) are not responsible. However, yarns strain (ε_{y1} and ε_{y2}) during deformation can be derived by relations (3.40) and (3.41). Quantity d_f is simultaneously deemed constant and known value. Hence, variables γ_1, γ_2, e_1 , e_2 can be determined by equations (3.35), (3.37), (3.39) and (3.38).

$$\varepsilon_{y1} = \frac{2l_{1C} - L_1}{L_1}100 \qquad if\ 2L_{1C} > L_1 \tag{3.40}$$

$$\varepsilon_{y2} = \frac{2l_{2C} - L_2}{L_2}100 \qquad if\ 2L_{2C} > L_2 \tag{3.41}$$

c. Packing density is reached to maximum amount of it and gap between yarns is vanished (situation 9-10 of table 3.1)

Lateral contact between yarns would occur when gaps vanished in warp and/or weft direction. This stated condition so called warp or weft yarns jamming. In this regard equations (3.32) and/or (3.33) become zero. Then, depend on jamming direction the equations (3.42), (3.44) and/or (3.43), (3.45) are valid. Where a'_{1S}, a'_{2S}, b'_{1S} and b'_{2S} are corresponding values to constant values just before gap vanished. Quantity/s γ_1 and/or

γ_2 can be obtained from (3.38) and/or (3.39) relations. Finally, equations (3.42)-(3.45) can be applied as well as in situation10 of table 3.1.

$$a_{1S} = \frac{1+e_2}{2D_1} \tag{3.42}$$

$$a_{2S} = \frac{1+e_1}{2D_2} \tag{3.43}$$

$$b_{1S} = \frac{2b'_{1S}a'_1D_1}{(1+e_2)\cos(\pi/2-\psi)} \tag{3.44}$$

$$b_{2S} = \frac{2b'_{2S}a'_2D_2}{(1+e_1)\cos(\pi/2-\psi)} \tag{3.45}$$

Exterior characteristics of a fabric

Some expressed parameters, such as warp-weft angle (ψ), strain of fabric in both warp and weft directions namely e_1, e_2 and fabric strain (e_f) are exterior characteristics of a fabric. According to this model, relationship between exterior characteristics could be deducted as equation (3.46).

$$e_f = \frac{\sin\left(\frac{\pi-\psi}{2}\right)\left(\frac{1+e_2}{D_1}+\frac{1+e_1}{D_2}\right)}{\frac{\sqrt{2}}{2}\left(\frac{1}{D_1}+\frac{1}{D_2}\right)} - 1 \tag{3.46}$$

Rupture mechanisms

Yarns features in rupture area in bias direction can be classified in two categories: slipped yarns and broken yarns (figure 3.6). Friction force and number of interlacing points determine the feature of a yarn in rupture area. Slippage can be expected on low friction force and contact number while yarn failure is occurred in condition of high friction force and contact numbers. Obviously, the width of specimen play vital role to determine rupture mechanisms. In this study "*Critical width*" is defined as the initial width of sample which at least one broken yarn is observed in rupture area (figure 3.7). This failure is generally taken place within weft yarns due to bigness of number of contacts in comparison with warp yarns in traditional fabrics.

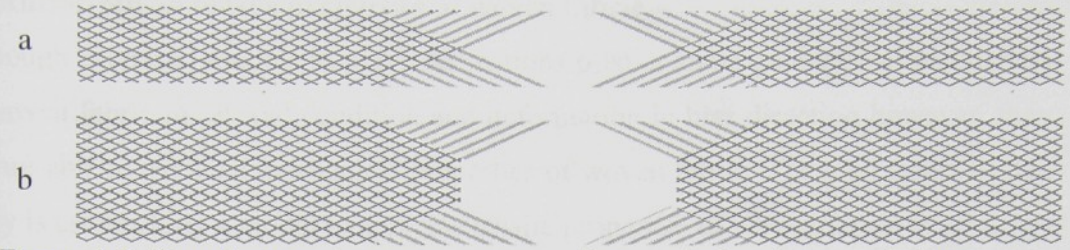

Figure 3.6- Yarn features in rupture area a: slippage b: breakage and slippage

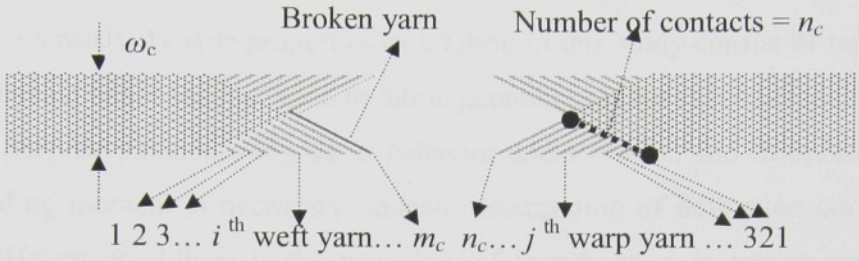

Figure 3.7- Schematic rupture mechanism in critical width of a fabric

3.2 Anisotropy in tensile properties of woven fabric

Although proposed models in previous sections predict some geometrical parameters of woven fabric in relaxed condition and deformation in bias direction however, they are not able to evaluate mechanical properties of woven fabric. The vital target of this study is establishing a model to appraise tensile properties of woven fabric in arbitrary direction. Tensile properties of fabric indicate how the fabric will react to forces being applied in tension. Tensile properties of a fabric in this study consist of tensile force-strain curve of fabric and variation in fabric geometrical characteristics simultaneity.

For this purpose understanding yarns behavior under tension and compressive forces and bending moment is necessary. Indeed, determining of deflection curve of yarn under different conditions is the main key of investigation in tensile properties of fabric. A yarn is constructed by assembling of fibers in different technologies and arrangements. Definition and determining of yarn deflection curve is difficult due to viscoelastic behavior of fibers and complex interaction within fibers in yarn structure. Accordingly, considering some simplifications are necessary to establish a comprehensive model for tensile properties of fabric.

3.2.1 Deflection curve of tensioned yarn

Figure 3.8 indicates the path of a yarn in unit cell of plain weave. Half path of yarn between two cross yarns is adequate to study deflection curve of yarn due to symmetry of path.

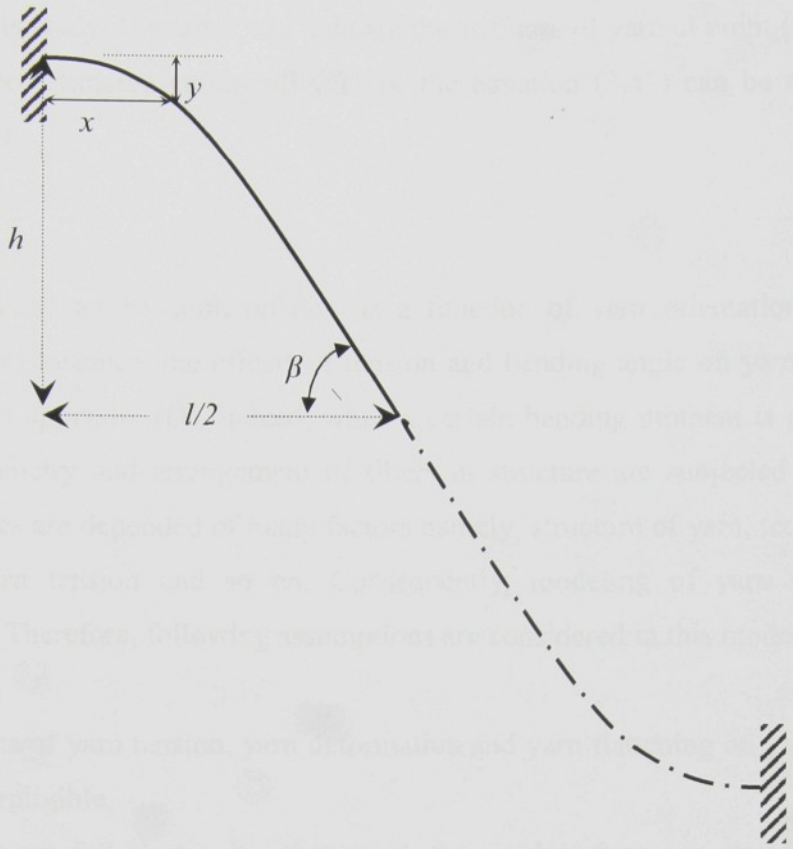

Figure 3.8- Yarn path between two cross yarns (fabric cross-section)

The well-known Euler-Bernoulli beam equation (3.47) is usually used in continuum mechanic for isotropic materials. This equation reveals the relation between beam curvature and moment at certain point of (x,y) by considering *EI* quantity. Where, *EI* shows stiffness of beam which it consists of *E*, Young's modulus of beam, and *I*, moment of inertia of beam cross-section.

$$\frac{1}{\rho_{(x,y)}} = \frac{M_{(x,y)}}{EI} \qquad (3.47)$$

To derive equation (3.47) it is assumed that the absolute values of deformation of materials in compressive and tensile stress are the same and the Hooke's law is governed. However, there are some restrictions for applying this equation to evaluate bending stiffness of textile materials as well as yarn due to non-isotropic behavior of textile materials. Therefore, behavior of textile materials is not the same as continuum materials when they are subjected to bending moment.

It is cleared that response of yarns in axial compressive and tensile stress are dissimilar. Thus, considering *EI* can not be used as yarn stiffness. Nevertheless, the yarn curvature at certain point (x,y) is logically proportional to the ratio of bending moment and yarn stiffness at this point. Therefore, the quantities *EI* do not exert

directly in this study. Hereafter, we indicate the stiffness of yarn at point (x,y) as $S_{(x,y)}$ which will be estimated empirically. Thus, the equation (3.47) can be rewritten as equation (3.48).

$$\frac{1}{\rho_{(x,y)}} = \frac{M_{(x,y)}}{S_{(x,y)}} \tag{3.48}$$

Yarn's stiffness can be contemplated as a function of yarn orientation and fiber properties. For instance, the effects of tension and bending angle on yarn's stiffness are studied in appendix (D). Indeed, when a certain bending moment is put on yarn then the geometry and arrangement of fibers in structure are subjected to change. These changes are depended of many factors namely; structure of yarn, technology of spinning, yarn tension and so on. Consequently, modeling of yarn stiffness is problematic. Therefore, following assumptions are considered in this model.

Assumption

1. Effects of yarn tension, yarn deformation and yarn flattening on yarn stiffness are negligible.
2. Yarns are full elastic. In other word, the residual forces in structure of bent yarn are disesteem.
3. The yarn geometry and properties through whole of the yarn do not vary.

According to diagram of forces and moments in figures 3.9 and 3.10, bending moment at point O can be computed as equation (3.49).

$$M_o = \frac{F_n l}{2} + Th \tag{3.49}$$

Also, bending moment at certain point of (x,y) follows equation (3.50).

$$M_{(x,y)} = F_n\left(x - \frac{l}{2}\right) + T(y-h) \tag{3.50}$$

The curvature mathematically corresponds with first and second order derivative of deflection curve like equation (3.51).

$$\frac{1}{\rho_{(x,y)}} = \frac{|y''|}{\left(1+(y')^2\right)^{\frac{3}{2}}} \tag{3.51}$$

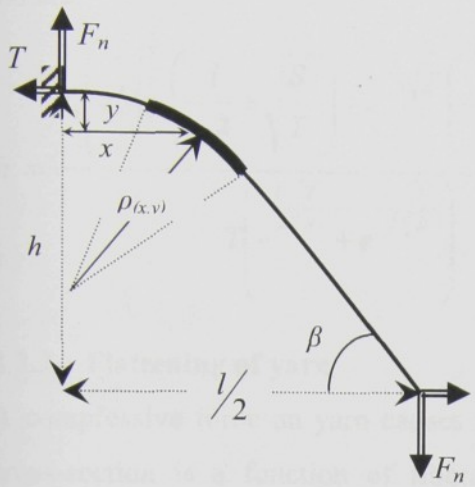

Figure 3.9- Curvature and cantilever bending at fixed point

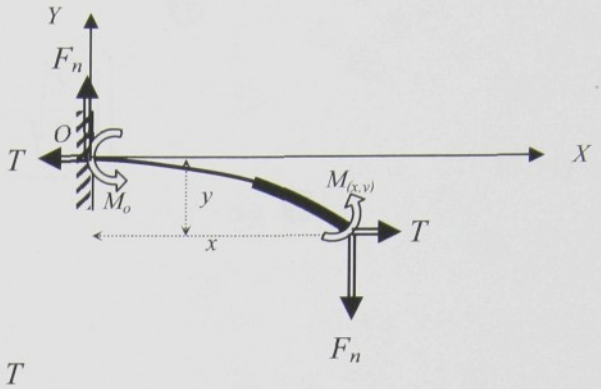

Figure 3.10- Diagram of force and bending moment at point (x,y)

Eventually, the equation (3.52) can be derived by substituting equations (3.50) and (3.51) in equation (3.48). Differential equation (3.52) indicates the relation among deflection function, yarn stiffness and exerted force/s on yarn. In addition, following two boundary conditions are valid.

$$\frac{y''}{\left(1+\left(y'\right)^2\right)^{\frac{3}{2}}}=\frac{F_n}{S}\left(x-\frac{l}{2}\right)+\frac{T}{S}\left(y-h\right) \qquad y(0)=0, y'(0)=0 \tag{3.52}$$

The differential equation (3.52) has been analytically solved under stipulation that $T>2F_n$ (appendixes (B), (C)). On the basis of this appendix, when planar force is bigger that normal force ($T>2F_n$) then the equations (3.53) would be solution of equation (3.52). Otherwise when $T\leq 2F_n$, numerical solution must be considered for equation (3.52). The authenticity of analytical solution in comparison with numerical solution in different conditions has been surveyed in appendix (C).

If $T>2Fn$ then:

$$y=\frac{F_n}{2T}e^{x\sqrt{\frac{T}{S}}}\left(-\frac{l}{2}-\frac{hT}{F_n}+\sqrt{\frac{S}{T}}\right) \tag{3.53}$$
$$+\frac{F_n}{2T}\left(e^{-x\sqrt{\frac{T}{S}}}\left(-\frac{l}{2}-\frac{hT}{F_n}-\sqrt{\frac{S}{T}}\right)-2x+l\right)+h$$

Where:

$$h = \frac{F_n\left(e^{\frac{l}{2}\sqrt{\frac{T}{S}}}\left(-\frac{l}{2}+\sqrt{\frac{S}{T}}\right)+e^{\frac{l}{2}\sqrt{\frac{T}{S}}}\left(-\frac{l}{2}-\sqrt{\frac{S}{T}}\right)\right)}{T\left(e^{\frac{l}{2}\sqrt{\frac{T}{S}}}+e^{\frac{l}{2}\sqrt{\frac{T}{S}}}\right)} \tag{3.54}$$

3.2.2 Flattening of yarn

A compressive force on yarn causes to flatten of cross-section. Deformation of yarn cross-section is a function of fibers arrangement in yarn structure, quantity and modality of compressive force, yarn tension, etc. However, in this study it is assumed flattening coefficient namely e_d is only function of compressive force F_n (equation (3.55) and (3.56). G function can be determined via empirical method which is expressed in chapter 4.

$$e_d = \frac{d - d_0}{d_0} \tag{3.55}$$

$$e_d = G\left(F_n\right) \tag{3.56}$$

The original diameter of yarn d can be computed for certain value of yarn packing density and fiber density.

Following classification can be contemplated in anisotropy of tensile properties of fabric.

Remark: the subscripts 1 and 2 refer to warp and weft respectively.

3.2.3 Relaxed fabric state:

In this condition, it is deemed that the planar force T_1 and T_2 are zero then, the differential equations (3.52) for both side of warp and weft yarns convert to (3.57) and (3.58) equations. These equations should be solved in numerical manner due to absence of planar force. Obviously, the interaction normal force F_n at interlacing point is unique for both warp and weft yarns.

$$\frac{y_1''}{\left(1+\left(y_1'\right)^2\right)^{\frac{3}{2}}} = \frac{F_n}{S_1}\left(x-\frac{l_1}{2}\right) \qquad y_1(0)=0, y_1'(0)=0 \tag{3.57}$$

$$\frac{y_2''}{\left(1+\left(y_2'\right)^2\right)^{\frac{3}{2}}} = \frac{F_n}{S_2}\left(x-\frac{l_2}{2}\right) \qquad y_2(0)=0, y_2'(0)=0 \tag{3.58}$$

The quantities l_1 and l_2 computed on the basis of relations (3.59) and (3.60).

$$l_1 = (1+e_1).\frac{1}{D_2} \tag{3.59}$$

$$l_2 = (1+e_2).\frac{1}{D_1} \tag{3.60}$$

Where, D_1, D_2 and e_1, e_2 are yarn sett (as known values) and fabric strain in relative warp or weft direction respectively. Evidently, in relax condition fabric strain in warp and weft direction is zero (e_1= e_2=0). In the other hand, the flattening functions for warp and weft can be written like (3.61) and (3.62) equations separately.

$$e_{d1} = G_1(F_n) \tag{3.61}$$

$$e_{d2} = G_2(F_n) \tag{3.62}$$

On the basis of fabric geometry, following relation is always true in all conditions (figures 3.1 and 3.2).

$$h_1 + h_2 = \frac{d_1 + d_2}{2} \tag{3.63}$$

Where, d_1 and d_2 are thickness of warp and weft yarns. Consequently, equation f_1 can be established by substituting equations (3.61) and (3.62) in equation (3.63).

$$f_1 = \left(d_{01}(1+e_{d1}) + d_{02}(1+e_{d2})\right)/2 + (h_1 + h_2) = 0 \tag{3.64}$$

On the other hand, the length of warp and weft yarns between two cross yarns can be calculated by relations (3.65) and (3.66) respectively.

$$L_1 = \frac{C_1/100+1}{D_2}, \tag{3.65}$$

$$L_2 = \frac{C_2/100+1}{D_1} \tag{3.66}$$

Where, C_1 and C_2 are warp and weft yarns crimp respectively (as known values). The length of yarn between two cross yarns can be calculated via deflection curve too. Therefore, equations (3.67) and (3.68) govern if the deflection curves of warp and weft determine.

$$f_2 = 2\int_0^{l_1/2} \sqrt{1+y_1'^2} - L_1 = 0 \tag{3.67}$$

$$f_3 = 2\int_0^{l_2/2} \sqrt{1+y_2'^2} - L_2 = 0 \tag{3.68}$$

Finally, a system of equations consist of equations (3.64), (3.67) and (3.68) can be contemplated to evaluate relaxed fabric state. Three unknown values F_n, S_1 and S_2 can

be computed from this system of equations numerically by utilizing mathematical methods. Accordingly, a script has been constructed in MATLAB program.

On the basis of assumptions, the stiffness of yarns which are derived by mentioned method in relaxed fabric state, are constant during deformation. Hence, warp and weft yarns stiffness is deemed as known values in next states.

3.2.4 Stress in principal direction:

Suppose that the direction of imposed stress is in warp direction. Then, the planar force in cross yarns, here weft yarn, is negligible. In this condition T_2 is zero, while both e_1 and e_2 are subjected to change. Evidently, quantity e_1 indicates the strain of fabric in warp direction and e_2 shows the contraction of fabric in weft direction. Equations (3.59) and (3.60) can be used to calculate new values of l_1 and l_2. Whereas, the planar force in warp direction T_1 is generally bigger than F_n, the equation (3.69) is responsible in warp yarn. However, to indicate deflection curve of cross yarn (weft yarn) the equation (3.71) must be used in this regard.

If $T_1 > F_n$ then:

$$y_1 = \frac{F_n}{2T_1} e^{x\sqrt{\frac{T_1}{S_1}}} \left(-\frac{l_1}{2} - \frac{h_1 T_1}{F_n} + \sqrt{\frac{S_1}{T_1}} \right) + \frac{F_n}{2T_1} \left(e^{-x\sqrt{\frac{T_1}{S_1}}} \left(-\frac{l_1}{2} - \frac{h_1 T_1}{F_n} - \sqrt{\frac{S_1}{T_1}} \right) - 2x + l_1 \right) + h_1 \tag{3.69}$$

Where:

$$h_1 = \frac{F_n \left(e^{\frac{l_1}{2}\sqrt{\frac{T_1}{S_1}}} \left(-\frac{l_1}{2} + \sqrt{\frac{S_1}{T_1}} \right) + e^{\frac{l_1}{2}\sqrt{\frac{T_1}{S_1}}} \left(-\frac{l_1}{2} - \sqrt{\frac{S_1}{T_1}} \right) \right)}{T_1 \left(e^{\frac{l_1}{2}\sqrt{\frac{T_1}{S_1}}} + e^{-\frac{l_1}{2}\sqrt{\frac{T_1}{S_1}}} \right)} \tag{3.70}$$

$$\frac{y_2''}{\left(1 + (y_2')^2\right)^{\frac{3}{2}}} = \frac{F_n}{S_2} \left(x - \frac{l_2}{2} \right) \qquad y_2(0) = 0, y_2'(0) = 0 \tag{3.71}$$

Apparently, maximum yarn strain ε_{1y} is occurred in inflection point due to bigness of tension at this point (3.72). Relation (3.73) reveals the inflection angle of warp yarn. Where, E_1 is the original warp yarn modulus which we consider it as one of the inputs data of this model. The maximum yarn strain quantity is considered for whole yarn strain. Thus, the equation (3.67) must be modified like equation (3.74). While the strain in cross yarns ε_{2y} is deemed negligible due to absence of T_2 then the equation (3.68) is still valid in this state.

$$\varepsilon_{y1} = \frac{T_1}{E_1 \cos\beta_1} \tag{3.72}$$

Where,

$$\tan\beta_1 = y_1'(l_1/2) \tag{3.73}$$

$$f_2 = 2\int_0^{l_1/2} \sqrt{1+y_1'^2} - L_1(1+\varepsilon_{1y}) = 0 \tag{3.74}$$

Now, the system of equations is composed of equations (3.64), (3.68) and (3.74). This system of equations can be solved for certain value of T_1 by applying mathematical methods. Eventually, the variables F_n, e_1 and e_2 can be estimated by this system of equations. When the fabric is suffering the stress in weft direction then proposed equations can be utilized by substituting relative subscripts in the same way (equations (3.75)-(3.80)).

If $T_2 > F_n$ then:

$$y_2 = \frac{F_n}{2T_2} e^{x\sqrt{\frac{T_2}{S_2}}}\left(-\frac{l_2}{2} - \frac{h_2 T_2}{F_n} + \sqrt{\frac{S_2}{T_2}}\right) \tag{3.75}$$

$$+\frac{F_n}{2T_2}\left(e^{-x\sqrt{\frac{T_2}{S_2}}}\left(-\frac{l_2}{2} - \frac{h_2 T_2}{F_n} - \sqrt{\frac{S_2}{T_2}}\right) - 2x + l_2\right) + h_2$$

Where:

$$h_2 = \frac{F_n\left(e^{\frac{l_2}{2}\sqrt{\frac{T_2}{S_2}}}\left(-\frac{l_2}{2} + \sqrt{\frac{S_2}{T_2}}\right) + e^{-\frac{l_2}{2}\sqrt{\frac{T_2}{S_2}}}\left(-\frac{l_2}{2} - \sqrt{\frac{S_2}{T_2}}\right)\right)}{T_2\left(e^{\frac{l_2}{2}\sqrt{\frac{T_2}{S_2}}} + e^{-\frac{l_2}{2}\sqrt{\frac{T_2}{S_2}}}\right)} \tag{3.76}$$

$$\frac{y_1''}{\left(1+(y_1')^2\right)^{\frac{3}{2}}} = \frac{F_n}{S_1}\left(x - \frac{l_1}{2}\right) \qquad y_1(0) = 0, y_1'(0) = 0 \tag{3.77}$$

$$\varepsilon_{y2} = \frac{T_2}{E_2 \cos\beta_2} \tag{3.78}$$

Where,

$$\tan\beta_2 = y_2'(l_2/2) \tag{3.79}$$

$$f_2 = 2\int_0^{l_2/2} \sqrt{1+y_2'^2} - L_2(1+\varepsilon_{2y}) = 0 \tag{3.80}$$

3.2.5 Stress in arbitrary direction, except of principal directions

When a strip fabric is subjected to stress in arbitrary direction except of principal direction all quantities e_1, e_2, ψ_1, ψ_2 and F_n are subjected to change. Current equations

are not adequate to achieve final solution. It seems more assumptions must be contemplated in this regard.

3.2.5.1 Exterior geometry of plain weave fabric after deformation in arbitrary direction

Figure 3.11-I describes the deformation of a specimen when the initial angle of force axis with weft yarns is φ. Suppose one imaginary square *abcd* on center of specimen which is parallel to edges. Square *abcd* is converted to parallelogram *a'b'c'd'* after deformation. Figure 3.3.11-II illustrates deformation of square *abcd* in details. On the basis of observations, following assumptions are deemed.

Assumptions

1. Deformation is symmetric around central point of specimen "O".
2. Lateral sides of imaginary parallelogram are parallel to force axis.
3. Deformation and distribution of force are homogonous for each yarn and cut end effects effect is negligible.
4. The perimeter of imaginary parallelogram is constant during deformation and is the same as initial imaginary square *abcd* before deformation.
5. Jaws effect on deformation on area under consideration is negligible.

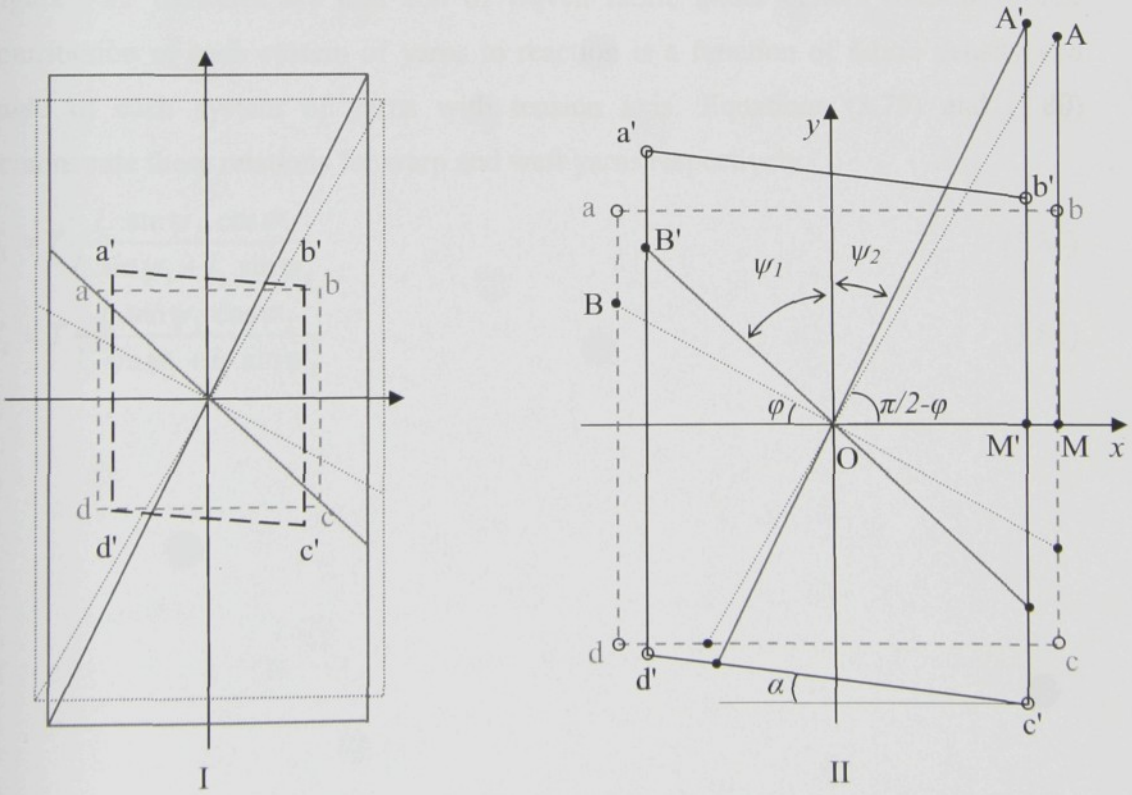

Figure 3.11- Imaginary square abcd on center and parallel with sample's edges. I: deformation of square II: converting square to parallelogram in details

On the basis of pure geometry and assumptions, subsequent arguments are valid. Lateral sides of parallelogram are parallel to force axis, thus:

$$e_1 = \frac{(1+e_2).\sin\psi_2}{\tan\varphi.\sin\psi_1} - 1 \tag{3.81}$$

Strain of fabric can be calculated as equation (3.76).

$$e_f = (1+e_1)\sin\varphi.\cos\psi_1 + (1+e_2)\cos\psi_2.\cos\varphi - 1 \tag{3.82}$$

Remark: the calculated fabric strain by equation (3.76) is not the same as the fabric strain recorded by Tensile Instron due to this equation computes real strain of fabric in direction of force axis.

Oblique angle of parallelogram can be accounted as subsequent equation.

$$\tan\alpha = \frac{(1+e_1).\cos\psi_1 - \sin\varphi - e_f.\cos\varphi}{(1+e_1).\sin\psi_1} \tag{3.83}$$

The subsequent equilibrium (3.78) is logically true when it is deemed that perimeter of parallelogram is constant.

$$f_4 = \frac{2(1+e_1).\sin\psi_1}{\cos\alpha} + 2\cos\varphi.(1+e_f) - 4\cos\varphi = 0 \tag{3.84}$$

3.2.5.2 Distribution of planar force

Figure 3.12 indicates the unit cell of woven fabric under certain tension *T*. The contribution of each system of yarns to reaction is a function of fabric density and angle of each system of yarns with tension axis. Equations (3.79) and (3.80) demonstrate these relations for warp and weft yarns respectively.

$$T_1 = T\frac{l_2.\sin\psi_2.\cos\psi_1}{l_1.\sin\psi_1 + l_2.\sin\psi_2} \tag{3.85}$$

$$T_2 = T\frac{l_1.\sin\psi_1.\cos\psi_2}{l_1.\sin\psi_1 + l_2.\sin\psi_2} \tag{3.86}$$

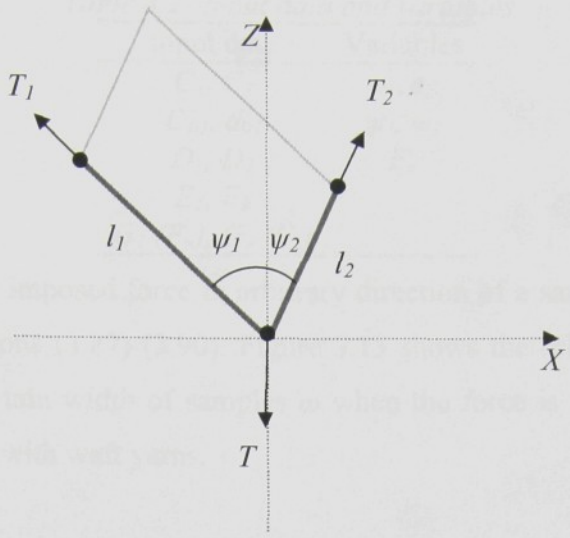

Figure 3.12- Forces diagram of unit cell (surface of fabric)

3.2.5.3 Solving system of equations

When a fabric is subjected to stress in arbitrary direction, except principal directions, then planar forces T_1 and T_2 are bigger than F_n. On the basis of previous arguments, the yarn deflection equation (5.53) can be applied in both warp and weft yarns by using relative subscripts (equations (3.69) and (3.75)). There are warp and weft yarns strain due to existence of planar force in both warp and weft direction. A system of equations includes of five equations (3.64), (3.74), (3.80), (3.81) and (3.84) can be applied to determine five variables for a certain value of T.

$$f_1 = (d_{01}(1+e_{d1}) + d_{02}(1+e_{d2}))/2 + (h_1 + h_2) = 0 \tag{3.64}$$

$$f_2 = 2\int_0^{l_1/2} \sqrt{1+y_1'^2} - L_1(1+\varepsilon_{1y}) = 0 \tag{3.74}$$

$$f_3 = 2\int_0^{l_2/2} \sqrt{1+y_2'^2} - L_2(1+\varepsilon_{2y}) = 0 \tag{3.80}$$

$$e_1 = \frac{(1+e_2).\sin\psi_2}{\tan\varphi.\sin\psi_1} - 1 \tag{3.81}$$

$$f_4 = \frac{2(1+e_1).\sin\psi_1}{\cos\alpha} + 2\cos\varphi.(1+e_f) - 4\cos\varphi = 0 \tag{3.84}$$

Table 3.2 illustrates the inputs and variables of this model when the stress is imposed in arbitrary direction except of principal directions. According stated arguments, a script has been constructed in MATLAB program to solve equations.

Table 3.2- Input data and variables

Input data	Variables
C_1, C_2	e_1, e_2
D_{01}, d_{02}	ψ_1, ψ_2
D_1, D_2	F_n
E_1, E_2	
$G_1(F_n)$, $G_2(F_n)$	

Eventually, the total imposed force in arbitrary direction of a sample width ω can be accounted by equations (3.87)-(3.90). Figure 3.13 shows the schematic arrangement of unit cells at a certain width of samples ω when the force is applied to sample in arbitrary direction φ with weft yarns.

$$\theta = \arctan(D_1 / D_2) \tag{3.87}$$

$$N = \frac{\omega . D_1 . D_2}{(D_2 \cos\theta + D_1 \sin\theta)\sin(\varphi + \theta)} \tag{3.88}$$

$$F = N..T \tag{3.89}$$

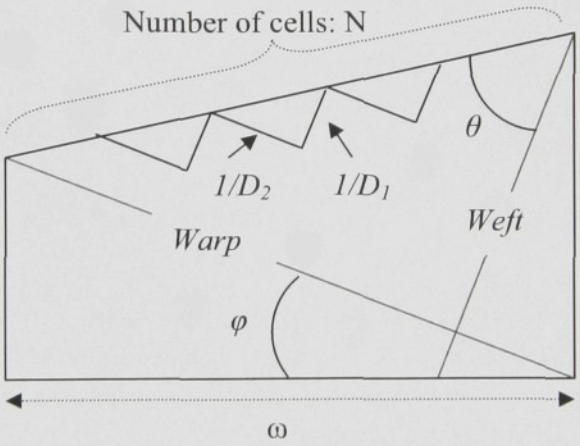

Figure 3.13- Calculating number of unit cells at certain width

4 Methods and materials

4 Methods and materials

4.1 Methods

4.1.1 Applying image processing to measure external geometry of fabric

a. 2D Fourier Transform

Suppose that the main image obtained from the fabric is included *f(x, y)* in grey level that *x, y* show the position of a pixel in row and column, respectively. Also this image is of $N \times N$ size. The discrete 2D FT of *f(x, y)* is given by equation (4.1).

$$F(u,v) = \frac{1}{N}\sum_{x=0}^{N-1}\sum_{y=0}^{N-1} f(x,y)\exp[-j2\pi(ux+vy)/N] \tag{4.1}$$

For frequency variable *u, v = 0, 1, 2..., (N-1)*. The above function is complex relation with these elements:

$$F(u,v) = R(u,v) + jI(u,v) \tag{4.2}$$

Where *R (u, v)* and *I (u, v)* are real parts and j is imaginary unit of *F (u, v)*:

$$R(u,v) = \frac{1}{N}\sum_{x=0}^{N-1}\sum_{y=0}^{N-1} f(x,y)\cos[2\pi(ux+vy)/N] \tag{4.3}$$

$$I(u,v) = \frac{1}{N}\sum_{x=0}^{N-1}\sum_{y=0}^{N-1} f(x,y)\sin[2\pi(ux+vy)/N] \tag{4.4}$$

The power spectrum *P (u, v)* of *f(x, y)* is defined as:

$$P(u,v) = \left|F(u,v)\right|^2 = R^2(u,v) + I^2(u,v) \tag{4.5}$$

To show spectrum as an intensity function in gray scale level, *P (u, v)* is converted by equation (4.6).

$$P(u,v) = \log(1 + \left|F(u,v)\right|^2) \tag{4.6}$$

As *f (x, y)* is real, 2D FT will be symmetric and the magnitude of the transform is centered in the main 2D FT image [52]. The FT domain image has 90° phase lag with the main image and is sensitive to rotation. Any angular change in the main image will be effected in the FT domain image with an angular 90° delay. It will be shown that to measure warp-weft angle during fabric deformation the present power spectrum is not suitable.

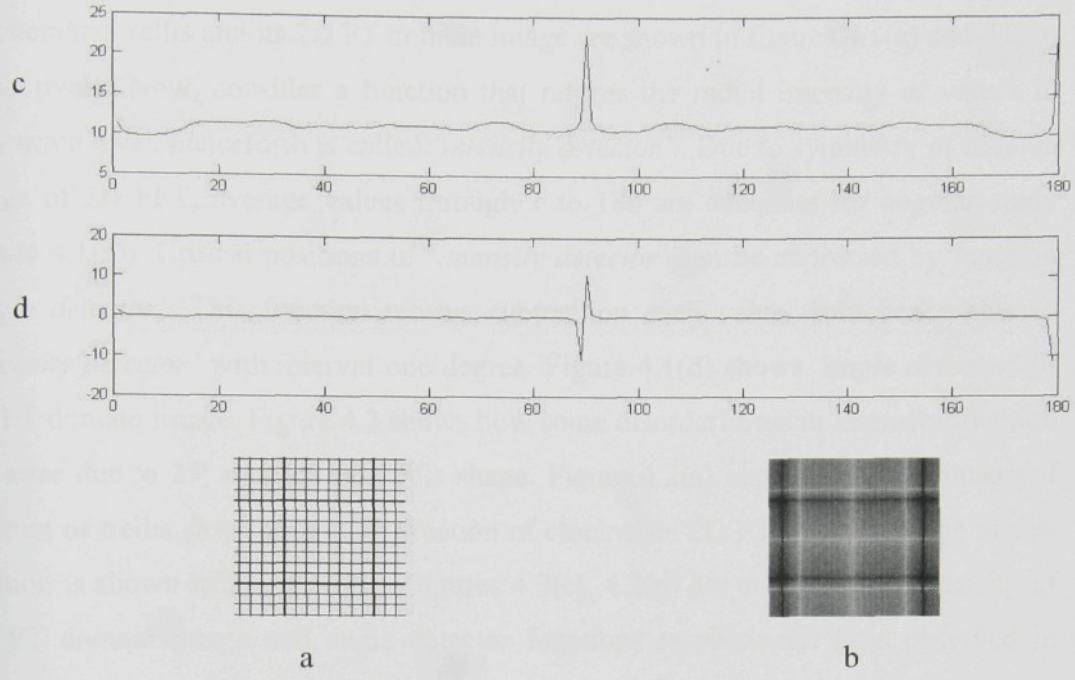

Figure 4.1- a: A schematic trellis and its b: 2D FT domain image c: intensity detector, d: angle detector

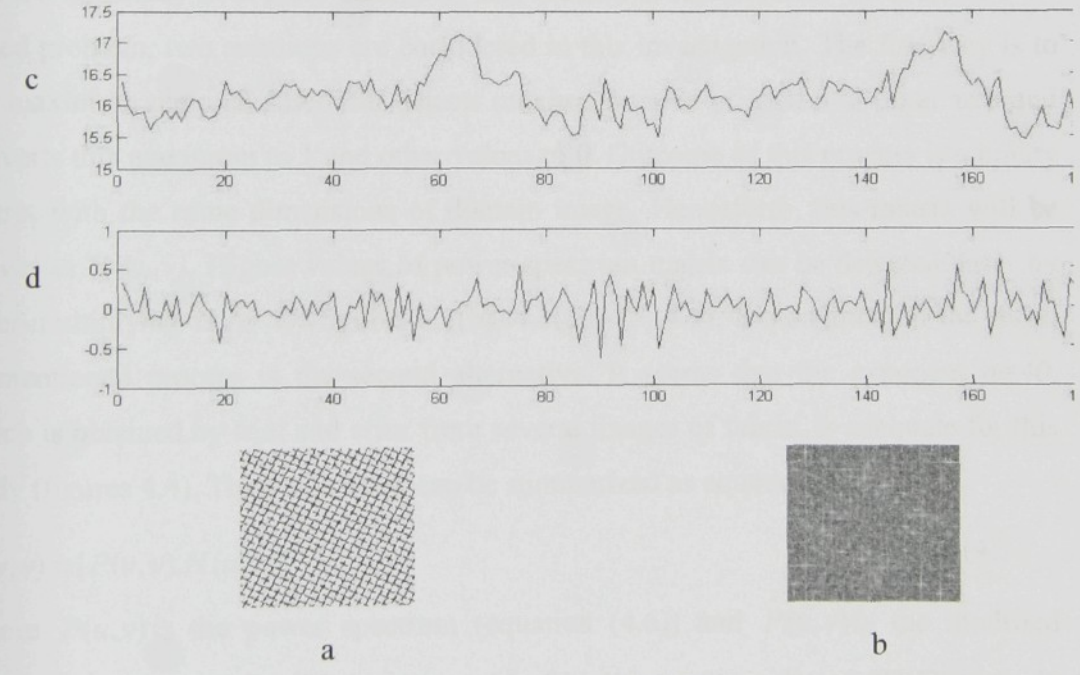

Figure 4.2- a: Trellis rotated in 25 ° (clockwise), b:2D FT domain image, c: intensity detector, d: angle detector

b. Modified Power Spectrum

A schematic trellis and its 2D FT domain image are shown in figures 4.1(a) and 4.2(b) respectively. Now, consider a function that returns the radial intensity of values in gray scale level, henceforth is called *'intensity detector'*. Due to symmetry of domain image of 2D FFT, average values through 1 to 180 are adequate for angular study (figure 4.1(c)). Critical positions of *'intensity detector'* can be expressed by function *'angle detector'*. This function returns subtraction each value from next value in *'intensity detector'* with interval one degree. Figure 4.1(d) shows *'angle detector'* of 2D FT domain image. Figure 4.2 shows how some disorderliness in intensity function are arise due to 25° rotation of trellis shape. Figure 4.2(a) shows the main image of rotation of trellis shape in 25° in direction of clockwise. 2D FT domain image of this rotation is shown in figure 42.(b). Figures 4.2(c), 4.2(d) are computed as intensity of 2D FT domain image and angle detector functions respectively. It is observed in figures 4.2(c) and 4.2(d) that disorderliness in angle detector does not show elements of rotated trellis clearly. It seems that power spectrum (4.6) is very sensitive to any rotation and study of angular change by this method is complicated. To overcome the stated problem, two solutions are considered in this investigation. The first way is to use maximum regional filter that detects maximum value of each 8×8 pixel area and converts this maximum to 1 and other values to 0. Outcome of this process is a binary matrix with the same dimensions of domain image. Henceforth, this matrix will be shown as *H (u, v)*. Higher values of power spectrum matrix can be detected easer by inner-multiplying *H (u, v)* (figures 4.3(b), 4.3(c), 4.5, 4.6). Exponentiation the result of mentioned process is the second alternative. It seems that the exponent $n=40$, which is obtained by trial and error from several images of fabric, is adequate for this study (figures 4.4). These solutions can be summarized as equation (4.7).

$$\hat{P}(u,v) = [P(u,v).H(u,v)]^n \qquad (4.7)$$

Where $P(u,v)$ is the power spectrum (equation (4.6)) and $\hat{P}(u,v)$ is the modified power spectrum and $H(u,v)$ is the matrix of high intensity point of 2D FT domain image. Effect of applying these functions on power spectrum can be observed in figures 4.3 and 4.4.

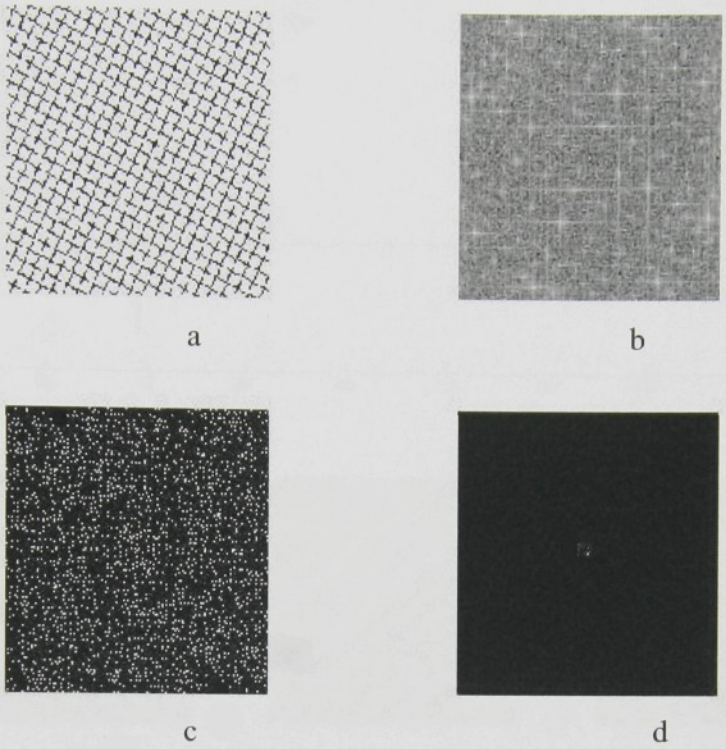

Figure 4.3- a: Rotated trellis in 25 degree (clockwise), b: domain image, c: domain image with using H (u, v), d: modified power spectrum image with 'n=40'.

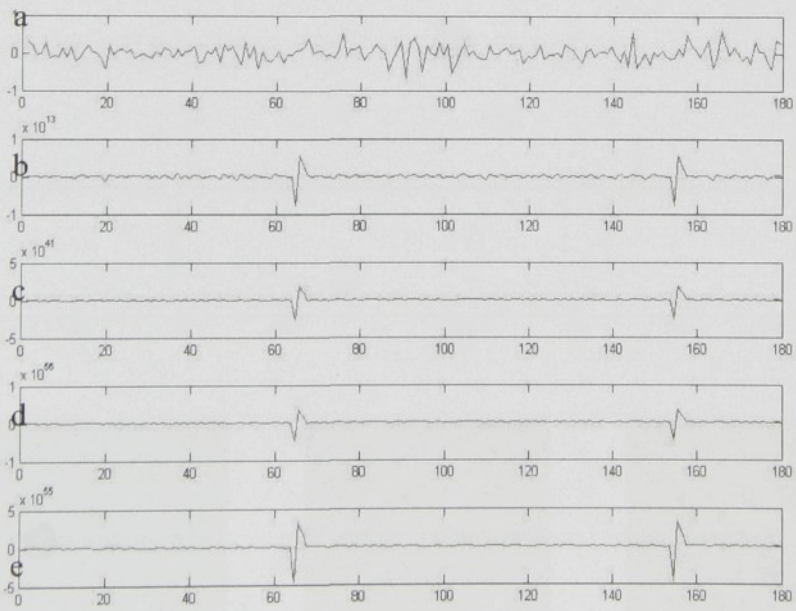

Figure 4.4- Angle detectors of a: standard power spectrum, b, c, d are modified by n= 10, 30, 40 respectively, e: modified without using H (u, v) filter.

Effects of exponent *"n"* on "angle detectors" can be observed in figure 4.4. Figure 4.4(a) displays 'angle detector' of trellis 4.3(a) with ordinary power spectrum. Figures

4.4(b), 4.4(c), 4.4(d) are connected with exponents 10, 30 and 40 of modified power spectrum respectively.

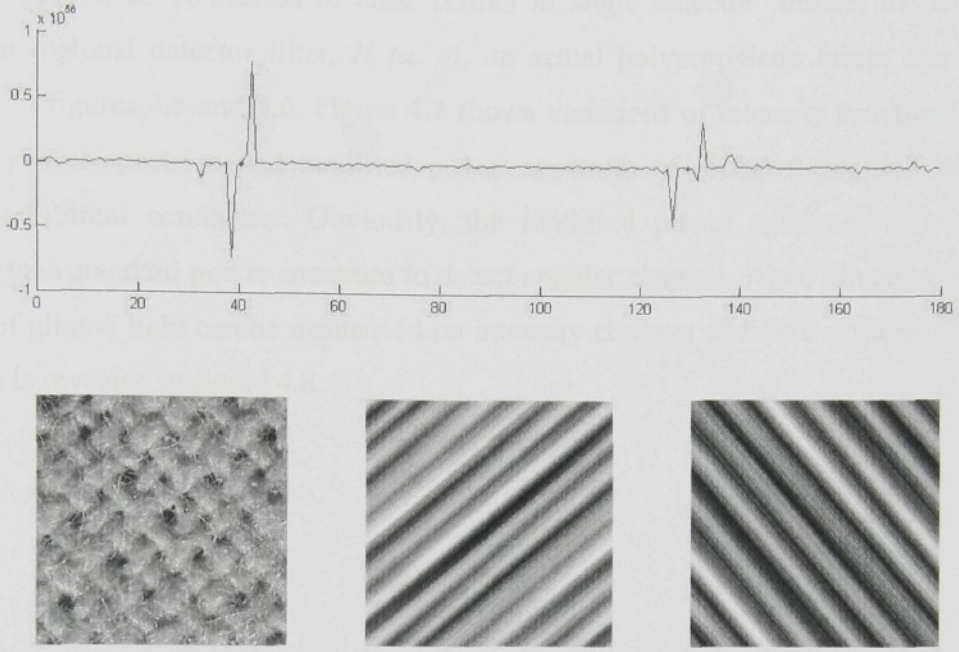

Figure 4.5- Yarn detecting without using H(u,v)

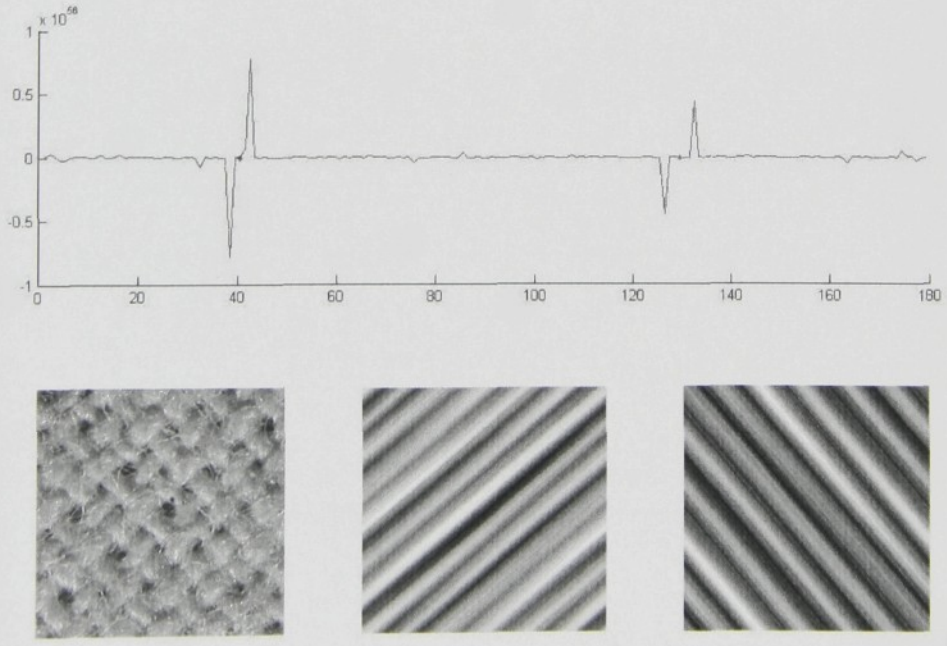

Figure 4.6- Yarn detecting with using H(u, v)

According to figure 4.4, when the exponent *'n'* is higher, the results of angle detector function are better. Also, trial and error in this work for traditional fabrics shows that exponent 40 can be conducted to clear results in angle detector. Impact of using maximum regional detector filter, *H (u, v)*, on actual polypropylene fabric can be observed in figures 4.5 and 4.6. Figure 4.7 shows variations of intensity functions in standard power spectrum and modified power spectrum of different position of a trellis at different conditions. Obviously, the modified power spectrum is more effective than standard power spectrum to detect angular changes. Also, direction and amount of glinted light can be influenced on intensity changes of fabric surface. This influence is revealed in figure 4.8.

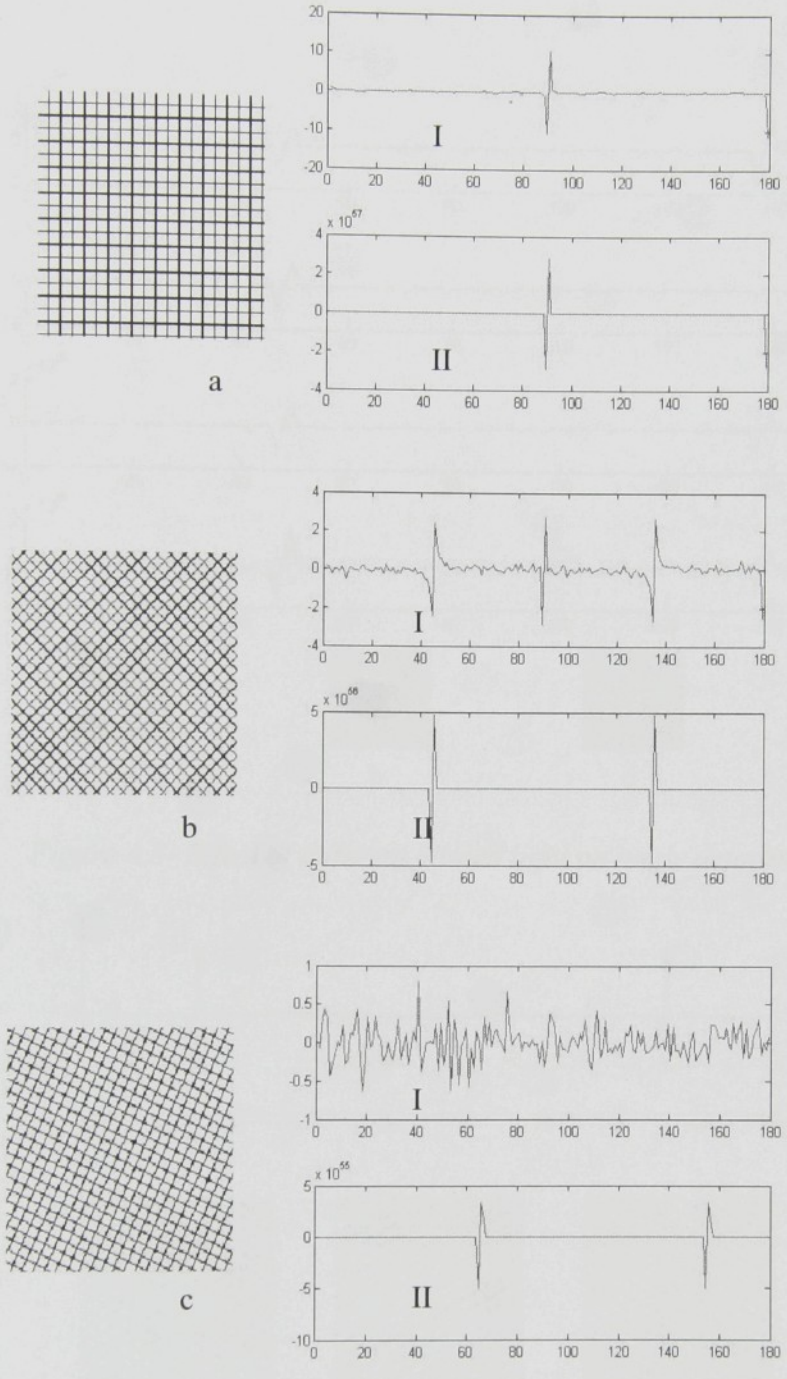

Figure 4.7- Using standard power spectrum and modified for a: trellis b: trellis in 45 degree rotation c: trellis in 25 (clockwise) rotation, I: standard, II: modified

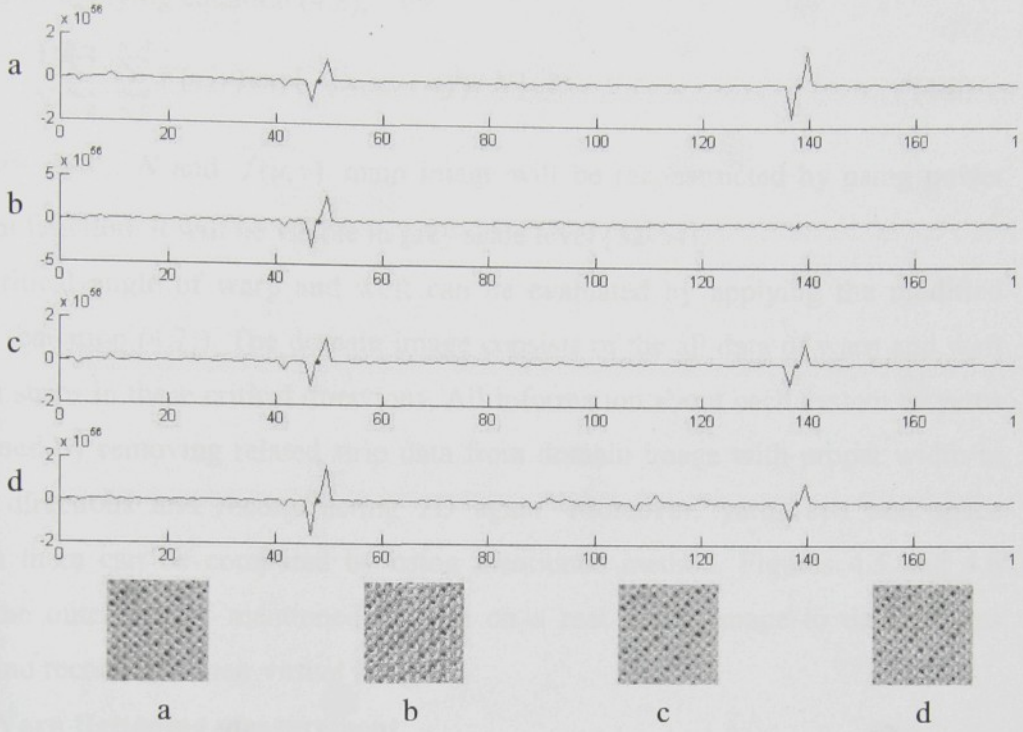

Figure 4.8- Effect of different glinted light on angle detector

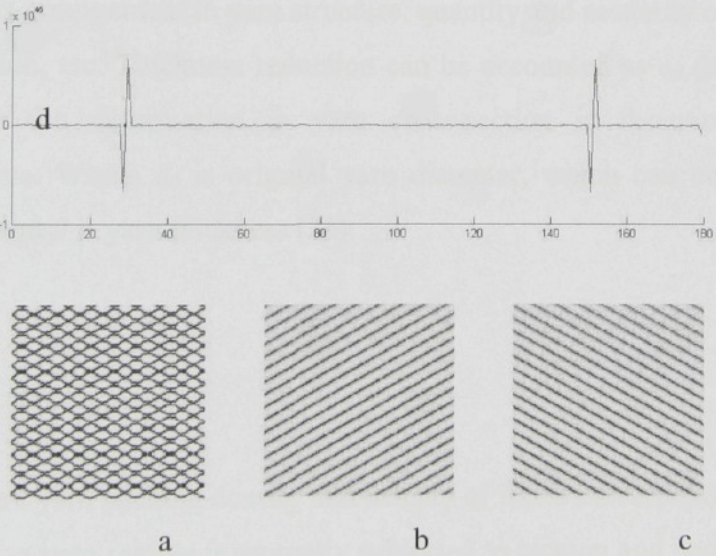

Figure 4.9- a: Schematic trellis with 30 and 150 degree liens(non-orthogonal) , b: 30° lines, c: 150° lines, d: lines angle detecting by modified spectrum

c. Detecting and measuring yarns sett

Furthermore, it is possible to remove all periodic components or part of them by using particular direction of FT domain image information and reconstructing new 2D FT with this information. Periodic components of main image will be visible by applying Inverse Fourier Transform (IFT) function on reconstructed domain image. If $\hat{F}(u,v)$

is considering as an image in the frequency domain the IFT of main image will be obtained by applying equation (4.8).

$$\hat{f}(u,v) = \frac{1}{N}\sum_{x=0}^{N-1}\sum_{y=0}^{N-1}\hat{F}(u,v)\exp[j2\pi(ux+vy)/N] \tag{4.8}$$

For $x, y = 1, 2 \ldots N$ and $\hat{f}(u,v)$ main image will be reconstructed by using power spectrum function. It will be visible in grey scale level [52-54].

Thus, critical angle of warp and weft can be evaluated by applying the modified method (equation (4.7)). The domain image consists of the all data of warp and weft yarns in strips in these critical directions. All information about each system of yarns is obtained by removing related strip data from domain image with proper width in critical directions and reconstructing 2D again. Moreover, yarns sett and space between them can be computed by using mentioned method. Figures 4.5 and 4.6 reveal the outcomes of mentioned method on a real fabric image to detect yarns angles and reconstruct their virtual images.

4.1.2 Yarn flattening measurement

As mentioned before, deformation of yarn cross-section due to compressive force is a function of fibers arrangement in yarn structure, quantity and modality of compressive force, yarn tension, etc. Thickness reduction can be accounted as e_d (equation (4.9)) which indicates the deformation in yarn cross-section in direction of exerted compressive force. Where d_0 is original yarn diameter, which can be obtained via equation (4.10) and d is yarn thickness ($2b$).

$$e_d = \frac{d - d_0}{d_0} \tag{4.9}$$

$$d_0 = \sqrt{\frac{4Tex}{10^9 \pi\mu\rho}} \tag{4.10}$$

Where μ and ρ are yarn packing density and density of fibers correspondingly.

For this purpose, a yarn sample is mutually subjected to tension and bending moment. Then, the effect of compressive forces on yarn flattening is observed by a microscope equipped with camera in different tension and angle. Figure 4.10 illustrates this concept schematically. Eventually, the thickness reduction is considered as a function of compressive force and this function is utilized to evaluate tensile properties of fabric. Appendix (E) represents the results of an investigation on flattening behavior of several yarns.

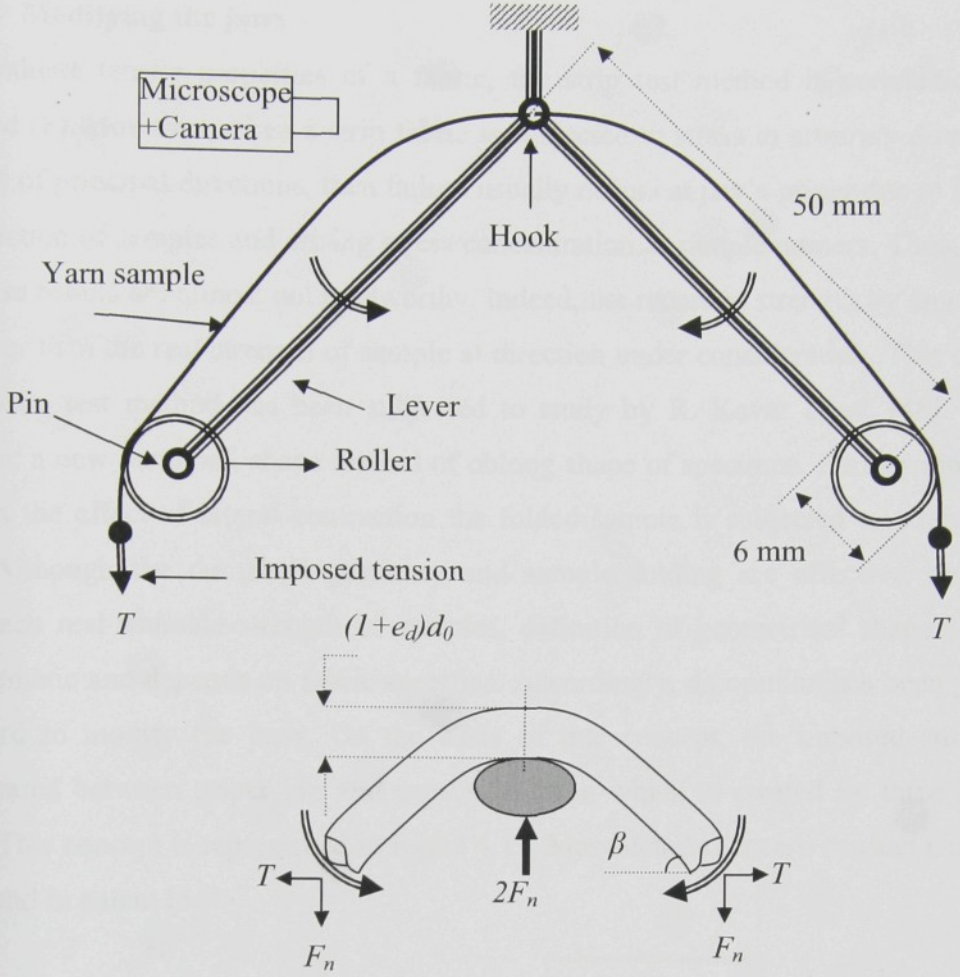

Figure 4.10- Yarn flattening measurement concept

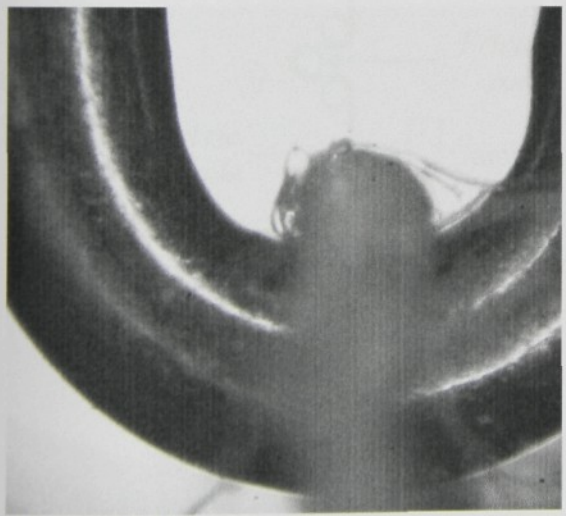

Figure 4.11- Sectional image of a cotton yarn F_n=0.98 [CN], β=30°, yarn tension =0.98 [CN]

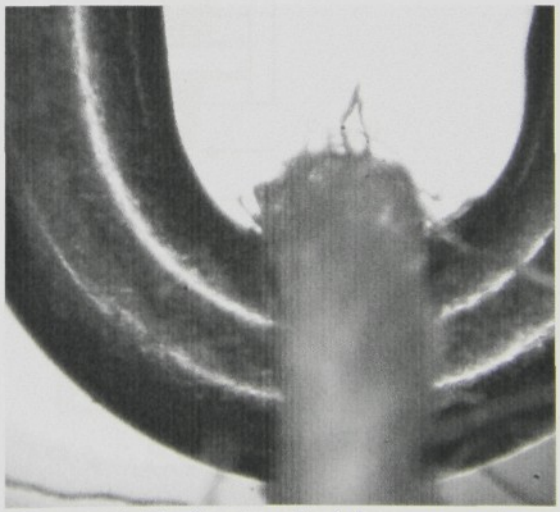

Figure 4.12- Sectional of the same point of cotton yarn in figure 4.11 at F_n=1.19[CN] β=80°, yarn tension =0.98 [CN]

4.1.3 Modifying the jaws

To evaluate tensile properties of a fabric, the strip test method is conventionally applied (F). However, when a strip fabric is subjected to stress in arbitrary direction, except of principal directions, then failure usually occurs at jaw's griper due to lateral contraction of samples and arising stress concentration at sample corners. Thus, most of these results are almost not trustworthy. Indeed, the recorded strength by apparatus is lower than the real strength of sample at direction under consideration. This defect of tensile test method has been subjected to study by R. Kovar *et al.* [48]. They suggest a new dumbbell shape instead of oblong shape of specimen. Further more, to deduct the effect of lateral contraction the folded sample is subjected to stress [48, 55]. Although the dumbbell geometry and sample folding are effective ways to approach real ultimate strength of samples, definition of geometrical shape is still problematic and depends on fabric specifics. Accordingly, an opinion has been put in forward to modify the jaws. On the basis of this concept, the imposed stress is moderated between griper nip and capstan friction which is created by three metal rods. This concept is represented in figure 4.13. More details concern capstan part can be found in patent [56].

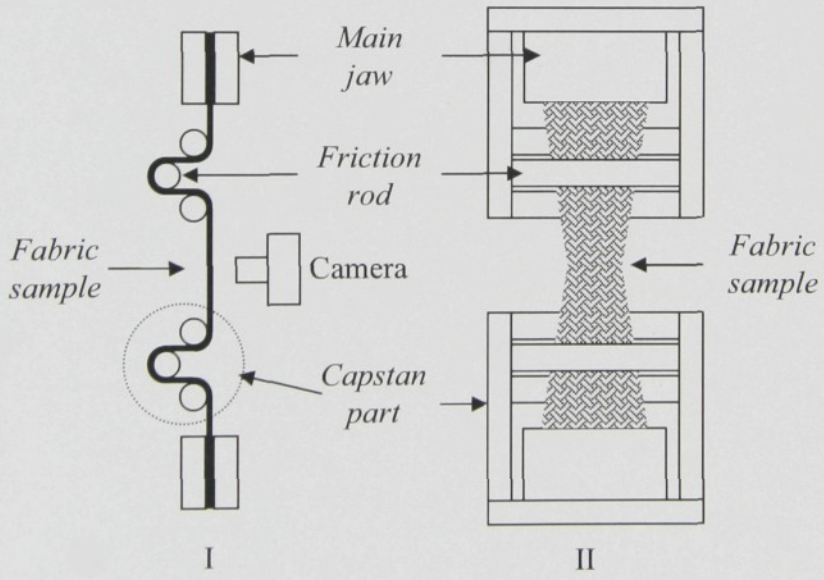

Figure 4.13- Modifying jaws to reduce concentrate stress at corners, I: Schematic cross-section of fabric path, II: Schematic modified jaws

Synchronizing strain

Obviously, the main disadvantage of this method is the strain reported by Instron is not synchronic with its force due to non-straight path of sample. Moreover, fabric

slippage would be occurred in capstan parts which affect on strain results. In order to solve stated problem, regional strain is measured by installing a camera at center of sample. The obtained images can be analyzed by image processing technique to measure exterior properties of fabric as well as regional strain. The regional strain would be synchronized with correspond force by mentioned method.

4.2 Materials

Several sets of fabrics at two level of grey and finished (washed and dyed only) have been subjected to study. Yarns of these fabrics are produced by three kinds of spinning technology. The fabric specifications are summarized in table 4.1.

Table 4.1- Specifications of fabrics under consideration

Fabric Code	Spinning Technology	Finishing Level	Yarns count/ Fiber density/ Material	Yarns sett		Yarns crimp		Yarn Packing Density**	Fabric Planar Weight
		Unit	[tex] gr/cm^3 [-]	[ends/m]	[picks/m]	[%]		[-]	[gr/m^2]
		Notation	tex_1, tex_2 ρ -	D_1	D_2	C_1	C_2	μ	W_0
R10G	Ring	Grey	10, 10 1.52 100% Cotton	4850	3090	8.2	6	0.541	88
R10F	Ring	Finished		5100	3010	5	11	0.541	84
N10G	Nova.*	Grey		4840	3110	8.6	5.9	0.547	84
N10F	Nova.	Finished		5090	3020	4.7	11.2	0.547	80
R20G	Ring	Grey	20, 20 1.52 100% Cotton	2580	2330	4.4	10.8	0.482	104
R20F	Ring	Finished		2760	2330	3.1	18.2	0.482	103
O20G	OE	Grey		2490	2430	7.4	8.7	0.438	103
O20F	OE	Finished		2730	2310	2.4	19.2	0.438	104
N20G	Nova.	Grey		2560	2370	5.6	9.5	0.462	105
N20F	Nova.	Finished		2770	2310	3	19.5	0.462	105
R30G	Ring	Grey	29.5, 29.5 1.52 100% Cotton	2360	2120	8.2	8	0.443	142
R30F	Ring	Finished		2570	2140	9.3	11.7	0.443	144
O30G	OE	Grey		2370	2060	8.2	7.3	0.404	148
O30F	OE	Finished		2450	2030	10.3	10.9	0.404	144
N30G	Nova.	Grey		2410	1960	7.6	7.4	0.441	141
N30F	Nova.	Finished		2480	2000	8.9	11.2	0.441	140
C14	Ring	Grey	14.48, 14.48 1.52 100% Cotton	3720	3460	6.2	6.9	0.512	115
P30	Ring	Grey	29.23, 29.23/ 0.91 100% Polypropylene	2350	2100	19.0	9.2	0.517	155

* *Novaspin is a spinning system technology which developed at VUTS Liberec.*
** *Yarns packing density are calculated on the basis of Neckar equation [51].*

An exhaustive Ph.D. study had been performed to analyze fabric cross-section by J. Drasarova [9]. In this study, geometry of fabrics R10G, R10F, N10G, N10F, R20G, R20F, O20G, O20F, N20G, N20F, R30G, R30F, O30G, O30F, N30G and N30F in warp and weft directions had been investigated. Yarns cross-section dimensions, inflection angles and relative high of yarns wave are measured by aide of LUCIA

program. These results are represented in table 4.2. We will compare some outcomes of our models with measured values.

Table 4.2- Internal geometry of fabrics in warp and weft directions investigated by J. Drasarova[9]

Fabric Code	Yarn dimension in cross-section								Inflection angle	
	[m^{-6}]		[m^{-6}]		[m^{-6}]		[m^{-6}]		[Degree]	
	a_1	S.D	a_2	S.D	b_1	S.D	b_2	S.D	warp	Weft
R10G	62.36	1.82	69.60	2.88	49.83	1.63	52.17	1.63	28	19
R10F	56.76	1.74	67.46	2.78	46.83	1.35	49.07	1.68	20	30
N10G	65.19	1.68	64.94	2.30	49.85	1.21	47.59	1.58	24	24
N10F	58.46	1.54	69.71	3.27	51.29	1.28	50.71	1.71	22	33
R20G	85.80	3.93	95.68	2.84	73.45	2.78	72.85	1.65	25	21
R20F	80.01	3.14	119.46	4.70	76.20	3.31	61.88	3.11	13	34
O20G	87.31	3.52	91.80	3.46	71.84	3.36	76.67	3.01	26	20
O20F	84.18	3.69	103.25	5.30	71.03	2.25	60.78	3.25	12	31
N20G	91.50	4.43	100.27	2.93	73.73	2.94	77.77	1.68	26	21
N20F	83.89	3.03	116.54	7.71	68.77	1.96	64.03	4.10	12	32
R30G	138.10	4.73	135.82	5.67	106.97	3.65	101.95	4.25	37	28
R30F	118.40	4.10	134.30	5.29	97.19	3.48	90.15	2.59	30	28
O30G	159.69	6.18	147.46	5.74	100.84	4.73	92.13	3.41	34	22
O30F	142.63	5.35	154.01	7.37	85.58	2.88	94.09	4.70	31	19
N30G	144.15	7.02	146.41	5.17	92.10	3.35	97.62	4.09	27	27
N30F	136.07	4.76	151.46	7.97	88.11	2.72	85.56	2.50	26	23

5 Results and discussion

5 Results and discussion

5.1 Geometry of plain weave fabric before deformation

To verify fabric geometry model a set of cotton fabric in different specifications and yarns spinning systems are considered. For this purpose, internal geometry of fabrics R10G, R10F, N10G, N10F, R20G, R20F, O20G, O20F, N20G, N20F, R30G, R30F, O30G, O30F, N30G and N30F in warp and weft directions before deformation are estimated by proposed method in section **3.1.1**. For each fabric all series of values which satisfied the equilibriums were collected then a series of results which conducts to minimum packing density was considered as final results. On the basis of this model, the elliptical shape is assumed for yarn cross-section. Accordingly, the major and minor radiuses are compared with measured values. Figure 5.1 shows the predicted warp and weft yarns cross-section dimensions in comparison with measured values by J. Drasarova [9]. Despite of fabrics variety bigness, it is observed that this model is responsible for all kinds of fabrics as well as finished and grey.

Relation between measured and predicted values in dimension is represented in figure 5.2. The correlation coefficient among predicted and measured values of yarn dimension in warp and weft direction is about 0.84 which is reasonable for this set of fabrics.

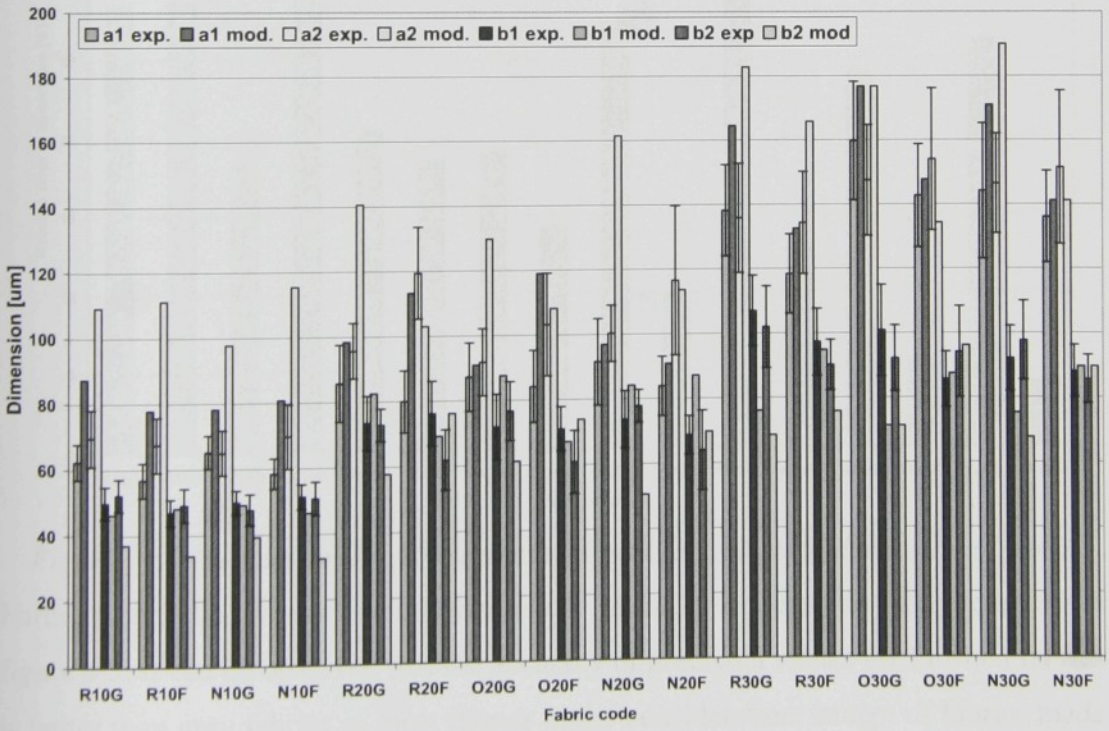

Figure 5.1- Dimensions of warp & weft yarns cross-section: measured & estimated

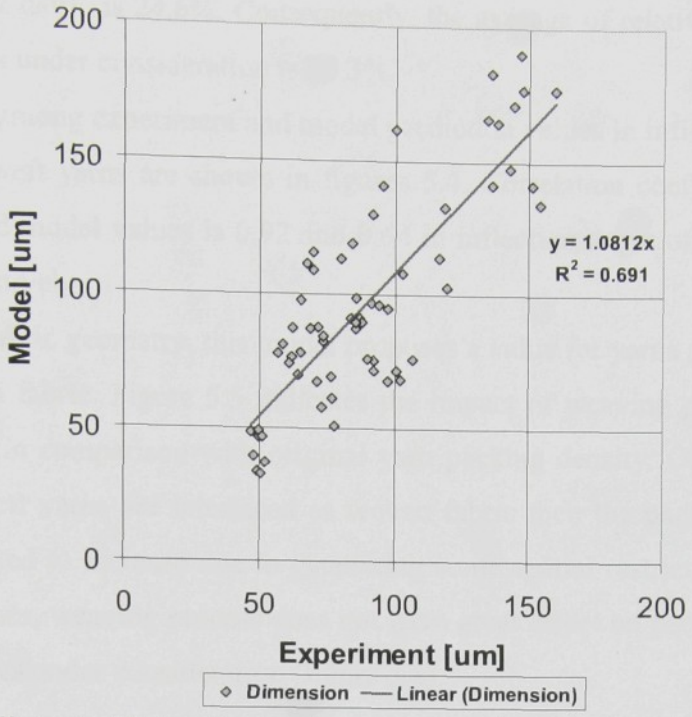

Figure 5.2- Coefficient of determination between experiment and model in dimension of yarns

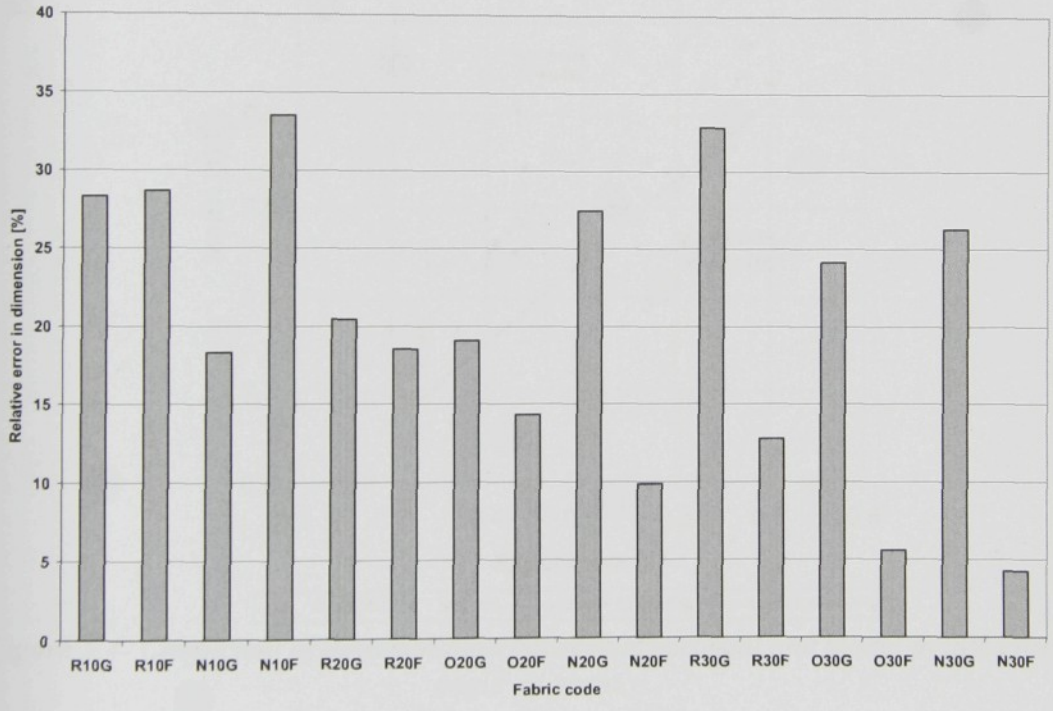

Figure 5.3- Average errors between experiment and model in dimension of yarns

Furthermore, the average of relative errors in yarns dimensions is represented in figure 5.3. It can be observed that the accuracy of predicted values for finished fabrics is better than grey fabrics in most fabrics under consideration, except of fabrics made by 10 *tex*. Indeed the average of relative errors for finished fabric is 15.9% while this

quantity for grey fabric is 24.6%. Consequently, the average of relative errors of this model for fabrics under consideration is 20.3%.

The association among experiment and model prediction values in inflection angle for both warp and weft yarns are shown in figures 5.4. Correlation coefficient between experimental and model values is 0.92 and 0.64 in inflection angle of warp and weft directions respectively.

On the base of fabric geometry, this model proposes a value for yarns packing density inside of relaxed fabric. Figure 5.5 indicates the impact of weaving process on yarn packing density in comparison with original yarn packing density. Obviously, when the warp and weft yarns are interlaced as woven fabric then the packing density of yarns are subjected to increase due to generating some spatial restriction. According to estimated values, weaving process does not have great effect on packing density in most of the fabrics under consideration (figure 5.5).

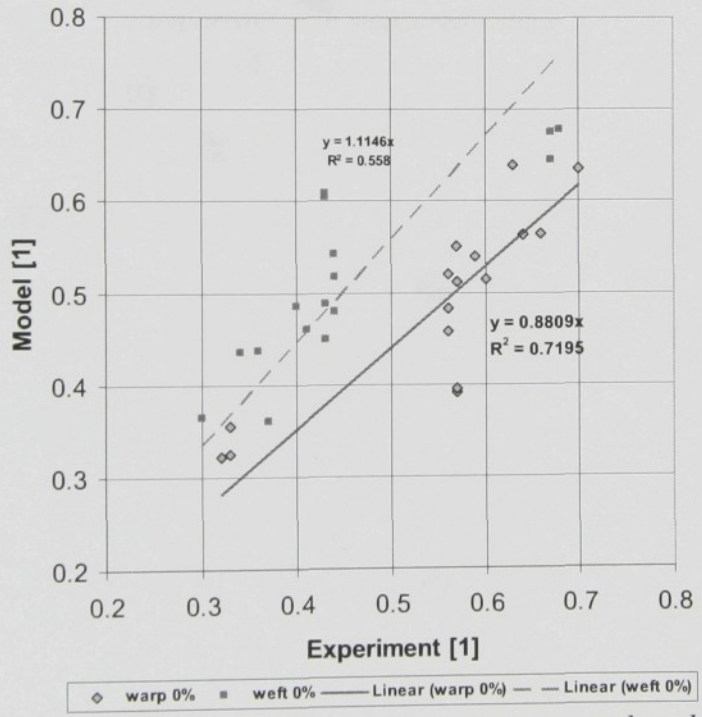

Figure 5.4- Coefficient of determination between experiment and model in inflection angle of yarns

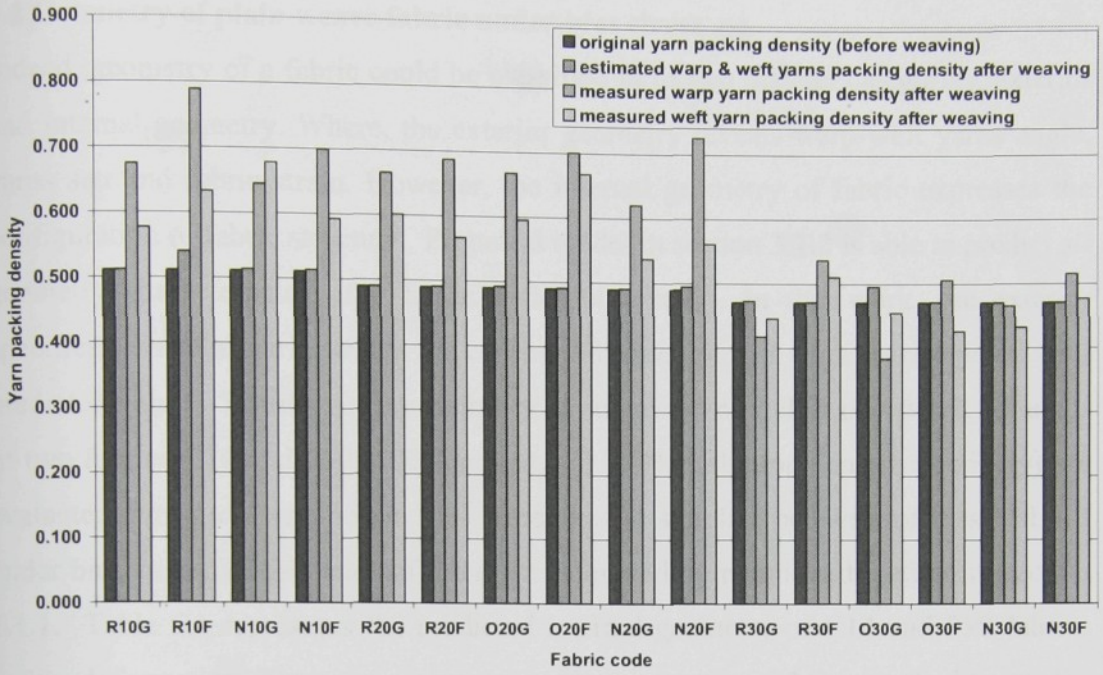

Figure 5.5- Estimated yarn packing density before and after weaving process in comparison with measured values

5.2 Geometry of plain weave fabric under bias stress

Indeed, geometry of a fabric could be classified in to two distinct categories; exterior and internal geometry. Where, the exterior geometry reveals warp-weft yarns angle, yarns sett and fabric strain. However, the internal geometry of fabric expresses the configuration of fabric structure. Proposed model in section **3.1.2** is able to predict all geometry characteristics of a fabric under bias stress. In this work, the exterior specifications of a fabric, which are obtained from empirical work, is compared with predicted values. To survey responsibility of suggested model in part **3.1.2**, behavior of two fabrics C14 and P30 (100% cotton and 100% polypropylene respectively) are evaluated during deformation in bias direction. To simulate behavior of these fabrics under bias stress, initial states of them are estimated by mentioned method in section **3.1.1.** Table 5.1 represents the predicted internal geometry of C14 and P30 fabrics before deformation. Then, the expressed method in section **3.1.2** is applied to predict fabrics geometry under bias stress by using initial data of these fabrics as input.

Table 5.1- Predicted values of internal geometry of P30 and C14 fabric

Internal geometry parameter	Unit	Polypropylene fabric Fabric code: P30		Cotton Fabric Fabric code: C14	
		Warp	Weft	Warp	weft
a_1, a_2	*cm*	0.0161	0.0141	0.0114	0.0106
b_1, b_2	*cm*	0.01103	0.0126	0.0049	0.0052
γ_1, γ_2	*degree*	62.72	71.56	75.42	79.89
γ_1', γ_2'	*degree*	53.23	69.63	61.78	71.6
μ_1, μ_2	-	0.5759	0.5759	0.5477	0.5477
L_{1L}, L_{2L}	*cm*	0.0022	-8E-6	0.0020	0.0017
k_1	-	1.46		2.3477	
k_2	-	1.14		1.08	
d_f	*cm*	0.0098		0.0030	
f_1	-	8.6E-5		-2E-7	
f_2	-	3.1E-8		-6.3E-8	
f_3	-	5.1E-5		9.7E-5	
f_4	-	0		0	

In the other hand, the exterior geometry of these fabrics under bias stress is studied by image analysis techniques (explained in section **4.1.1**). For this purpose, the specimens are prepared in oblong shape with aspect ratio 10 in three different widths and length namely; 10×100 mm, 15×150 mm and 20×200 mm in direction of 45 degree from warp and weft (bias direction). The numbers of trials for each fabric in each width were three. Simultaneously, to record the external features of specimens, a

microscope equipped camera is adjusted in center of samples. The exterior specifications of fabrics, which are obtained by this manner, will be compared with predicted values in following.

Polypropylene fabric:

On the basis of initial data of polypropylene fabric (code: P30), the linear part of weft yarns of negligible (table 5.1). Therefore, this fabric can be classified in situation 2 of table 3.1. Empirical evaluations of warp-weft yarns angle are judged against predicted values in figure 5.6. Meanwhile, the values of Weissenberg's model [18, 19] are revealed in this figure. As it is observed in figure 5.6 there is a critical angle (about 48 degree in 38% strain) which the ratio of angle variations after this angle reduces significantly. This critical angle, so called locking angle or jamming angle, is subjected to study by many researchers [20, 25-26]. Actually, shear deformation of fabric is limited by locking angle. At this point, warp-weft yarns rotation would be limited by lateral contacts of yarns. Anyway, proposed model indicates this critical angel. The relative errors between predicted and measured values in warp-weft angle are demonstrated in figure 5.7. Average of relative errors in predicting warp-weft angle is 3.6% for this fabric which is reasonable.

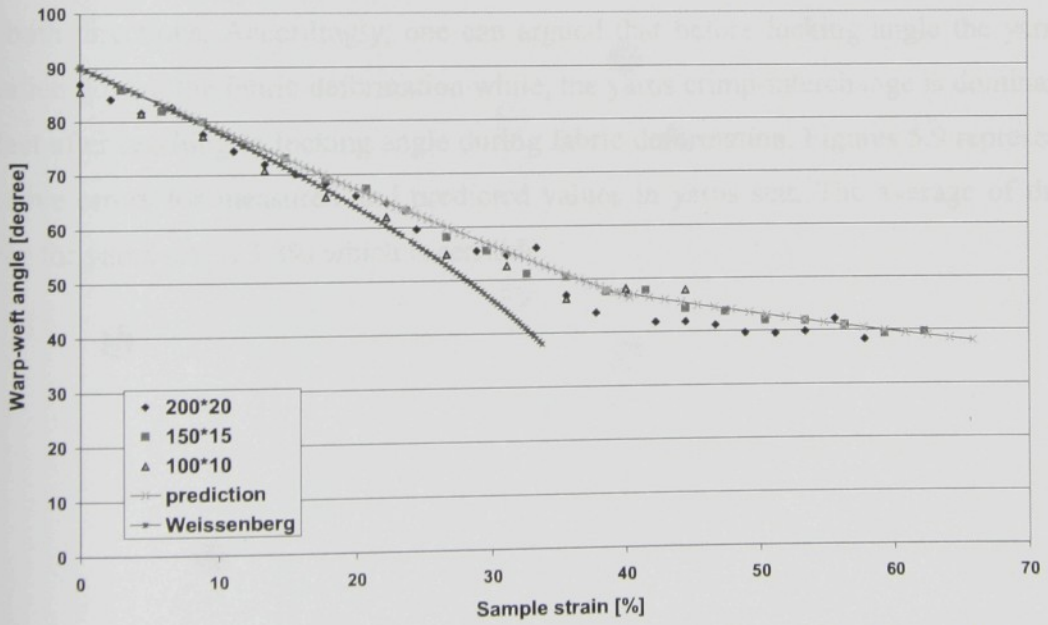

Figure 5.6- Measured and predicted values of warp-weft angle for fabric (P30) during bias deformation

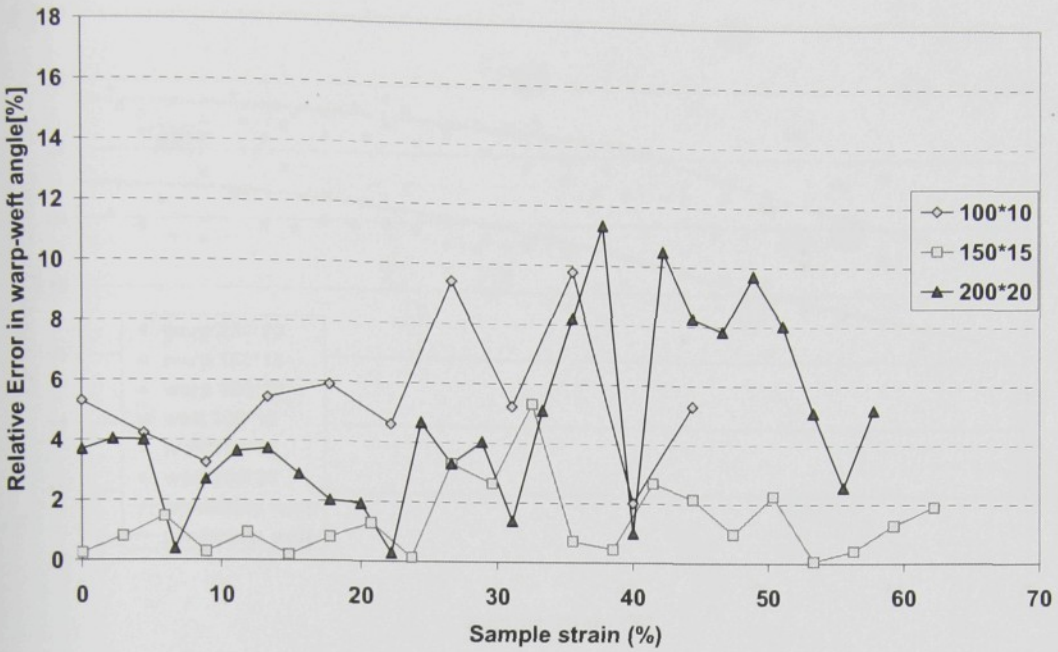

Figure 5.7- Relative error between measured and predicted values in warp-weft angle for fabric (P30)

Moreover, variations in yarn sett can be investigated by applying image analysis technique on exterior features of a fabric under bias stress. Figure 5.8 shows the predicted and measured values of shear yarn setts in warp and weft yarns. Unlike shear angle behavior, slope of reduction in yarns sett after locking angle are increased in both directions. Accordingly, one can argued that before locking angle the yarns rotation govern the fabric deformation while, the yarns crimp-interchange is dominant effect after reaching to locking angle during fabric deformation. Figures 5.9 represent relative errors for measured and predicted values in yarns sett. The average of this error for yarns sett is 3.8% which is sensible.

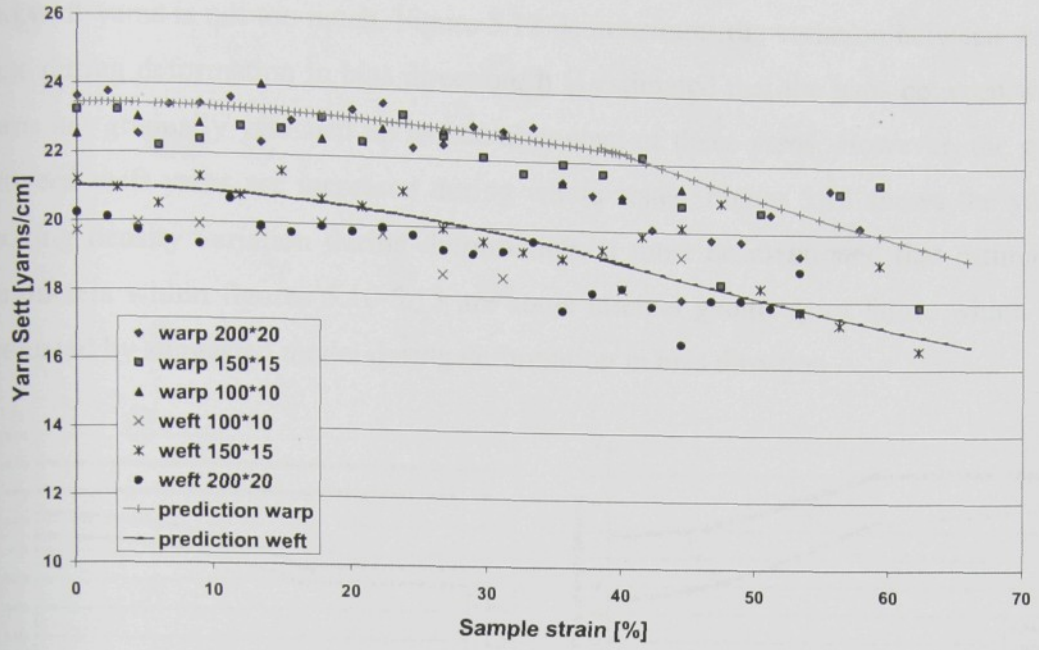

Figure 5.8- Yarns sett comparison between measured and predicted values (fabric P30)

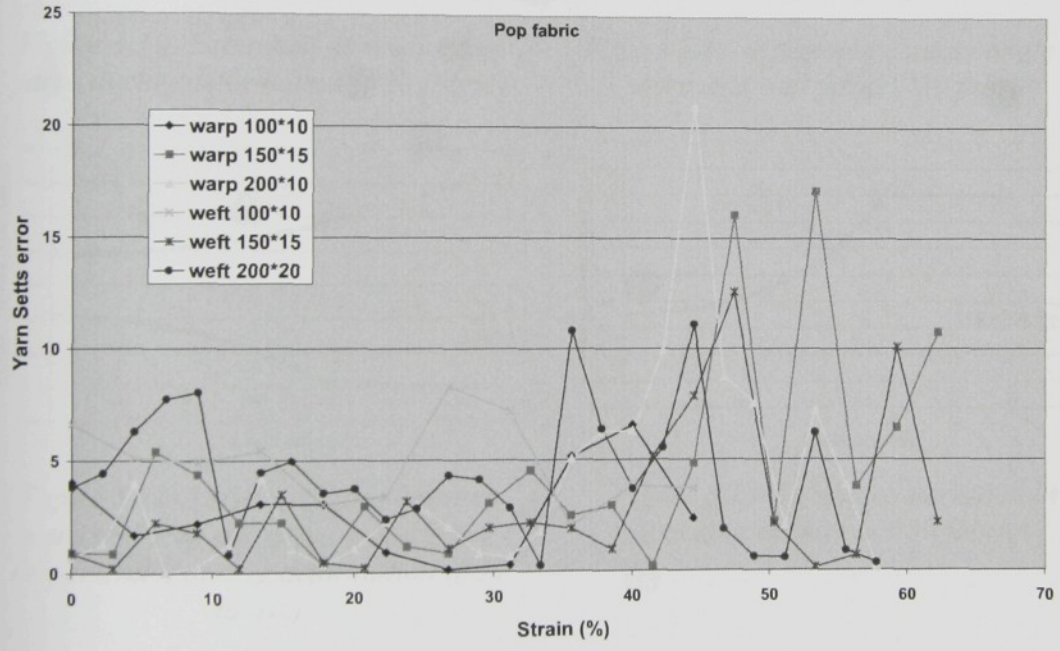

Figure 5.9- Relative error between measured and predicted values in yarns sett for fabric (P30)

Figures 5.10 indicates the estimated values of warp and weft yarns dimensions during deformation. On the basis of this evaluation, major radius of yarns is constant during shear deformation however; minor radius of these yarns is subjected to reduction up to maximum packing density. Figure 5.11 reveals the variation in contact angle of yarns. It seems that after locking angle the increasing in contact angles for both warp

and weft yarns is not too much. Figure 5.12 demonstrates the variation between yarns gaps during deformation in bias direction. It is estimated that the gaps between warp yarns are gradually vanished up to lateral contact of these yarns. However, the gaps between weft yarns are increased during whole states. Figure 5.13 shows the yarns packing density variation during deformation. It must be mentioned that estimated parameters within figures 5.10-5.13 are some internal geometry of fabric which are evaluated by suggested model during deformation in bias direction.

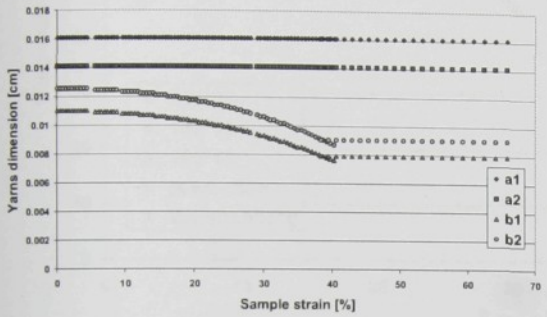

Figure 5.10- Estimated dimensions of yarns during deformation (P30 fabric)

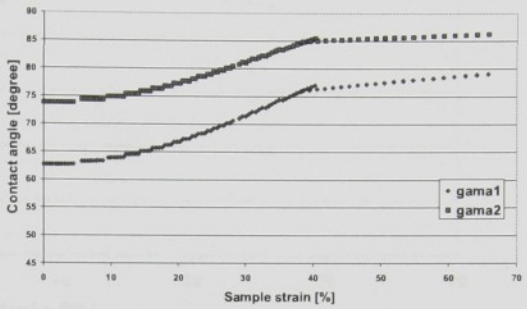

Figure 5.11- Estimated contact angle of warp and weft yarns(P30 fabric)

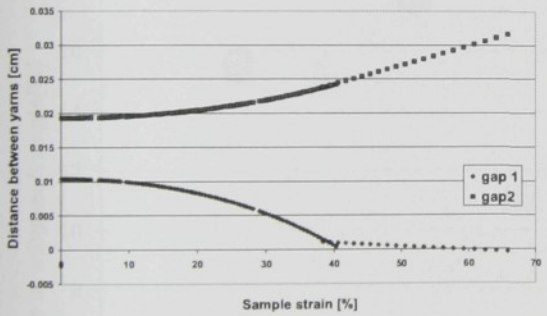

Figure 5.12- Estimated gaps between warp and weft yarns(gap1 and gap 2 respectively) during deformation (P30 fabric)

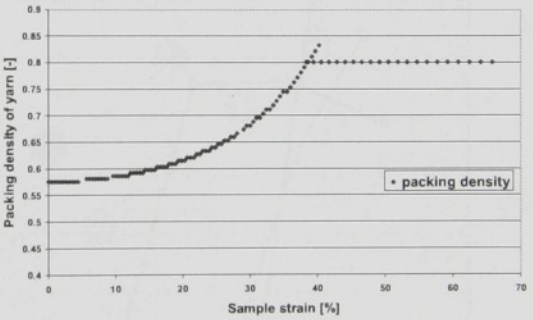

Figure 5.13- Predicted variation in packing density in P30 fabric

Cotton fabric (C14)

Estimated initial state of cotton fabric (table 5.1) indicates that there are linear parts in warp and weft yarns. According to table 3.1 this fabric can be classified in situation 1. Figure 5.14 discloses the variations of warp-weft angle experimentally and theoretically when the fabric is subjected to bias stress. Similar to P30 fabric, locking angle can be observed in this fabric as well as. The estimated locking angle for this fabric is about 58 degree, but the measured locking angel is about 48 degree.

Nevertheless, the average of relative errors for estimated and measured values is 3.9% (figure 5.15).

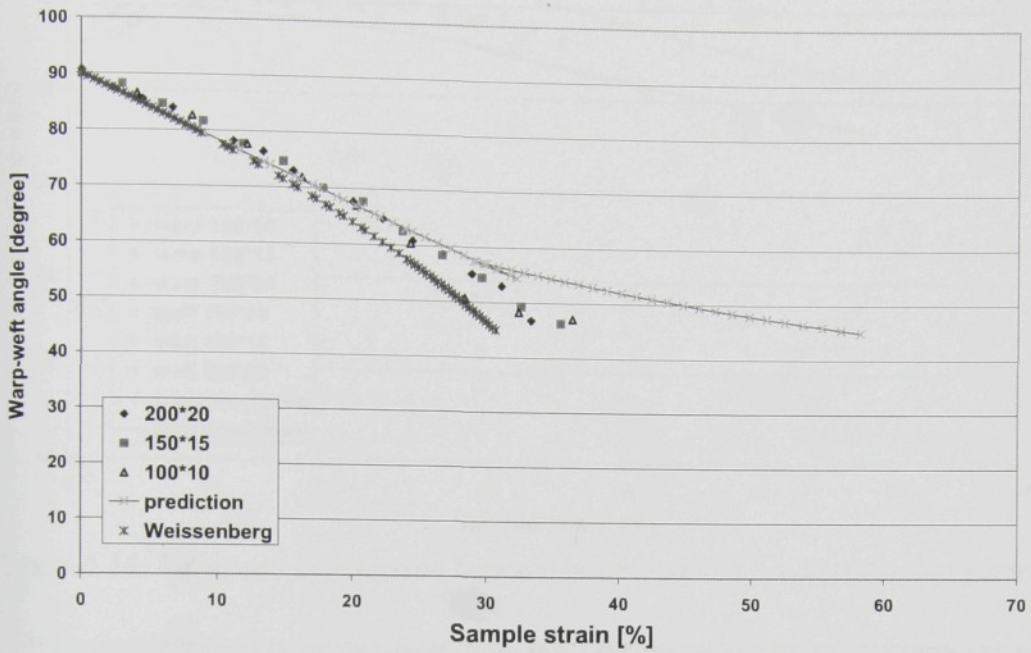

Figure 5.14- Measured and predicted values of warp-weft angle for fabric (C14) during bias deformation

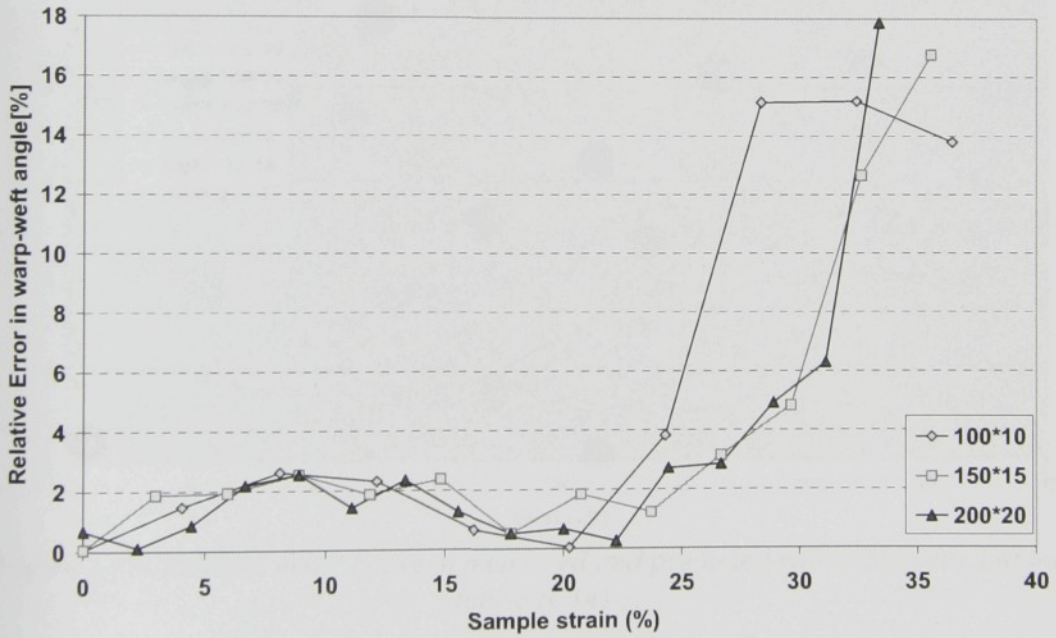

Figure 5.15- Relative error between measured and predicted values in warp-weft angle for fabric (C14)

Estimated and measured values of yarns sett is summarized in figure 5.16. According to mentioned arguments it is seems that before locking angle the yarns rotation govern the fabric deformation but, the yarns crimp-interchange is dominant effect after reaching to locking angle during fabric deformation. The average of relative errors in estimated and measured yarns sett is 2.7% (figure 5.17).

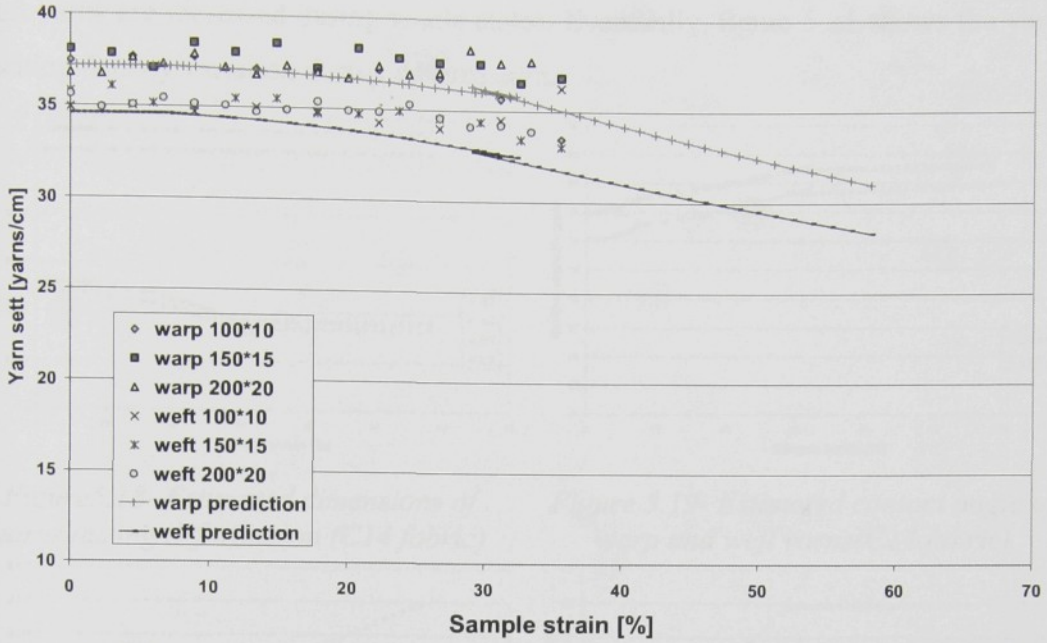

Figure 5.16- Yarns sett comparison between measured and predicted values (fabric C14)

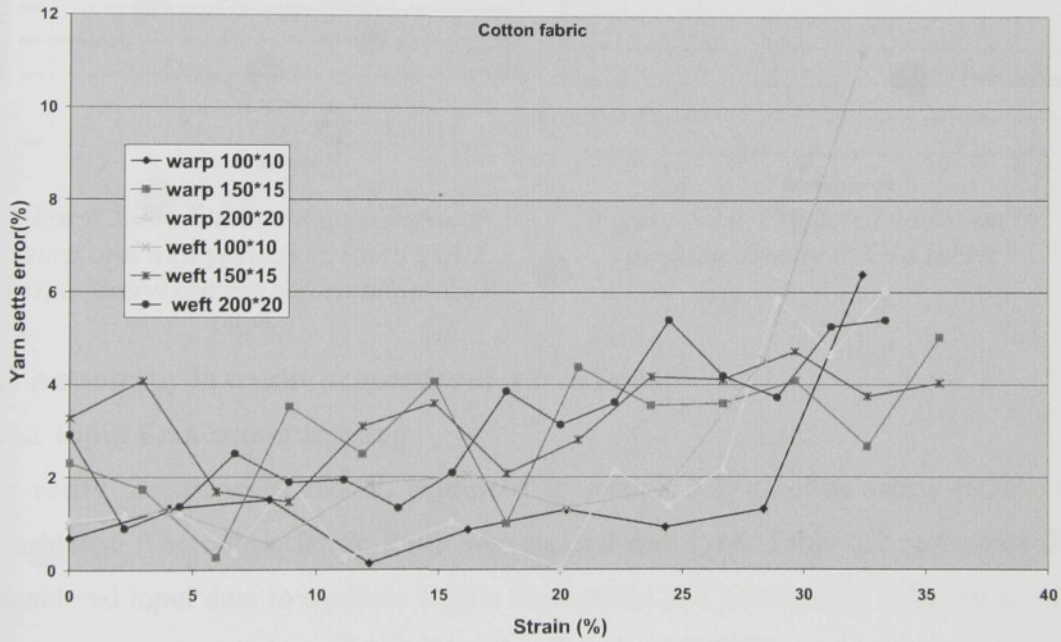

Figure 5.17- Relative error between measured and predicted values in yarns sett for fabric (C14)

Figures 5.18 indicates the estimated values of warp and weft yarns dimensions during deformation of C14 fabric. Like fabric P30, major radius of yarns is constant during shear deformation however; minor radius of these yarns is subjected to reduction up to maximum packing density. Figure 5.19 reveals the variation in contact angle of yarns as well as. Moreover, figure 5.20 illustrates the variation between yarns gaps during deformation in bias direction. It is estimated that the gaps between warp yarns are gradually vanished up to lateral contact of these yarns. However, the gaps between

weft yarns are increased during whole states. Eventually, figure 5.21 shows the yarns packing density variation during deformation.

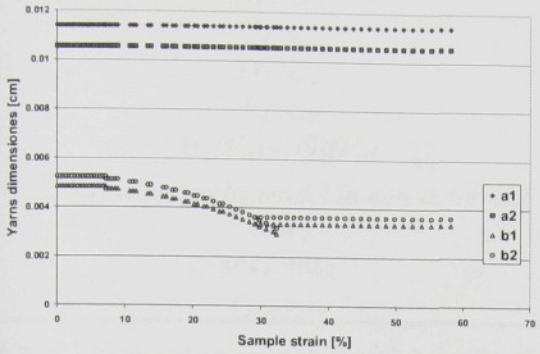

Figure5.18- Estimated dimensions of yarns during deformation (C14 fabric)

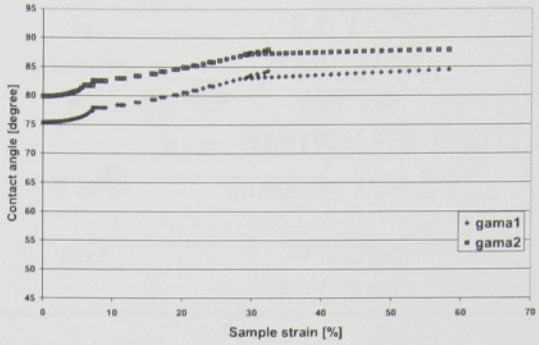

Figure 5.19- Estimated contact angle of warp and weft yarns(C14 fabric)

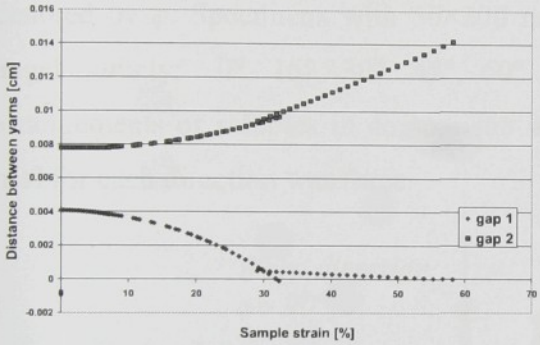

Figure 5.20- Estimated gaps between warp and weft yarns(gap1 and gap 2 respectively) during deformation (C14 fabric)

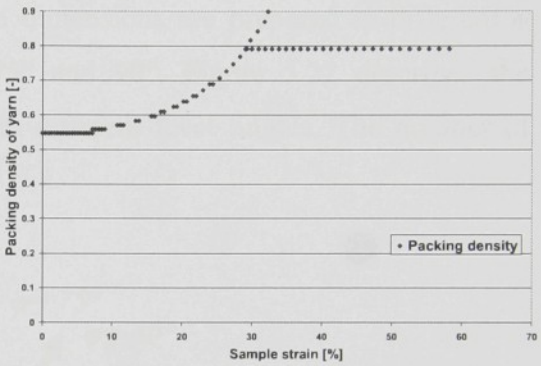

Figure 5.21- Predicted variation in packing density in C14 fabric

5.3 Anisotropy in tensile properties of woven fabric

5.3.1 Input data and estimating

To verify the proposed model, expressed in section **3.2**, a cotton fabric (R30F) is considered. The cotton fabric R30F was resized and dyed. Table 5.2 represents the considered input data to evaluate tensile force strain and geometrical behavior of this fabric. It must be mentioned that flattening function ($G(F_n)$) is obtained by empirical work performed on 30 tex cotton yarn expressed in appendix (E). Also, it is deemed that this function is unique for warp and weft. The yarns stiffness (S_1, $S2$) can be estimated by solving the system of equations in non-deformed fabric condition.

Table 5.2- Input data for fabric R30F

Parameter	Unit	Value
$\mu_1 = \mu_2$	-	0.35
C_1, C_2	%	9.3, 11.7
D_1, D_2	yarns/m	2540, 2140
E_1, E_2	N	100, 70
$G_1(F_n) = G_2(F_n)$	-	$e_d = -0.0815\ln(F_n) - 0.5712$
S_1, S_2[evaluated by model in non-deformed state]	$N.m^2$	2.09E-9 , 1.34 E-9
tex_1, tex_2	tex	29.5, 29.5
$\varepsilon_{y1u}, \varepsilon_{y2u}$	-	0.05, 0.065

5.3.2 Preparing samples and installing apparatuses

Henceforth, the angle of force axis and weft yarns would be called force angle and denoted by φ. Specimens with 50×200 mm dimensions are prepared in different φ angel namely; 0°, 15°, 30°, 45°, 60°, 75° and 90°. Figure 5.22 describes the arrangements of samples in comparison with different force angles. The number of trial for each direction was three.

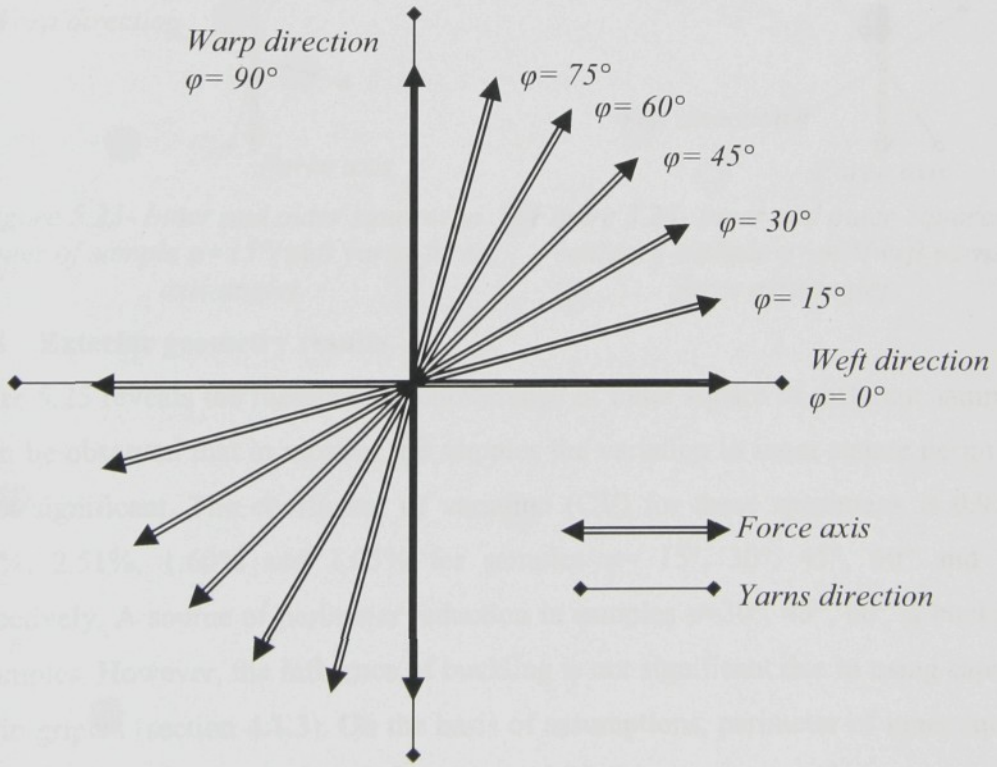

Figure 5.22- Sample arrangement in comparison with force axis

To evaluate exterior geometry of fabrics, two squares are drawn in center of each sample. The dimension of first square was 20×20 mm in parallel to sample edges, hereafter so called inner square. Second square was depicted in parallel with warp and

weft yarns directions and out of the first one, so it is called outer square. Figures 5.23 and 5.24 indicate these squares for samples with φ=15° and φ=60° typically.

Instron 4411 with testing speed 100 [mm/min] was employed for measuring tensile force. The jaws are modified by mentioned method in section **4.1.3**. To synchronize the strain with recorded force and measuring exterior deformation of sample a camera is installed and focused in center of sample.

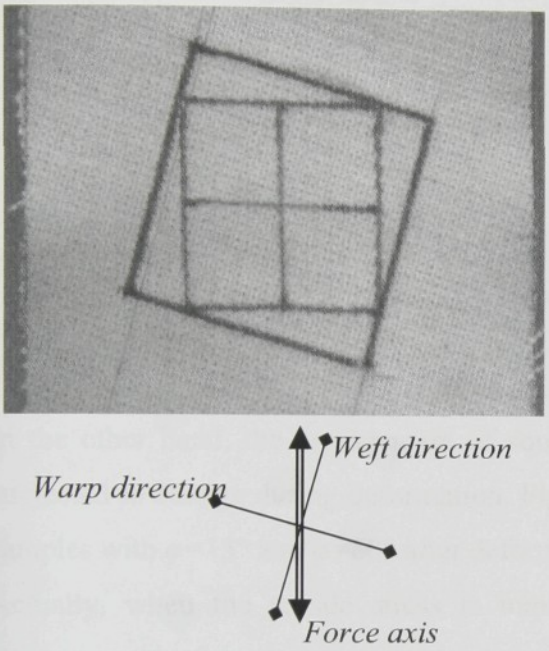

Figure 5.23- Inner and outer squares in center of sample φ=15°(weft yarns-force axis angle)

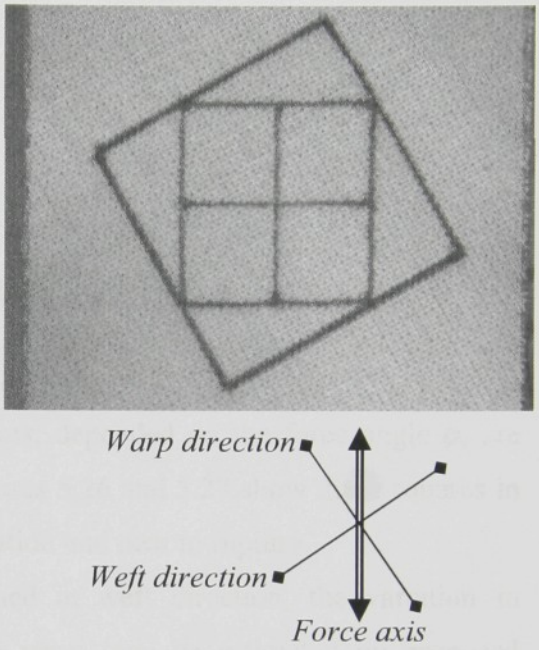

Figure 5.24- Inner and outer Squares in center of sample φ=60°(weft yarns-force axis angle)

5.3.3 Exterior geometry results

Figure 5.25 reveals the measured circumference of inner square of different samples. It can be observed that in most of the samples the variation in inner square perimeter is not significant. The coefficient of variation (CV) for these specimens is 0.92%, 2.02%, 2.51%, 1.60% and 1.05% for samples φ= 15°, 30°, 45°, 60° and 75° respectively. A source of perimeter reduction in samples φ=30°, 45°, 60° is buckling of samples. However, the influence of buckling is not significant due to using capstan part in gripers (section **4.1.3**). On the basis of assumptions, perimeter of inner square is assumed as constant during deformation which is agreement with measurements (figure 5.25).

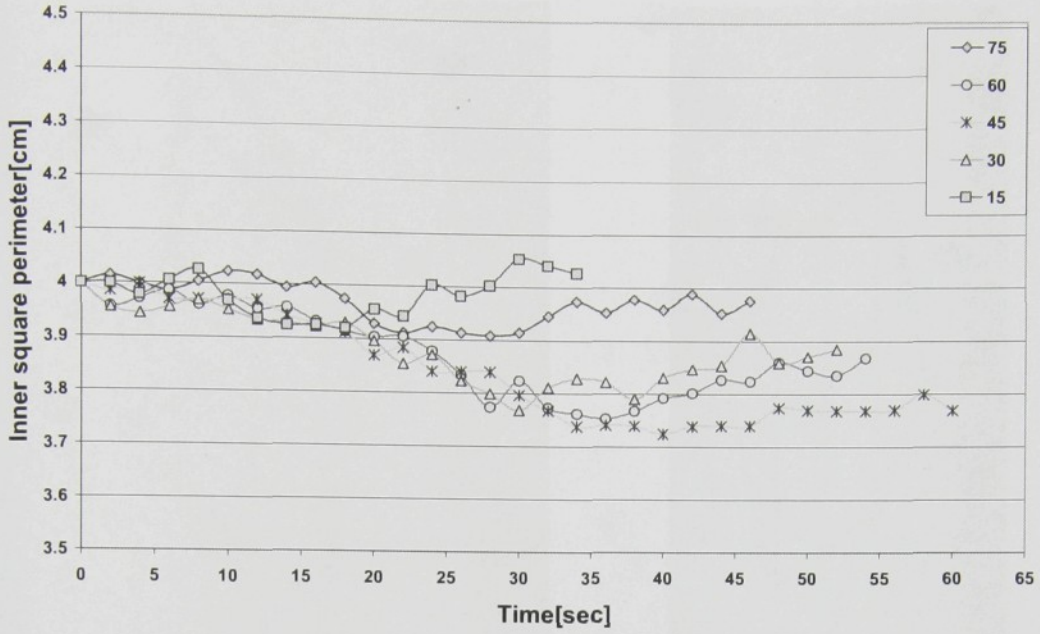

Figure 5.25- Circumference of inner square in samples with different φ (weft yarns-force axis angle)

In the other hand, the arrangement of squares, depended on the force angle φ, are subjected to change during deformation. Figures 5.26 and 5.27 show these squares in samples with φ=15° and φ=60° after deformation and near to rupture.

Actually, when the tensile stress is imposed in weft direction, the variation in arrangements of contrary yarns, here warp yarns, can be estimated by proposed model. As well as, this method can be applied when the fabric is suffering tensile stress in warp direction. The outcomes of experimental and predicted values of warp and weft yarns sett is summarized in figure 5.28. Evidently, the estimated values are higher than measured values. It can be justified by restriction in yarns sett. In real fabric, there are some geometrical restrictions which cause to limit sett for contrary yarns [17]. This limitation do not considered in this model. Thus, the predicted values are higher than measured values.

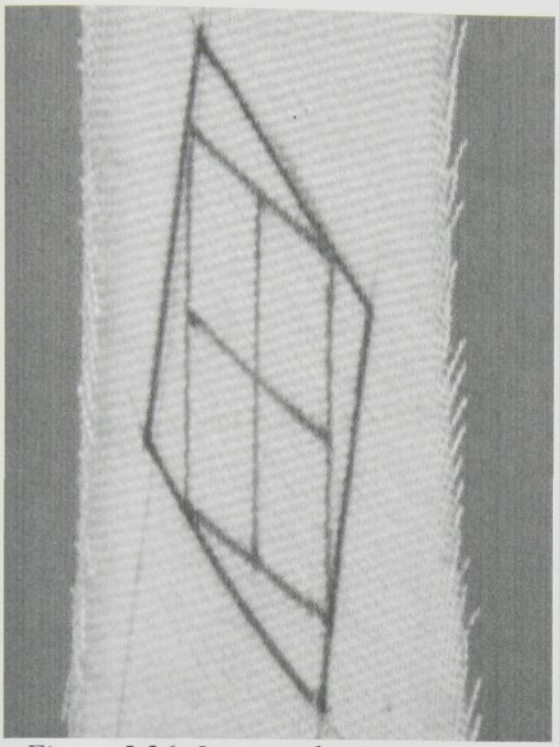

Figure 5.26- Inner and outer squares in center of sample φ=15°(weft yarns-force axis angle) after deformation and near to rupture point

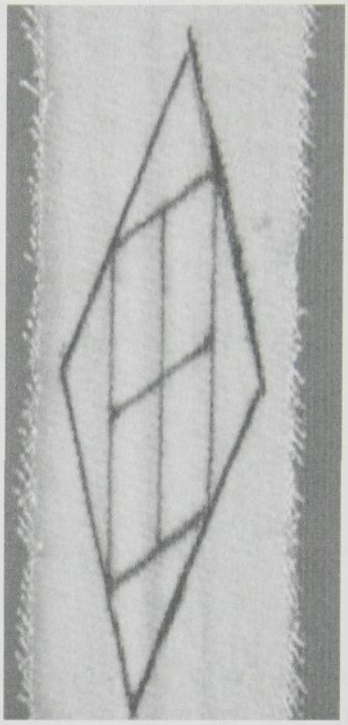

Figure 5.27- Inner and outer Squares in center of sample φ=60°(weft yarns-force axis angle) after deformation and near to rupture point

Indeed, in comparison with the condition that the stress is applied in principal directions, the variation in yarns arrangements is really more complex when the tensile stress is inflicted in arbitrary direction. For instance, when the tensile stress is inflicted in warp direction then the warp yarns sett increased and yarns sett in weft direction starts to reduce. But, when the stress is imposed in arbitrary direction of a fabric then both warp and weft yarns arrangements are subjected to non-uniform changes. It is strongly depended on planar and normal forces which are generated on yarns during deformation. Figures 5.29-5.33 depict the average of measurements and evaluated yarns sett when the tensile stress is imposed in different angles. In figure 5.29 and 5.30 can be observed that if the force angel is closer to weft yarns, yarns sett in weft direction start to reduce continuously, but warp sett is gradually increased then starts to decrease. The rivers trend is detected in figure 5.33 for force angel 75°. However, both warp and weft yarns setts begin to reduce when the force axis angle is 45° (figure 5.31). Whereas the predicted values depict the trend of variations in yarns sett as well as the measured values, it can deducted that the proposed model is responsible to estimate yarns sett changes during deformation in arbitrary direction.

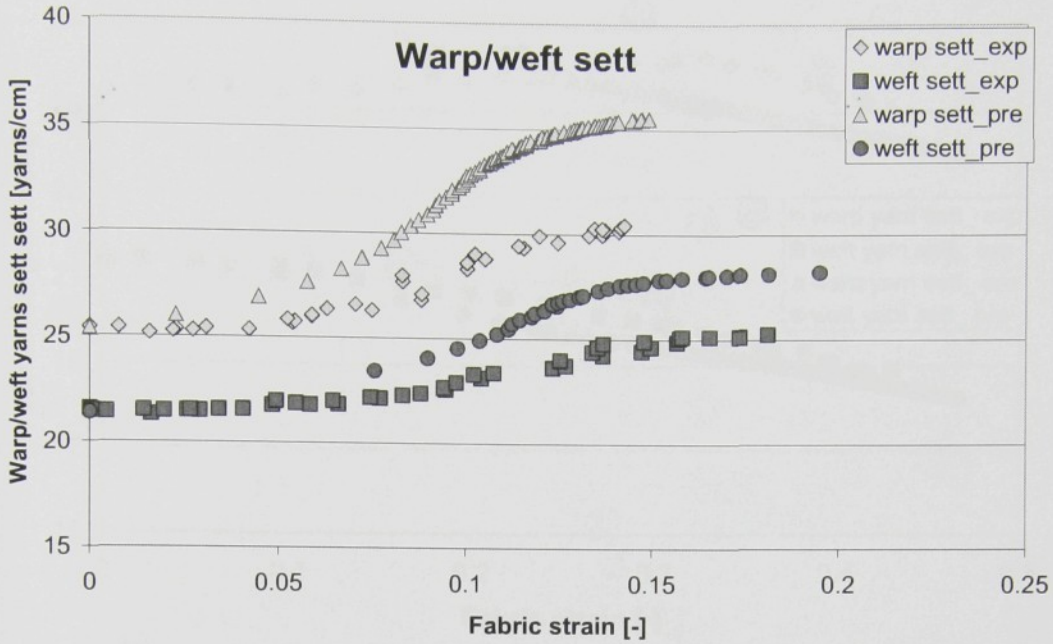

Figure 5.28- Comparison between predicted and measured values: Change in warp and weft yarns sett when the fabric is subjected to tensile stress in weft and warp direction respectively.

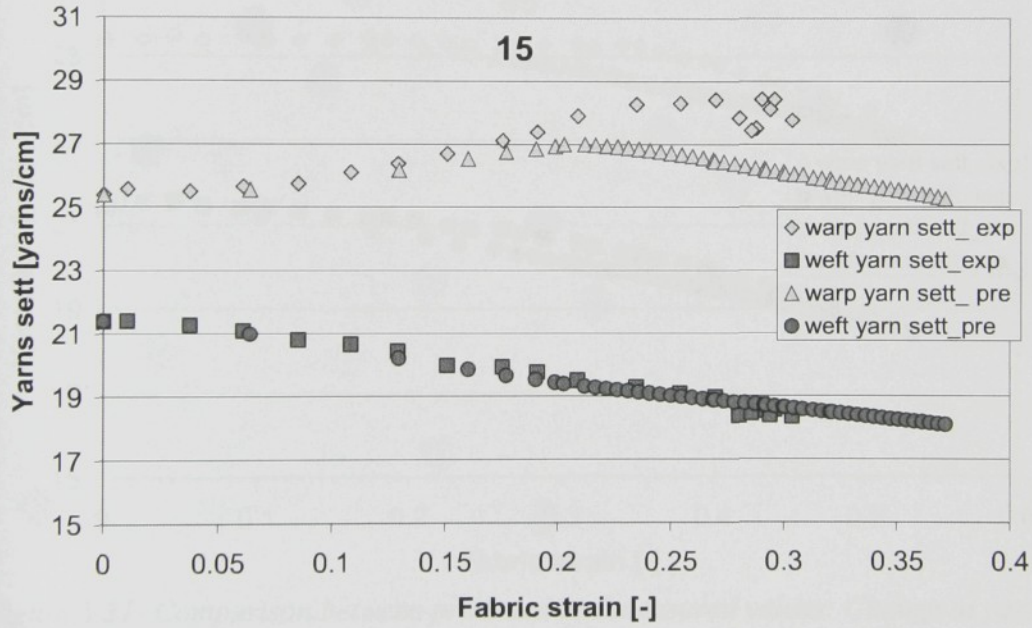

Figure 5.29- Comparison between predicted and measured values: Change in yarns sett for force angle φ=15 °

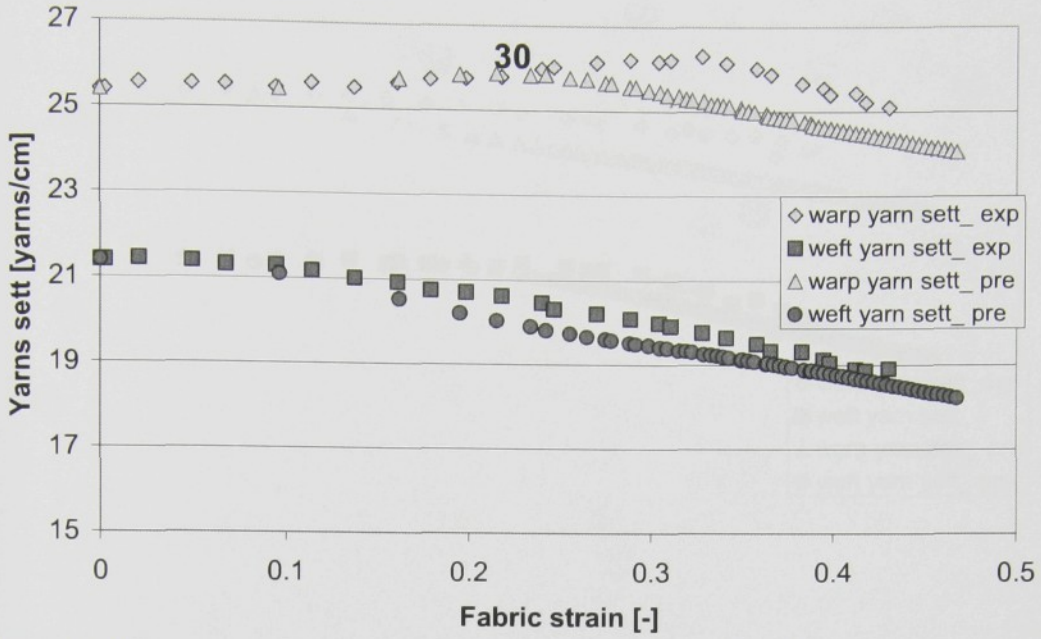

Figure 5.30- Comparison between predicted and measured values: Change in yarns sett for force angle φ=30 °

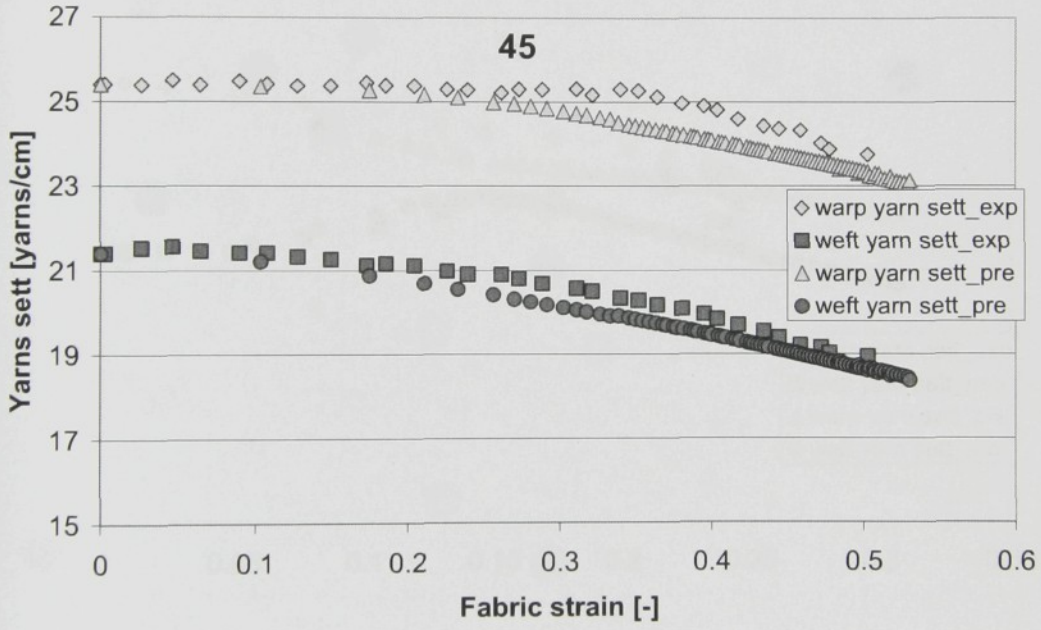

Figure 5.31- Comparison between predicted and measured values: Change in yarns sett for force angle φ=45 °

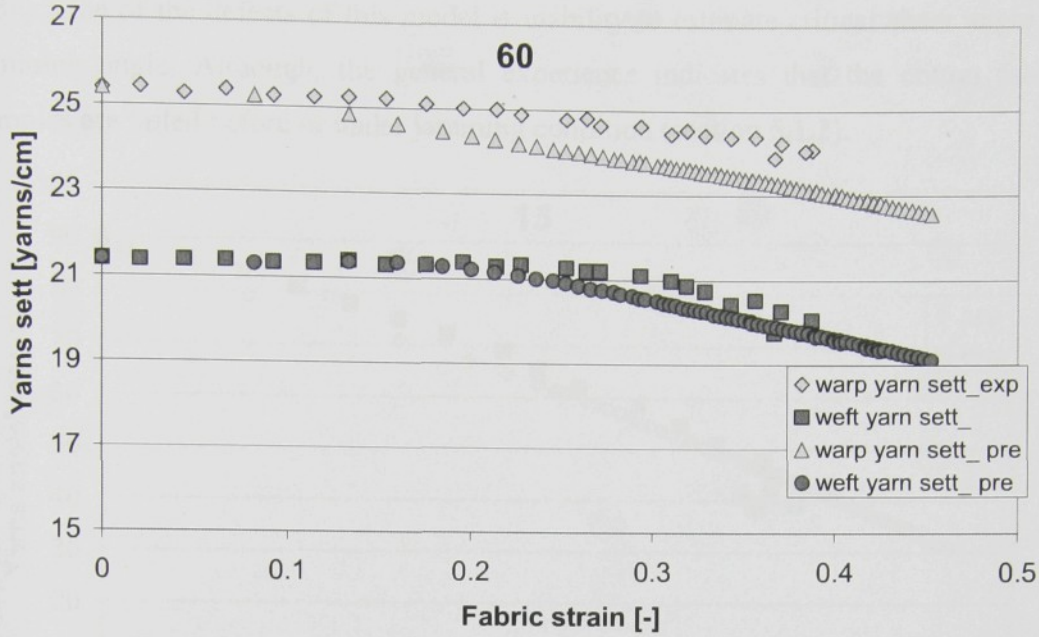

Figure 5.32- Comparison between predicted and measured values: Change in yarns sett for force angle φ=60 °

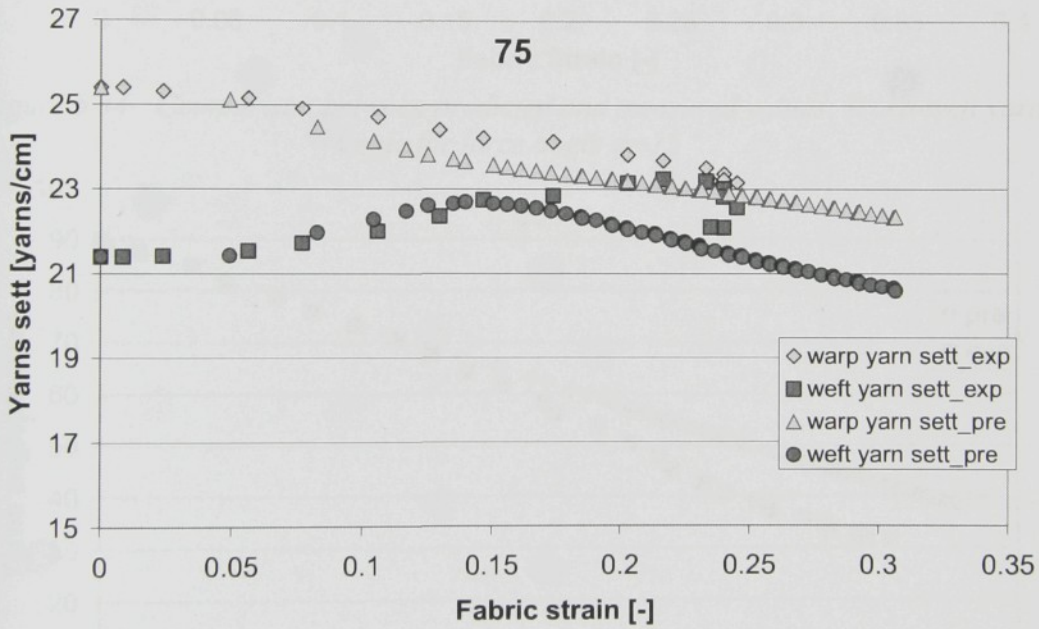

Figure 5.33- Comparison between predicted and measured values: Change in yarns sett for force angle φ=75 °

One of the important quantities in exterior properties of a fabric during deformation is warp-weft yarns angle which indicates the shear angle and shear strain [20, 25-26]. The samples with bigger change in warp-weft yarns angle are known as more deformable than others. This model is able to estimate warp-weft angle too. Figures 5.34-5.38 reveal the comparison between estimated and measured values of warp-weft angle in different force angle. It can be observed that maximum shear angle (minimum warp-weft angle) can be achieved when the force angle is 45° (figure

5.36). One of the defects of this model is inability to estimate critical shear angle or jamming angle. Although, the general experience indicates that the cotton fabric samples are failed before or under jamming condition (section **5.1.2**).

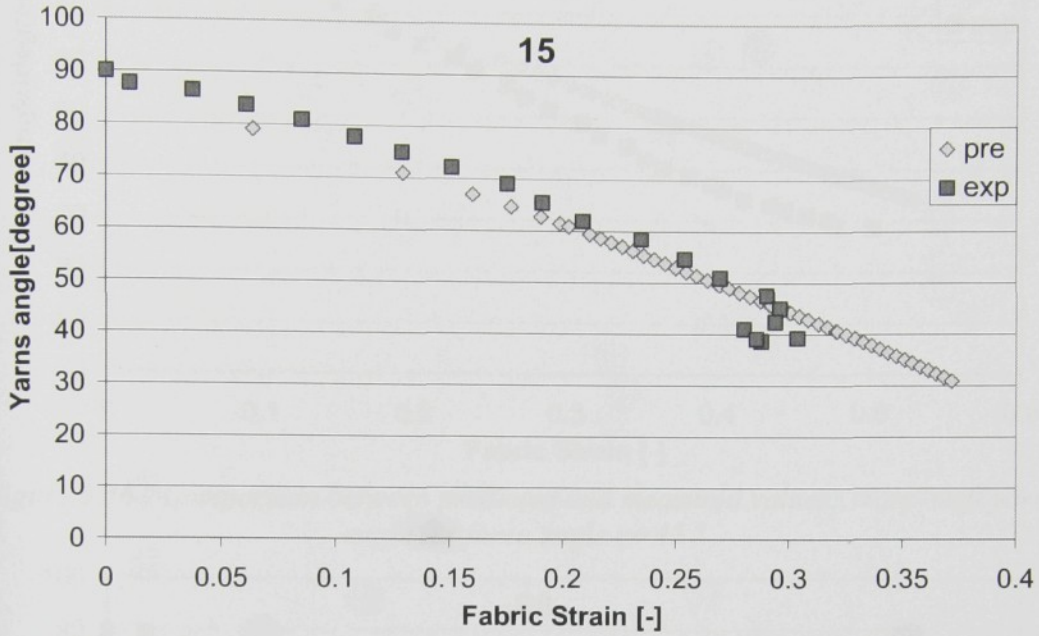

Figure 5.34- Comparison between predicted and measured values: Warp-weft yarns angle for force angle φ=15 °

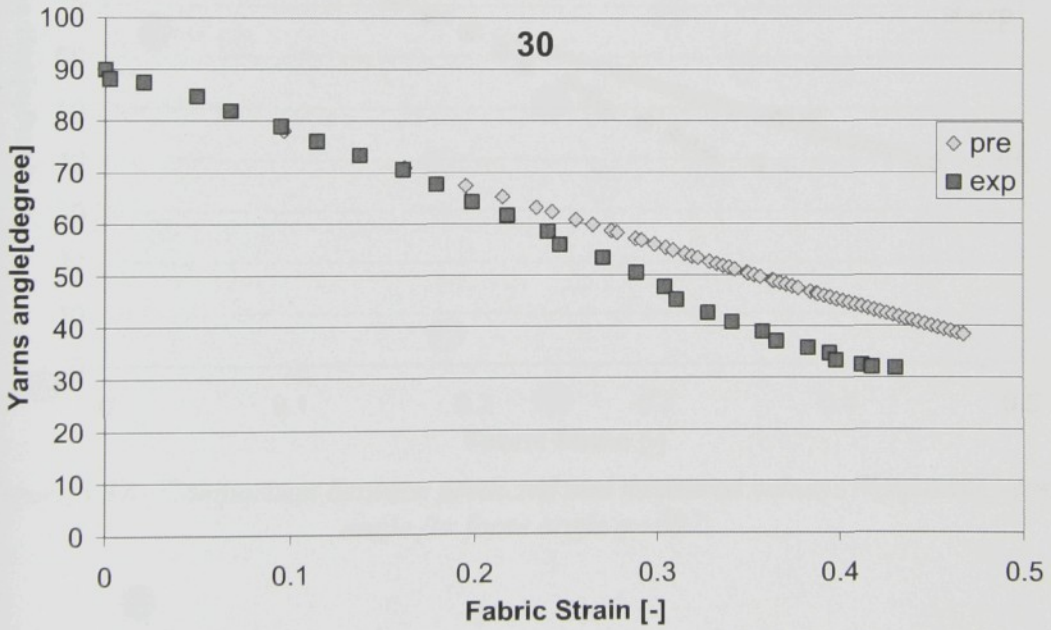

Figure 5.35- Comparison between predicted and measured values: Warp-weft yarns angle for force angle φ=30 °

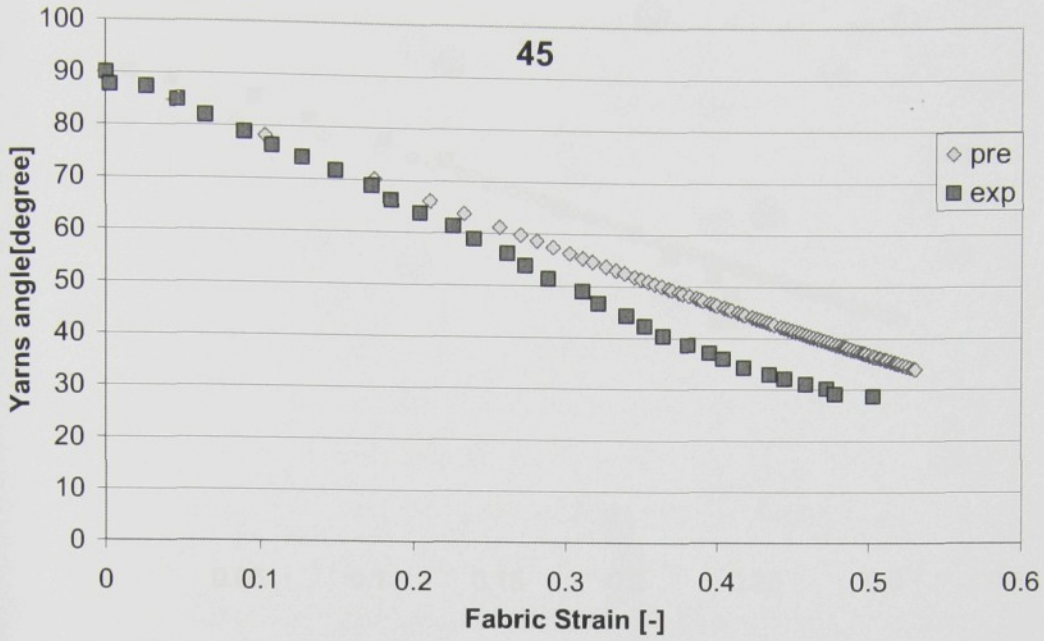

Figure 5.36- Comparison between predicted and measured values: Warp-weft yarns angle for force angle φ=45 °

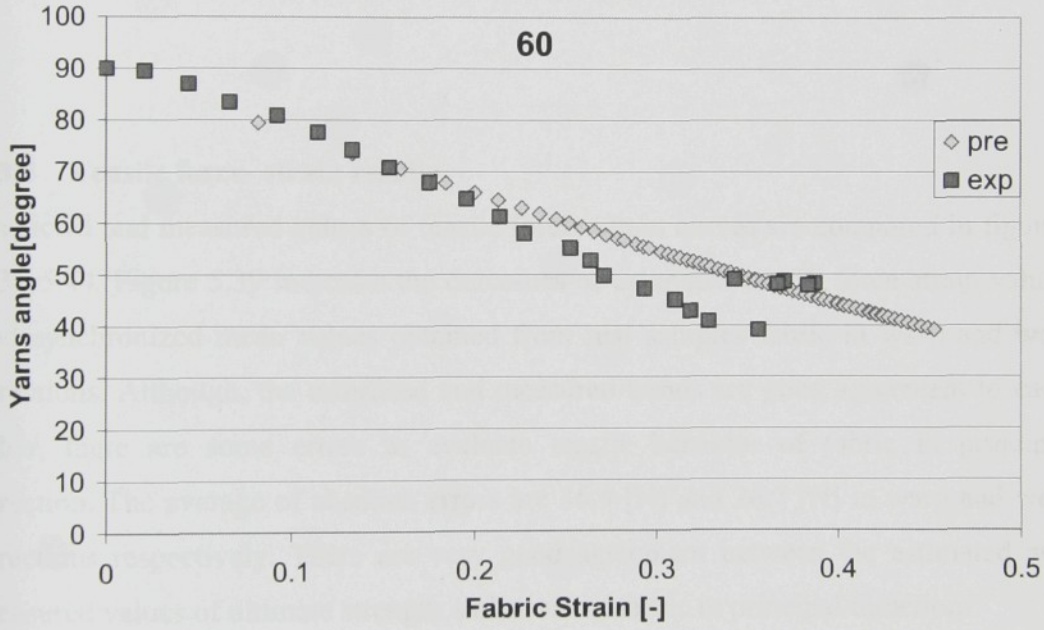

Figure 5.37- Comparison between predicted and measured values: Warp-weft yarns angle for force angle φ=60 °

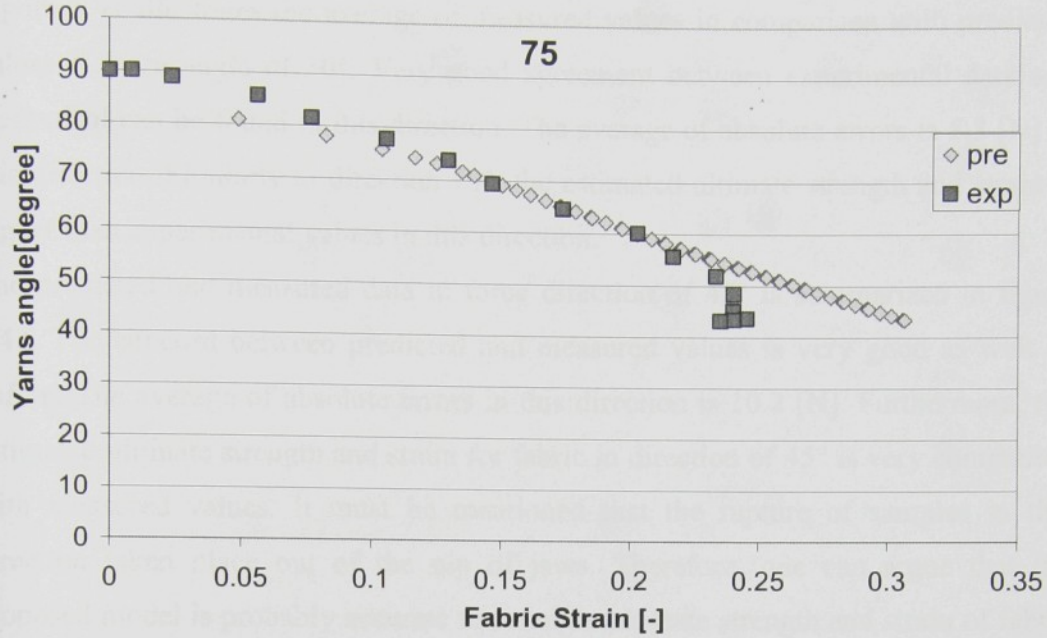

Figure 5.38- Comparison between predicted and measured values: Warp-weft yarns angle for force angle φ=75 °

5.3.4 Tensile force- strain results

Predicted and measured values of tensile force -strain curves are compared in figures 5.39-5.44. Figure 5.39 indicates the outcomes of estimated tensile force-strain values and synchronized mean values obtained from real samples fabric in warp and weft directions. Although, the estimated and measured trends are good agreement to each other, there are some errors to evaluate tensile behavior of fabric in principal direction. The average of absolute errors are 36.4 [N] and 26.7 [N] in warp and weft directions respectively. There are very good agreement between the estimated and measured values of ultimate strength and strain of fabric in principal direction.

Figure 5.40 depicts the results of estimated and average of measured values when the tensile stress is applied in 15° direction (from weft yarns). The estimated values in this direction are better in comparison with principal directions. The average of absolute errors in this direction is 10.2 [N]. Despite of using the modified jaws in this study, all the samples in this direction are failed in the nip of jaws. Therefore, the predicted ultimate strength and strain of fabric in this direction are really higher than the measured value. It is demonstrated that using the modified jaws conducts to better results (appendix (F)).

Figure 5.41 illustrates the average of measured values in comparison with predicted values if force angle of 30°. Very good agreement between experimental data and theoretical can be found in this direction. The average of absolute errors is 5.3 [N] in this direction. Similarly to direction 15°, the estimated ultimate strength and strain is higher than experimental values in this direction.

The predicted and measured data in force direction of 45° is summarized in figure 5.42. The concord between predicted and measured values is very good as well as before. The average of absolute errors in this direction is 10.2 [N]. Furthermore, the estimated ultimate strength and strain for fabric in direction of 45° is very compatible with measured values. It must be mentioned that the rupture of samples in this direction taken place out of the nip of jaws. Therefore, one can argue that the proposed model is probably accurate to estimate ultimate strength and strain of fabric in arbitrary direction as well as tensile force-strain estimation.

Figure 5.43 and 5.44 show the comparison between measured and evaluated data of tensile force-strain of this fabric in directions of 60° and 75°. The samples in these directions were broken at jaws, so the estimated values are higher than experimental data. As well as, the rate of increasing force in the obtained data from this model is bigger than tentative values. Nevertheless, the trend of predicted curve is acceptable and the averages of absolute errors are 26.6 [N] and 32.1 [N] in 60° and 70° directions respectively.

Figure 5.45 represents the tensile force-strain curve of samples in all directions to comparison. Clearly, the fabric in direction of 45° has a great strain and good strength (a bit higher that warp/weft direction). On the basis of estimations of this model, the maximum strength of this fabric can be expected when the tensile stress is imposed in axis 60° direction (φ=60° form weft yarns). Figure 4.46 describes the absolute errors of samples in different directions. The measured and estimated values of ultimate strength are summarized in figure 4.47 at different direction. There is good agreement between estimated and measured values in principal and bias directions. However, despite of using modified jaws the samples in other directions are broken at the jaws. Thus, the more strength is anticipated in this direction. The effect of modified jaws on anisotropy of tensile properties is investigated in appendix (F).

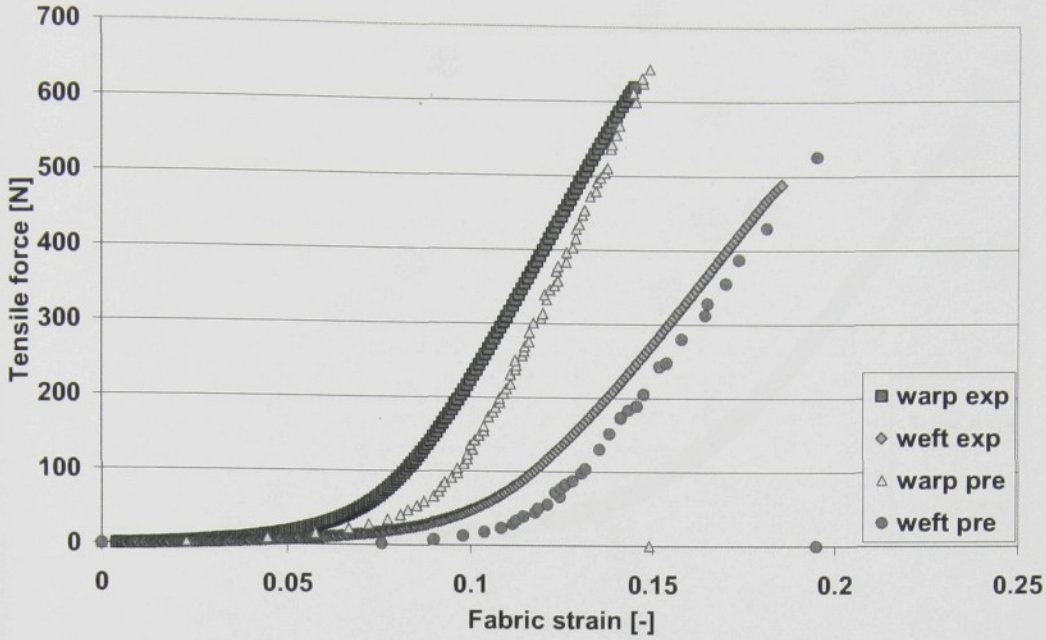

Figure 5.39- Comparison between predicted and measured values: tensile force-strain curve in warp weft direction (φ=90 ° and φ=0 ° respectively)

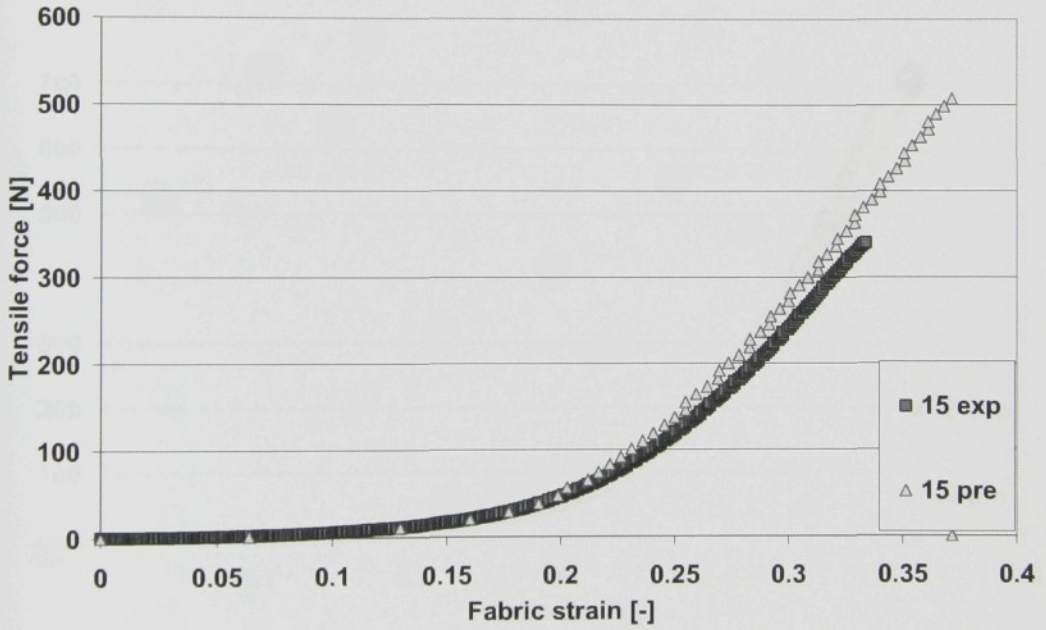

Figure 5.40- Comparison between predicted and measured values: tensile force-strain curve in φ=15 ° direction

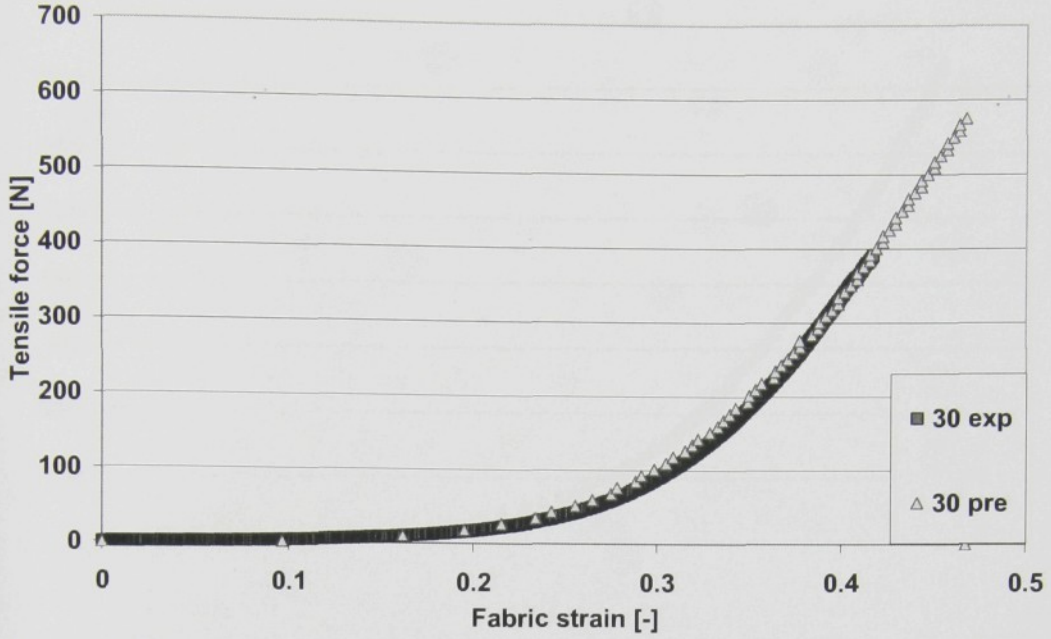

Figure 5.41- Comparison between predicted and measured values: tensile force-strain curve in φ=30 ° direction

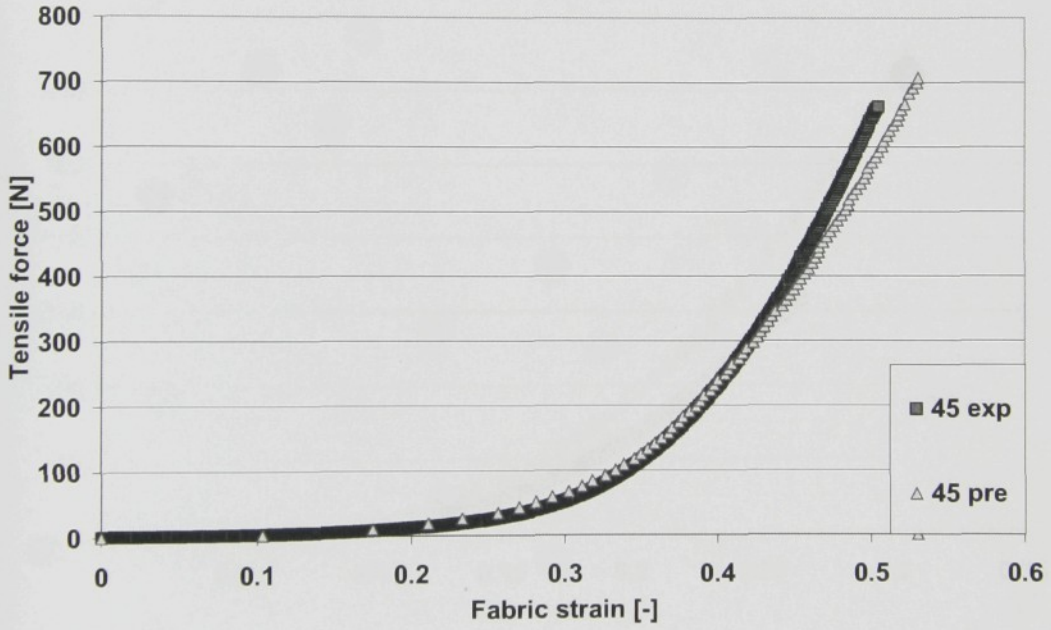

Figure 5.42- Comparison between predicted and measured values: tensile force-strain curve in φ=45 ° direction

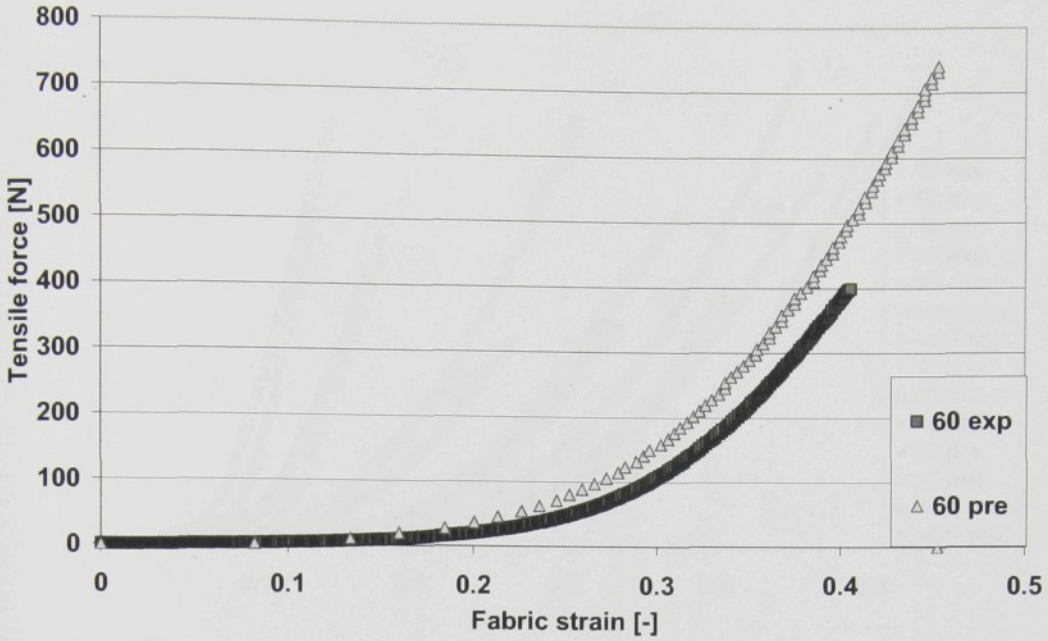

Figure 5.43- Comparison between predicted and measured values: tensile force-strain curve in φ=60 ° direction

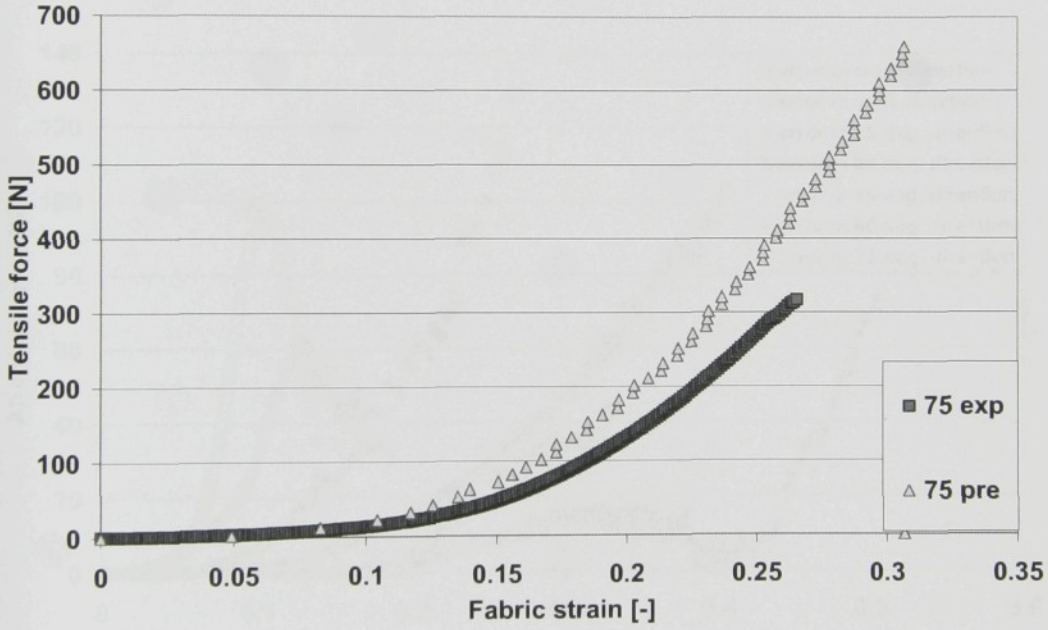

Figure 5.44- Comparison between predicted and measured values: tensile force-strain curve in φ=75 ° direction

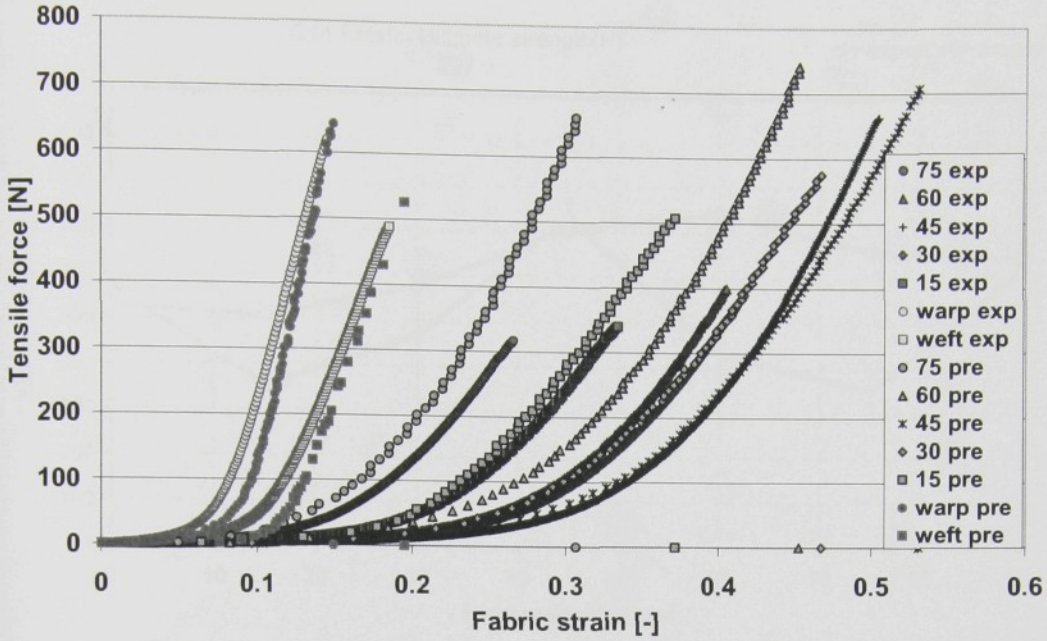

Figure 5.45- Comparison between predicted and measured values: tensile-strain curves of samples in different directions

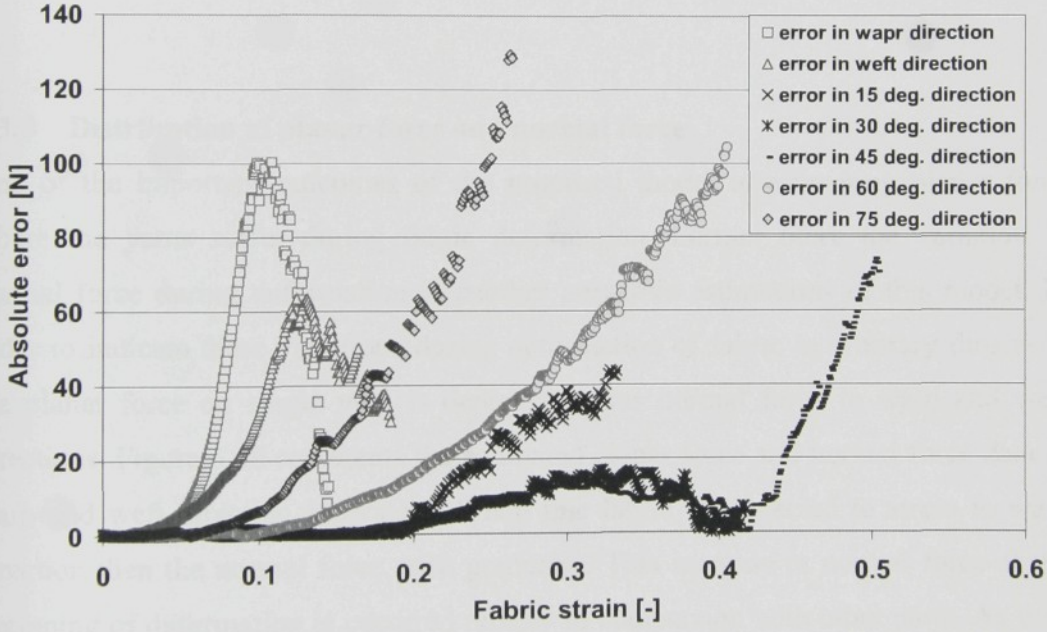

Figure 5.46- Absolute errors in predicated and average of measured values of tensile force-strain curve

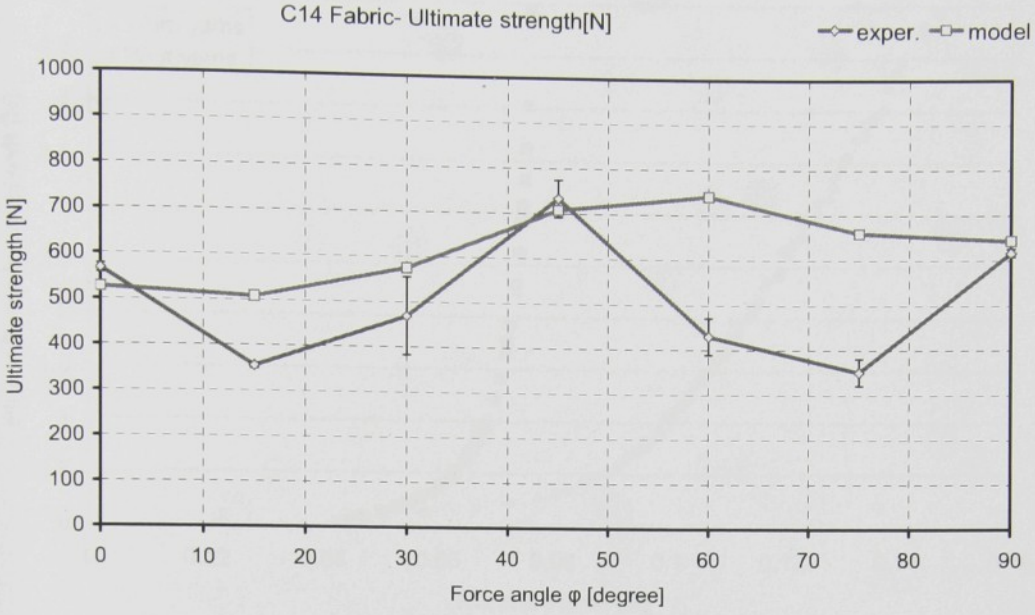

Figure 5.47- Comparison between measured and estimated ultimate strength of fabric C14 in different directions

5.3.5 Distribution of planar force and normal force

One of the important outcomes of the proposed model is estimating planar force where the yarns suffer during fabric deformation. Further more the variation in normal force during deformation is another attractive estimations of this model. In order to indicate these variations during deformation of fabric in arbitrary direction, the planar force on single yarn is depicted versus normal force in warp and weft directions. Figure 5.48 represents the estimated planar force and normal force data in warp and weft direction separately. When this fabric is subjected to stress in warp direction then the normal force arise gradually. This increase in normal force at the beginning of deformation is occurred rapidly in comparison with other parts. As well as, if the fabric under consideration subjected to stress in weft direction then the normal force increase quickly then limited to some value.

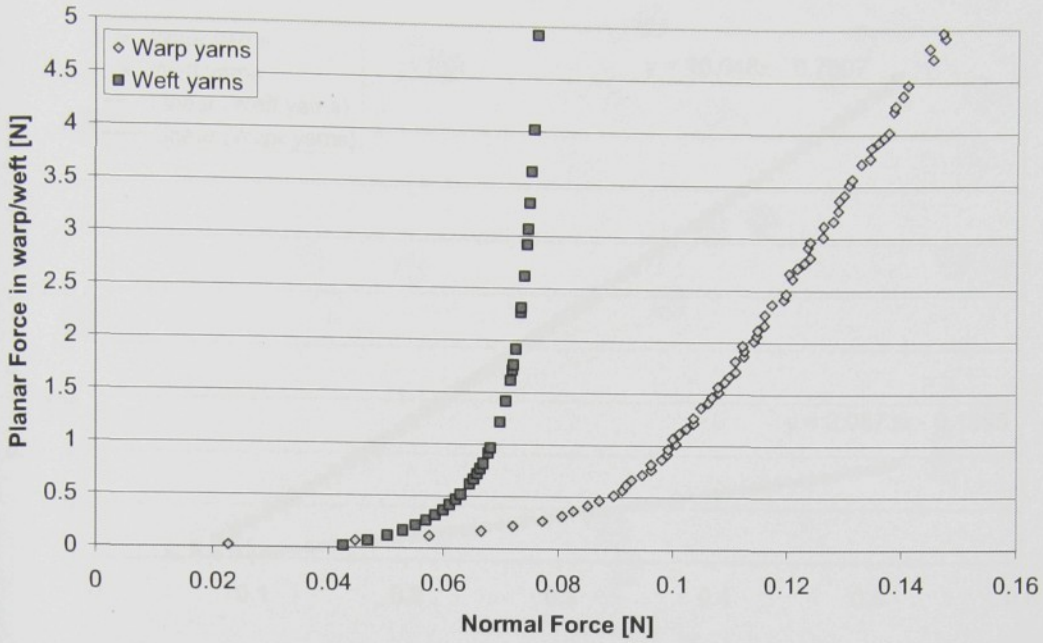

Figure 5.48- Variation of planar force and normal force on single yarn in warp and weft direction (φ=90° and φ=0° respectively)

Figure 5.49 shows attractive linear trend in variation of planar and normal force in single warp and weft yarns when the force angle is 15°. As it was anticipated, the planar force in weft yarns is higher than warp yarns due to closing of weft yarns with force angle. Thus it is expected that weft yarns are failed sooner than warp yarns. Consequently, the ultimate strength of fabric in this direction is low than the strength of fabric in higher force angles due to lack of weft sett yarns and small contribution of warp yarns in fabric resistance. The proportion planar force to normal force is 2.1 and 10.0 for warp and weft yarns respectively.

Figure 5.50 indicates variation of planar force in single yarn in warp and weft yarns of a sample under 30° force angle. The trend of planar and normal force is still linear. However, contribution of warp yarns to suffer stress is increased in comparison with 15° force angle. Nevertheless, weft yarns are anticipated to rupture sooner than warp yarns. The respect of planar force and normal force is 2.8 and 6.3 for warp and weft yarns respectively.

Figure 4.51 specifies the planar and normal force on a single yarn of warp and weft when the fabric is suffering bias stress. The involvement of both warp and weft yarns bear force is almost the same. Therefore, the superior strength is expected in this direction. Maximum normal force is predicted in this direction. The proportion planar force to normal force is 3.4 and 4.6 for warp and weft yarns respectively.

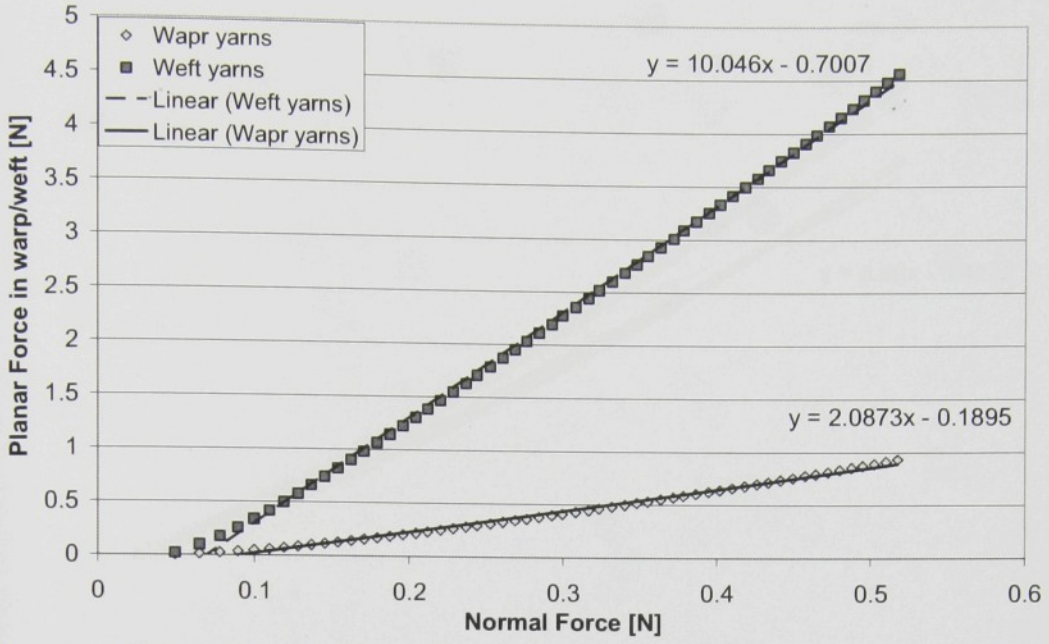

Figure 5.49- Variation of planar force and normal force on single yarn under force angle 15° (φ=15°)

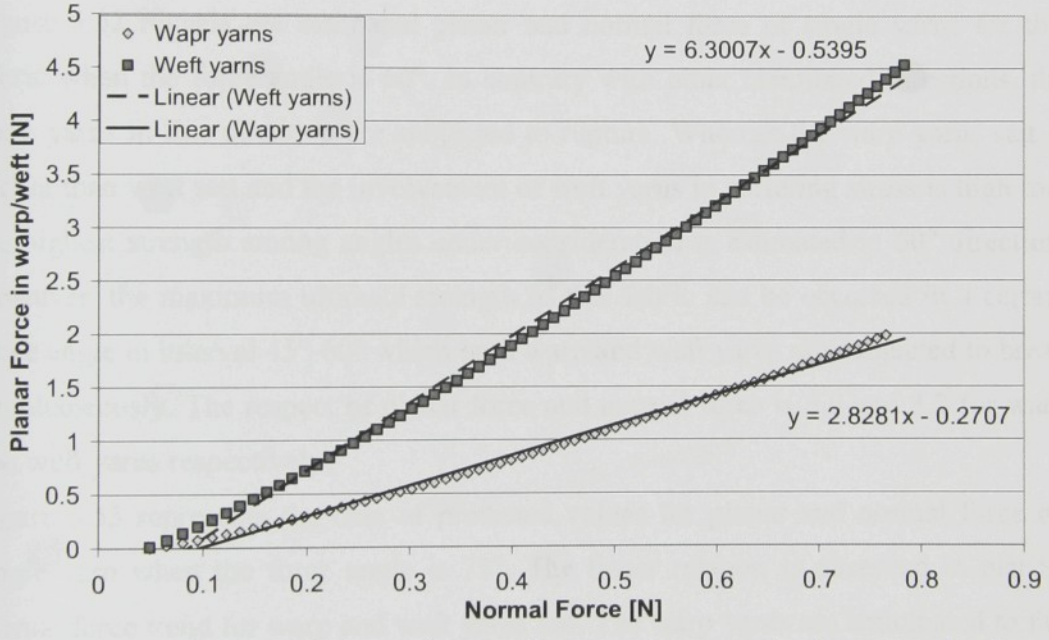

Figure 5.50- Variation of planar force and normal force on single yarn under force angle 30° (φ=30°)

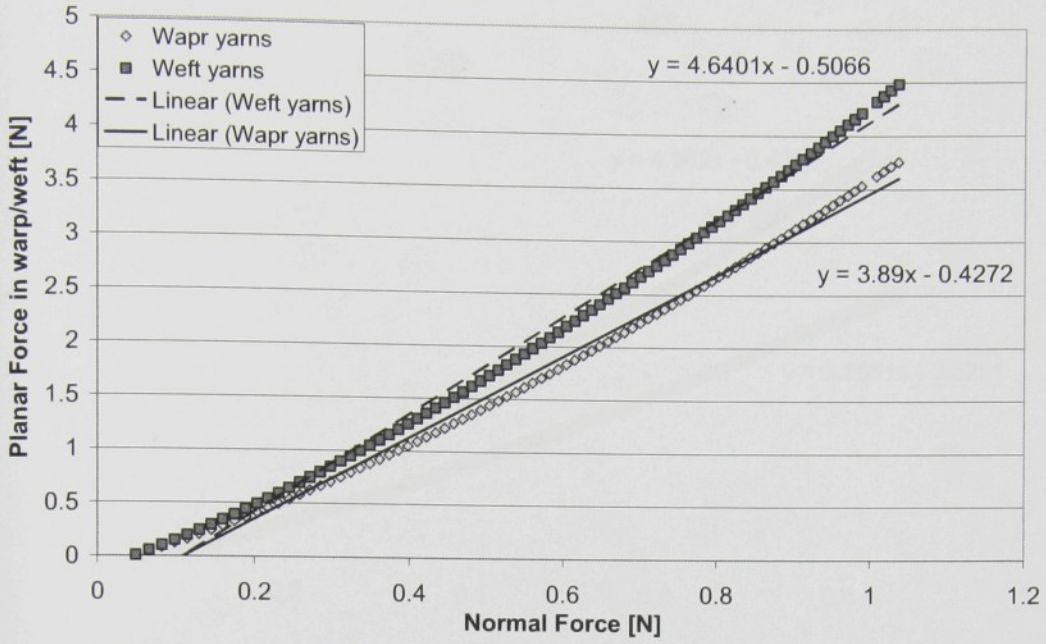

Figure 5.51- Variation of planar force and normal force on single yarn under force angle 45° (φ=45°)

Figure 5.52 reveals the estimated planar and normal force of single yarns for this fabric when the force angle is 60°. In contrary with other mentioned directions, the warp yarns in this direction are subjected to rupture. Whereas the warp yarns sett is higher than weft sett and the involvement of weft yarns in suffering stress is high too, the highest strength among angles under consideration is estimated in 60° direction. However, the maximum ultimate strength of this fabric can be occurred in a certain force angle in interval 45°-60° which both warp and weft yarns are subjected to break simultaneously. The respect of planar force and normal force is 5.0 and 3.2 for warp and weft yarns respectively.

Figure 5.53 represents the data of predicted values for planar and normal force on single yarn when the force angle is 75°. The linear relation is observed in planar-normal force trend for warp and weft yarns too. The warp yarns are anticipated to fail sooner than weft yarns due to closing force axis to warp yarns in this direction. The proportion planar force to normal force is 8.0 and 2.2 for warp and weft yarns respectively.

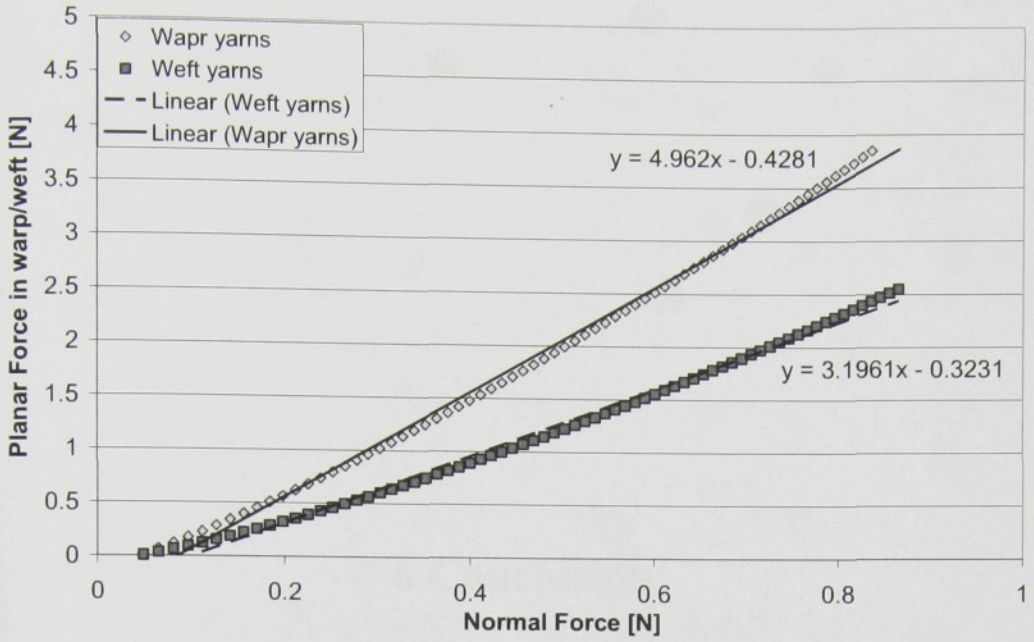

Figure 5.52- Variation of planar force and normal force on single yarn under force angle 60° (φ=60°)

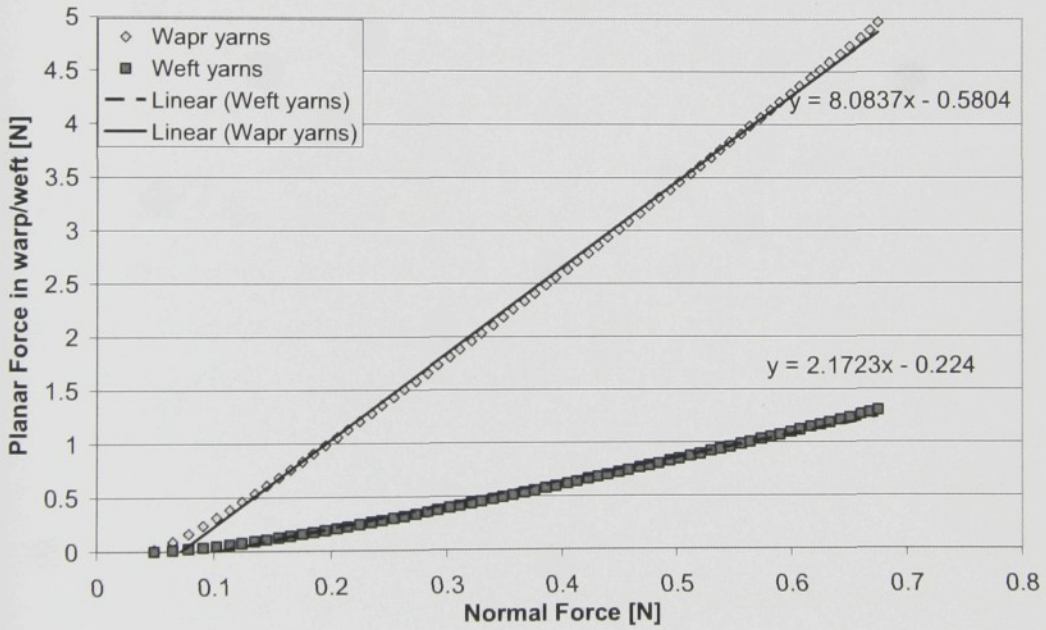

Figure 5.53- Variation of planar force and normal force on single yarn under force angle 75° (φ=75°)

6 Conclusion

6 Conclusion

Tensile properties of fabric indicate how the fabric will react to forces being applied in tension. Tensile properties of a fabric in this study consist of tensile force-strain curve of fabric and variation in fabric geometrical characteristics simultaneity. To challenge anisotropy of tensile properties of fabric, a geometrical model for understanding bias deformation has been put forward then a micro-mechanical for evaluating fabric in arbitrary direction has been established successfully. The conclusions of each of these models and developed methods are presented in following:

6.3 Geometry of fabric during bias deformation

Very simple geometrical model has been constructed with numbers of assumptions. This model had been utilized to evaluate geometry of a set non-deformed cotton fabrics. The comparison between tentative and estimated data indicates that this model is responsible in internal fabric geometry before deformation. Then this model is expanded to assess geometry of deformed fabric in bias direction by considering some more assumptions. To evaluate deformed fabric, the outcomes of this model had been compared with experimental work. It is found that suggested model reveal geometry of fabric as well as. Estimating of locking angle can be pointed out as another advance of this model. According to proposed model and observations one can argued that before locking angle the yarns rotation govern the fabric deformation while, the yarns crimp-interchange is dominant effect after reaching to locking angle during fabric deformation.

Notwithstanding the capacities of this model to evaluate fabric geometry before and after deformation in bias direction, this geometrical model does not satisfy whole targets of our study. Consequently, a micro-mechanical model has been established.

6.4 Micro-mechanical model for evaluating fabric in arbitrary direction

When a woven fabric is subjected to stress in arbitrary direction then a complex behavior for the fabric can be anticipated. Relative rotation between yarns, crimp interchange in warp and weft yarns, yarns flattening, yarns extension etc. are the well known reactions of fabric's yarns when the fabric is suffering stress in arbitrary direction. For this purpose, deflection curve of a yarn under planar and normal forces has been determined by considering yarn bending stiffness and some assumptions. Moreover, behavior of tensioned yarn under compressive force is empirically determined. Thus, a system of equations include of some differential equations has

been constructed. Whereas the yarns stiffness can be determined in relaxed fabric condition, the mentioned system of equations can be solved for certain force and force angle. It has been demonstrated that the established model is successful to appraise tensile properties of fabric by comparing the empirical and theoretical data. Despite of capacities of proposed model to simulate behavior of fabric under stress in arbitrary direction, lack of ability to estimate jamming condition is the main defect of this model. Some sources of errors in model are summarized in following categories:

1. Bending rigidity of tensioned yarn is a function of tension and bending angle, however in this study we contemplate is as a constant value during deformation.
2. Mechanical properties of a yarn inside of fabric are not the identical as free yarn.
3. Distinguishing yarn deformation under tension and compressive force is complicate. Nevertheless, we applied an empirical approach to measuring yarn cross-section deformation under a certain interval tension and compressive forces.

6.5 Developed methods

To investigate external geometry of woven fabric, the 2D FFT technique is modified and used effectively in this study. It is demonstrated that this technique can be employed to detect yarns shear angle and change yarns density during deformation.

Moreover to evaluate flattening of tensioned yarn when it is subjected to normal force a simple method is suggested in this study. The exponential behavior in deformation of yarn cross-section under formal force is observed by applying this method. The flattening of tensioned yarn is accompanied with yarn consolidation by increasing tension. To better understanding this behavior of yarn an independent investigation is proposed.

As other researchers, to measure ultimate tensile strength and strain of woven fabric in arbitrary direction there were a dilemma due to rupture of samples at nip of jaws. Beside of other solutions a new concept to overcome stated problem is put forward. On the basis of this concept, the jaws can equipped with capstan parts to apply tension on the sample gradually. The observations indicate that this method is more effective than the other solution to measuring tensile properties of woven fabric in arbitrary direction.

Appendixes

Appendix A: Minimum packing density of yarn inside of two real fabric

As mentioned in section **3.1.1**, four equilibriums (3.10), (3.21), (3.22) and (3.25) can be inferred from geometry of a fabric which are depended on six variables. To obtain variables, all series of results which satisfy equilibriums are to be computed by considering two arbitrary values for proportions (A.1) and (A.2). It can be graphically shown that, there is one pair of k_1 and k_2 among arbitrary values which corresponds with minimum possibility of packing density.

$$k_1 = \frac{a_1}{b_1} \tag{A.1}$$

$$k_2 = \frac{b_2}{b_1} \tag{A.2}$$

To demonstrate relation among k_1, k_2 and packing density, two plain weave fabrics C14 and P30 are considered (their specifications are presented in table 4.1).

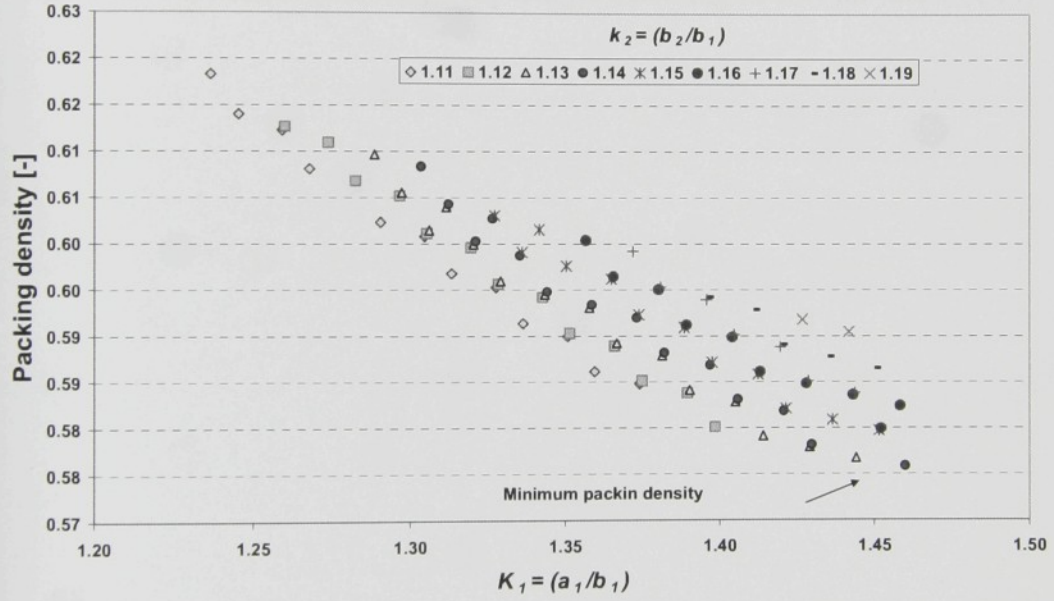

Figure A.1- Relationship among k_1, k_2 and yarn packing density for fabric (P30)

All possibilities in results which satisfy equilibriums (3.10), (3.21), (3.22) and (3.25) are computed and collected in figures A1 and A2 for fabrics C14 and P30 respectively. Then, a series of data which is conducted to minimum packing density is picked out as a final result for each fabric. The minimum calculated packing densities for polypropylene and cotton yarns inside of fabric are 0.576 and 0.548 respectively. The results of this evaluation are summarized in table 5.1.

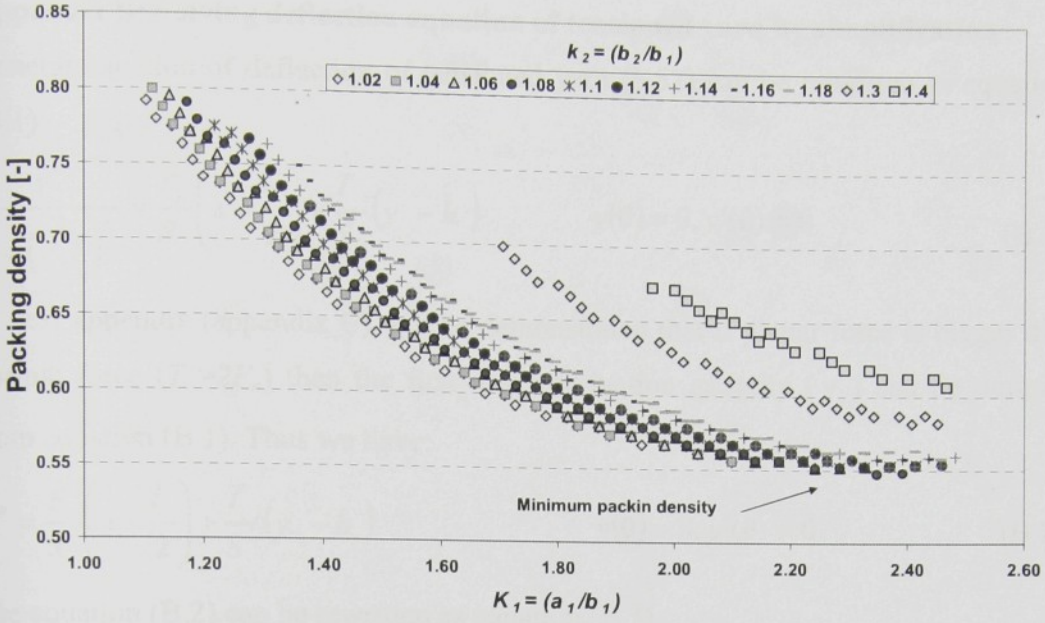

Figure A.2- Relationship among k_1, k_2 and yarn packing density for fabric (C14)

Appendix B: Solving deflection equation of tensioned yarn by simplification

General equation of deflection of tensioned yarn (3.52) can be rewritten as equation (B.1):

$$\frac{y''}{\left(1+(y')^2\right)^{\frac{3}{2}}}=\frac{F_n}{S}\left(x-\frac{l}{2}\right)+\frac{T}{S}\left(y-h\right) \qquad y(0)=0, y'(0)=0 \tag{B.1}$$

In next appendix (appendix C) will be demonstrated that if planar force is bigger that normal force ($T>2F_n$) then the first order derivation quantity (y') can be omitted from equation (B.1). Thus we have:

$$y''=\frac{F_n}{S}\left(x-\frac{l}{2}\right)+\frac{T}{S}\left(y-h\right) \qquad y(0)=0, y'(0)=0 \tag{B.2}$$

The equation (B.2) can be rewritten as equation (B.3).

$$y''S-Ty=F_n x-\left(\frac{F_n l}{2}+Th\right) \tag{B.3}$$

Outcome equation is a differential equation with a general answer (B.4) which it consists of two parts namely; particular and homogeneous answers. Each of them can be solved by regarding to differential equation theorems as equations (B.5) and (B.6). Eventually, equation (B.7) is deducted as general answer of this equation.

$$y=y_p(x)+y_h(x) \tag{B.4}$$

$$y_p=-\frac{F_n x}{T}+\frac{F_n l}{2T}+h \tag{B.5}$$

$$y_h=C_1 e^{x\sqrt{\frac{T}{S}}}+C_2 e^{-x\sqrt{\frac{T}{S}}} \tag{B.6}$$

$$y=-\frac{F_n x}{T}+\frac{F_n l}{2T}+h+C_1 e^{x\sqrt{\frac{T}{S}}}+C_2 e^{-x\sqrt{\frac{T}{S}}} \tag{B.7}$$

To obtain quantities C_1 and C_2 boundary conditions (B.8) and (B.9) can be applied.

$$\begin{cases} x=0 \\ y=0 \end{cases} \mapsto C_1+C_2+\frac{F_n l}{2T}+h=0 \tag{B.8}$$

$$\begin{cases} x=0 \\ y'=0 \end{cases} \mapsto C_1\sqrt{\frac{T}{S}}-C_2\sqrt{\frac{T}{S}}-\frac{F_n}{T}=0 \tag{B.9}$$

Therefore:

$$C_1=-\frac{F_n l}{4T}-\frac{h}{2}+\frac{F_n}{2T}\sqrt{\frac{S}{T}} \tag{B.10}$$

$$C_2=-\frac{F_n l}{4T}-\frac{h}{2}-\frac{F_n}{2T}\sqrt{\frac{S}{T}} \tag{B.11}$$

Eventually, If $T > 2Fn$ then the deflection equation of tensioned yarn can be derived as equation (B.12) and (B.13).

$$y = \frac{F_n}{2T} e^{x\sqrt{\frac{T}{S}}} \left(-\frac{l}{2} - \frac{hT}{F_n} + \sqrt{\frac{S}{T}} \right) + \frac{F_n}{2T} \left(e^{-x\sqrt{\frac{T}{S}}} \left(-\frac{l}{2} - \frac{hT}{F_n} - \sqrt{\frac{S}{T}} \right) - 2x + l \right) + h \quad \text{(B.12)}$$

Where:

$$h = \frac{F_n \left(e^{\frac{l}{2}\sqrt{\frac{T}{S}}} \left(-\frac{l}{2} + \sqrt{\frac{S}{T}} \right) + e^{\frac{l}{2}\sqrt{\frac{T}{S}}} \left(-\frac{l}{2} - \sqrt{\frac{S}{T}} \right) \right)}{T \left(e^{\frac{l}{2}\sqrt{\frac{T}{S}}} + e^{\frac{l}{2}\sqrt{\frac{T}{S}}} \right)} \quad \text{(B.13)}$$

Appendix C: Verifying the deflection equation of tensioned yarn

In this appendix it is tried to verify the validity of deflection equation (B.12) which is obtained by considering first order derivation quantity (y') as zero. Nevertheless the equation (B.1) can be solved numerically. Following diagrams compare the difference between numerical and analytical solutions in different conditions. Figure C.1 indicates the analytical and numerical solutions when the planar force is zero. When the normal force arises then the distortion form numerical solution and analytical solution is observed. Therefore, using analytical equation does not suggest when the planar force is absent or negligible compared to normal force.

Figure C.2 and C.3 verify the numerical and analytical solution for a yarn with 1E-9 [N.m^2] as stiffness and 2.33E-4 [m] as *l/2* in different planar force (T). Figures 5.47-5.51 demonstrated the planar/normal force ratio was varying within 2-10 rang. Accordingly, the ratio of planar force and normal force is considered as three ratios namely 10, 5 and 2 in this appendix. Distortion from numerical values is indicated by absolute errors. This comparison between analytical and numerical is repeated by assuming 2E-9 and 4E-9 [N.m^2] as yarn stiffness and different planar forces. The outcomes are pointed out in figures C.4-C.7. It can be argued that when the planar/normal force ratio increases then the first order derivation (y') of equation (B.1) tends to zero. As a conclusion it can be observed from figures C.2-C.7 that the

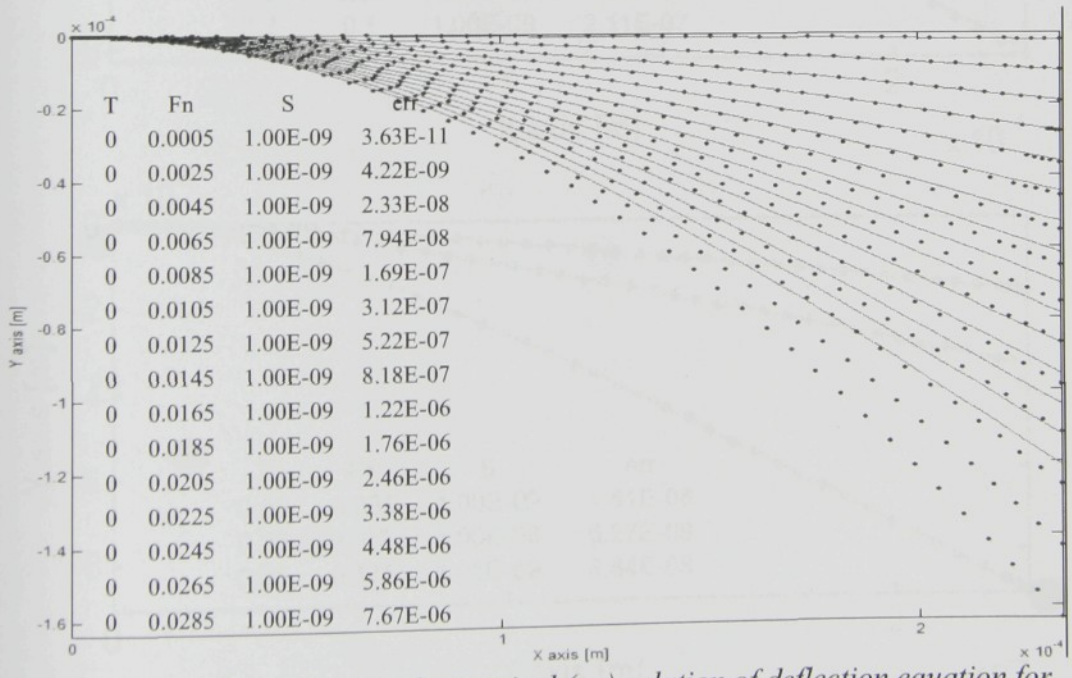

Figure C.1- Analytical (—) and numerical (...) solution of deflection equation for S=1E-9[N.m^2]: planar force is zero and normal force increase gradually

analytical solution (Equation (B.12)) is a good estimation of numerical solution (B.1) if the planar/normal force ratio is equal or bigger than 2.

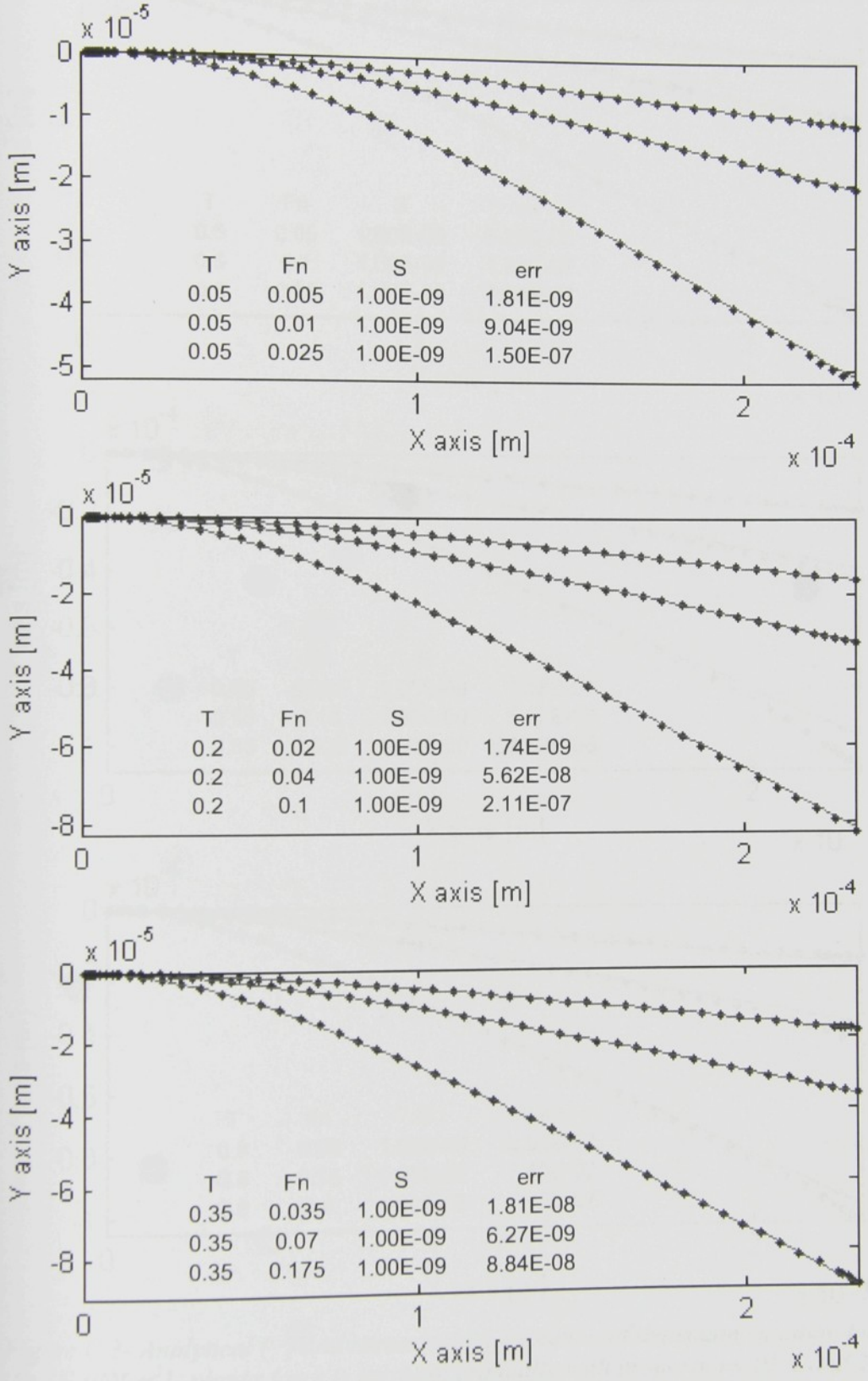

Figure C.2- Analytical (—) and numerical (...) solution of deflection equation for S=1E-9[N.m^2]: planar force is increase gradually with proportions 10, 5 and 2

respectively

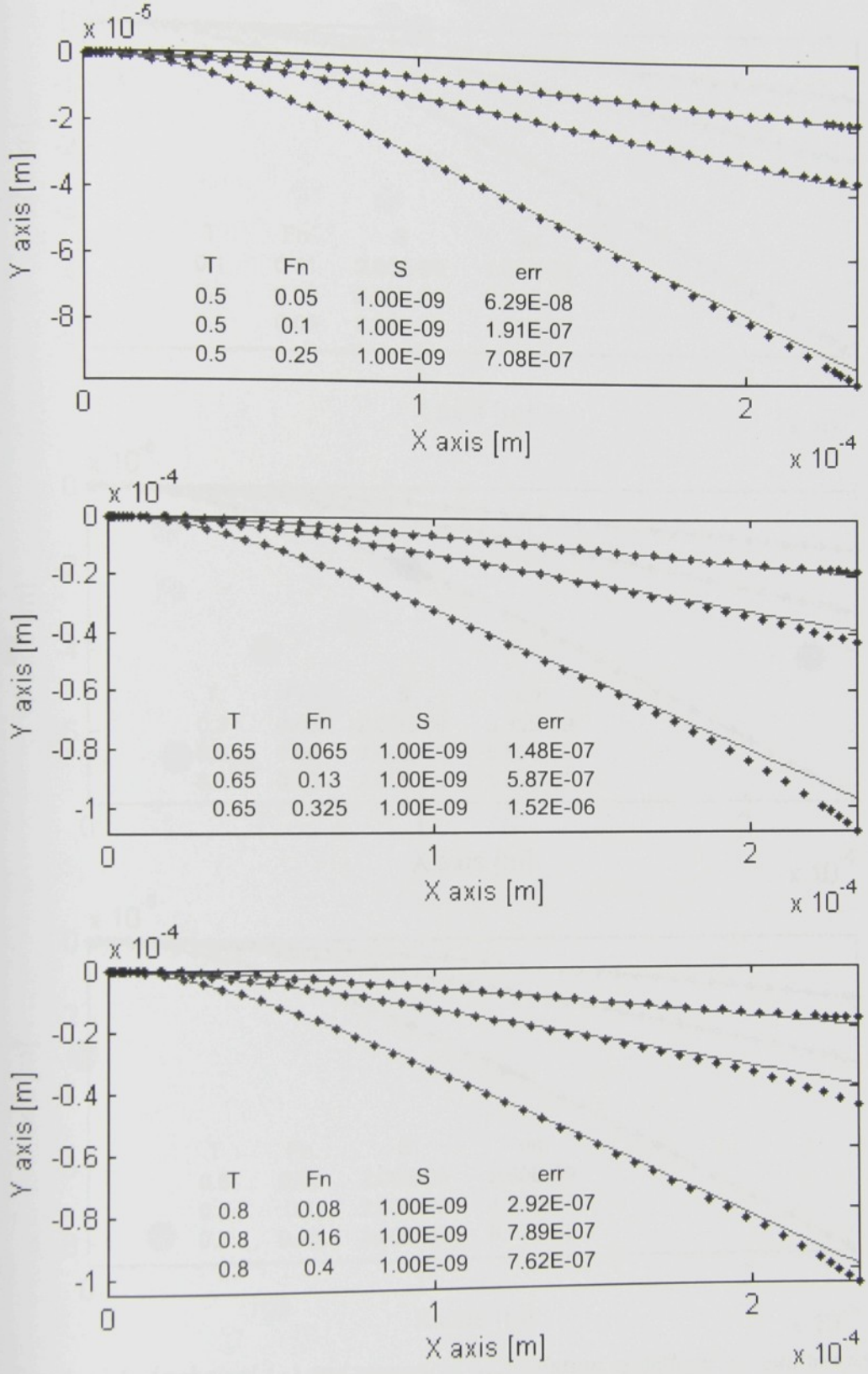

Figure C.3- Analytical (—) and numerical (...) solution of deflection equation for S=1E-9[N.m^2]: planar force is increase gradually with proportions 10, 5 and 2 respectively

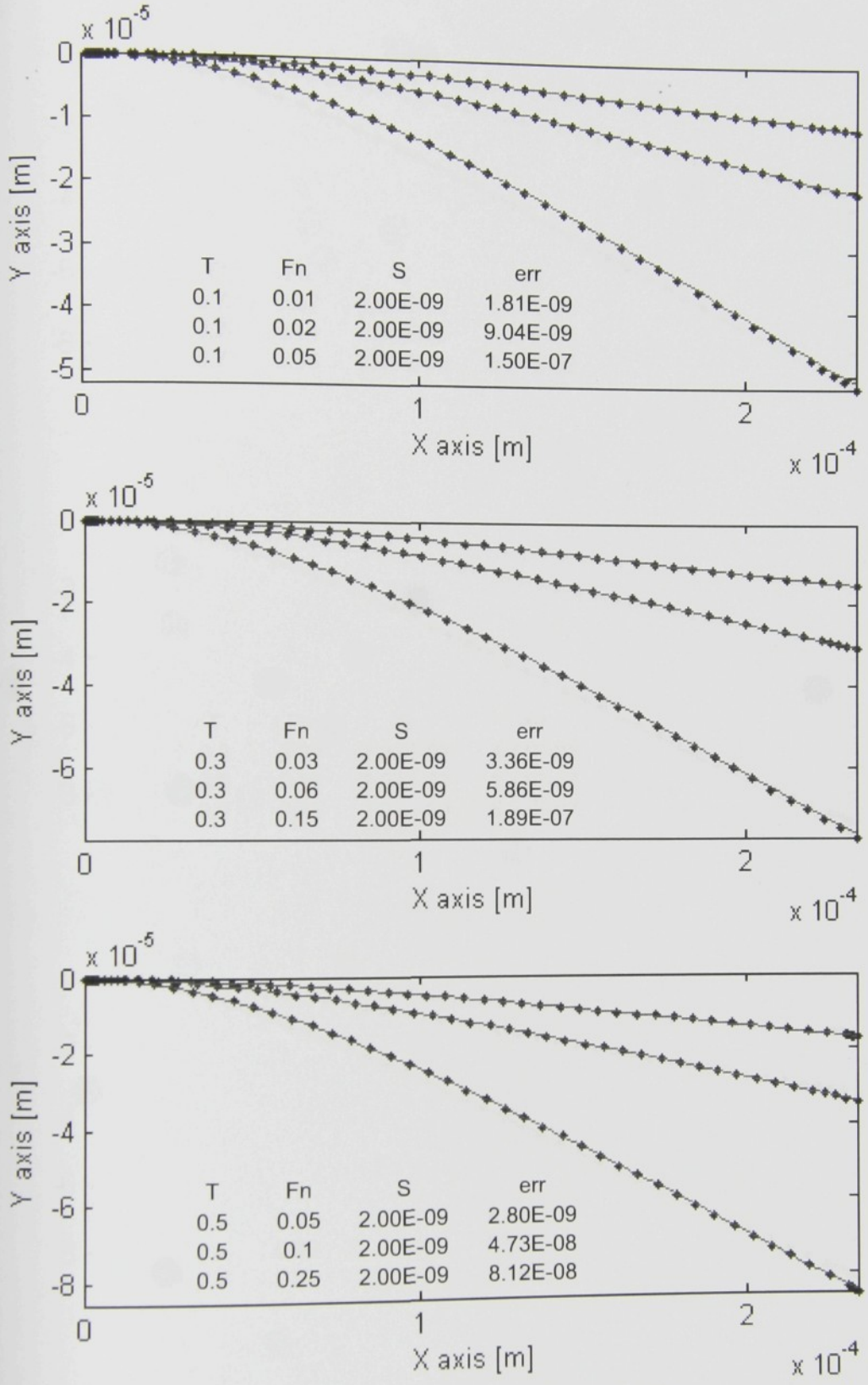

Figure C.4- Analytical (—) and numerical (...) solution of deflection equation for S=2E-9[N.m^2]: planar force is increase gradually with proportions 10, 5 and 2 respectively

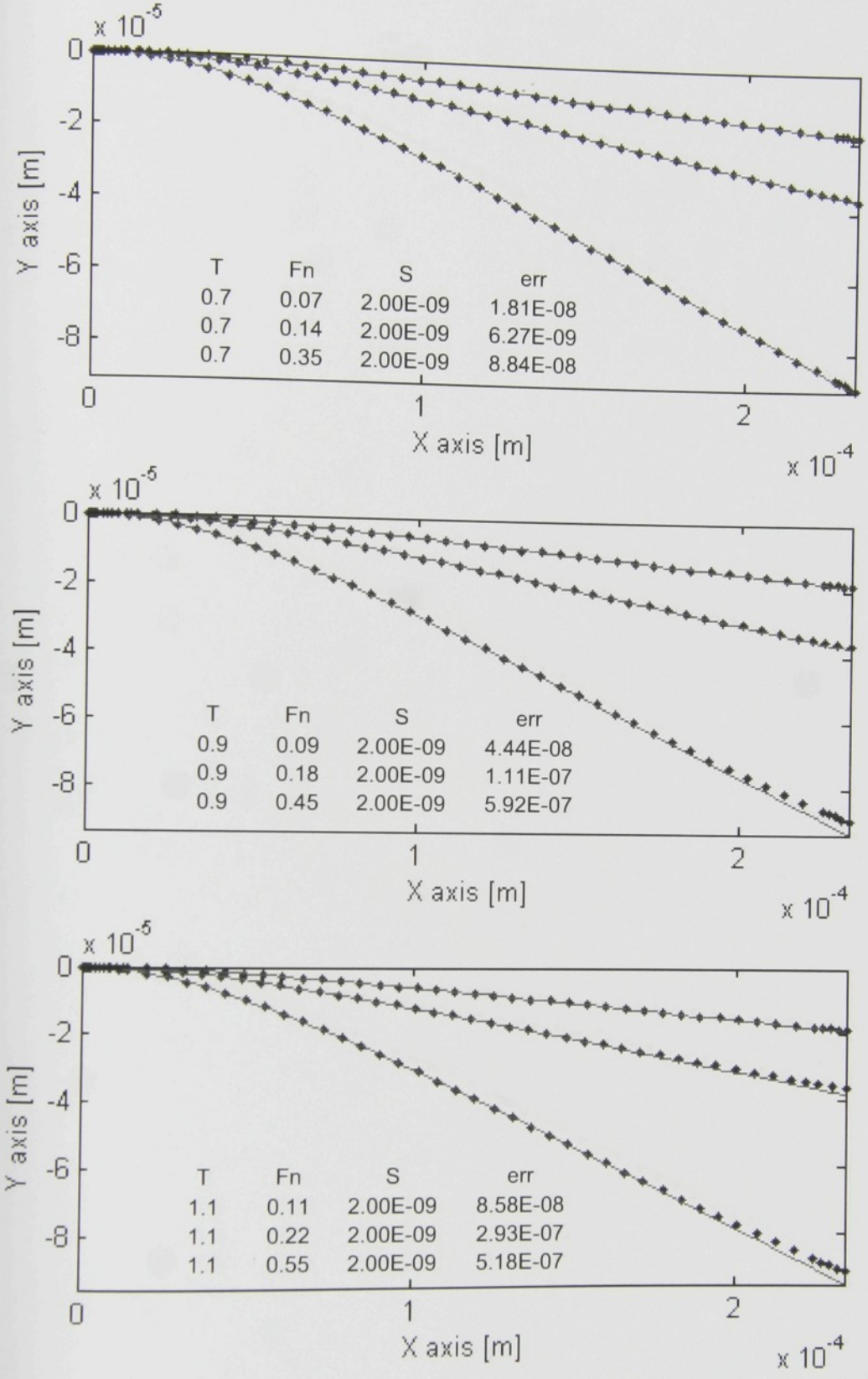

Figure C.5- Analytical (—) and numerical (...) solution of deflection equation for S=2E-9[N.m^2]: planar force is increase gradually with proportions 10, 5 and 2 respectively

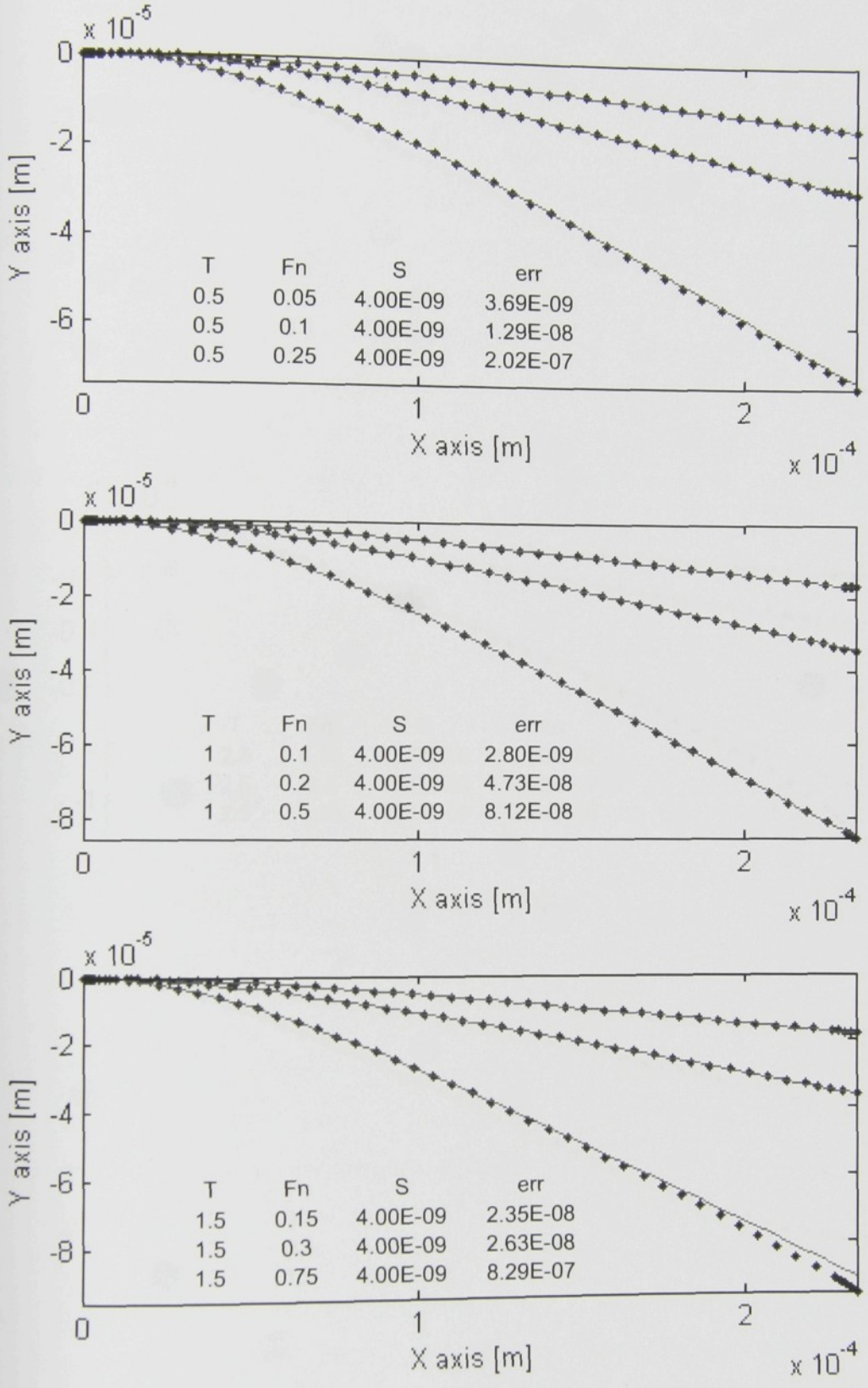

Figure C.6- Analytical (—) and numerical (...) solution of deflection equation for S=4E-9[N.m^2]: planar force is increase gradually with proportions 10, 5 and 2 respectively

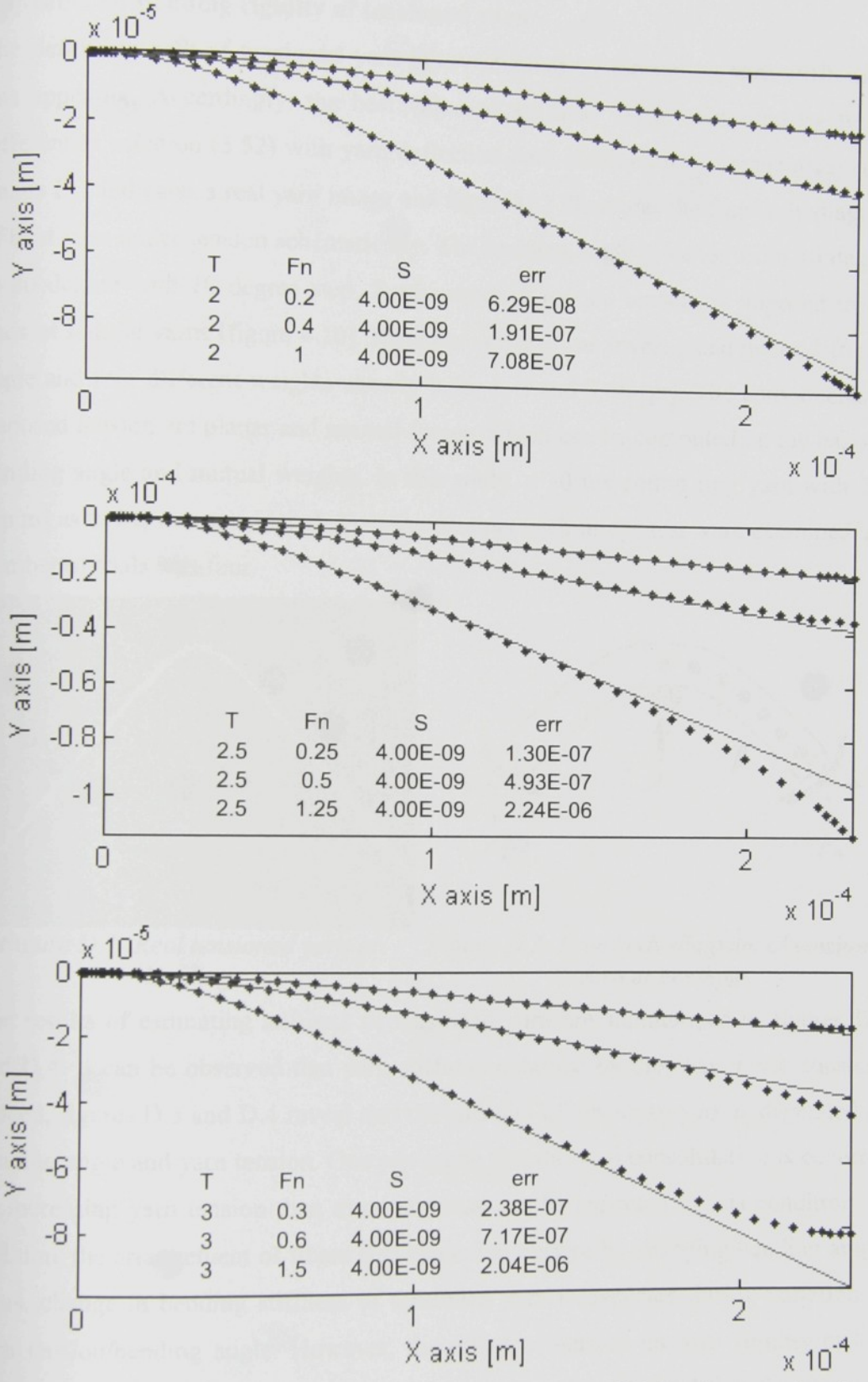

Figure C.7- Analytical (–) and numerical (...) solution of deflection equation for S=1E-9[N.m^2]: planar force is increase gradually with proportions 10, 5 and 2 respectively

Appendix D: Bending rigidity of tensioned yarn

The deflection path of tensioned yarn is investigated by estimating yarn stiffness in this appendix. Accordingly, the best value of stiffness (S) is computed by fitting differential equation (3.52) with yarn deflection path obtained form image analyzing. Image D.1 indicates a real yarn image and figure D.2 illustrates the free body diagram of bent yarn under tension schematically. The bending angle is varied from 10 degree to 80 degree with 10 degree step. Furthermore, a mutual tension is imposed in the ends of sample yarns (figure 4.10). Behavior of yarn was investigated under different angle and four different weights namely 0.36, 1, 2 and 3.66 [gr]. The components of imposed tension are planar and normal forces, which can be computed on the basis of bending angle and mutual weights. In this study, a 30 tex cotton ring yarn with 710 [t.p.m] as twist, was considered. Two samples per each image test were examined and number of trials was four.

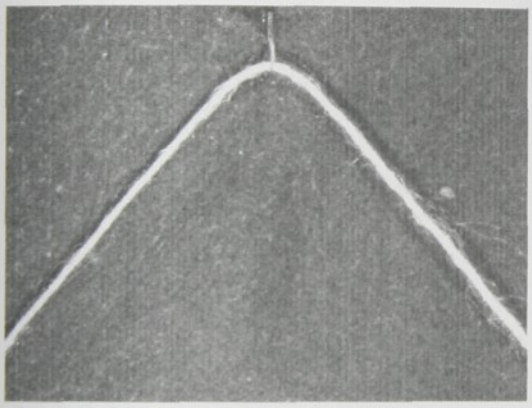

Figure D.1- Real tensioned yarn at bending

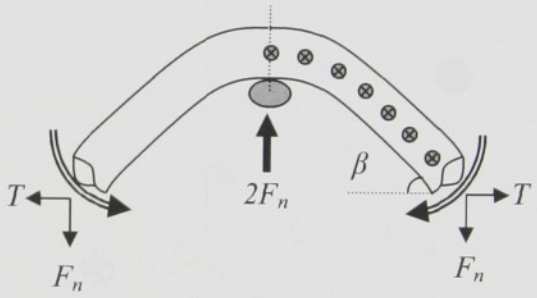

Figure D.2- Free body diagram of tensioned yarn at bending

The results of estimating stiffness of tensioned yarn are summarized in figures D.3 and D.4. It can be observed that yarn stiffness obtained by this way is not constant. Indeed, figures D.3 and D.4 reveal that the stiffness of tensioned yarn is depended on bending angle and yarn tension. One can argue that the yarn consolidation is occurred by increasing yarn tension then more stiffness can be expected in this condition. In addition, the arrangement of fibers is subjected to change by changing bending angle. Thus, change in bending stiffness of tensioned yarn is expected during variation of yarn tension/bending angle. However, the effect of tension on yarn rigidity at low bending angle is higher than the higher angle. It can be deducted that the effect of yarn tension on bending rigidity of yarn for bending angle bigger than 60° is negligible. Furthermore, the variation between observations is reduced by increasing bending angle.

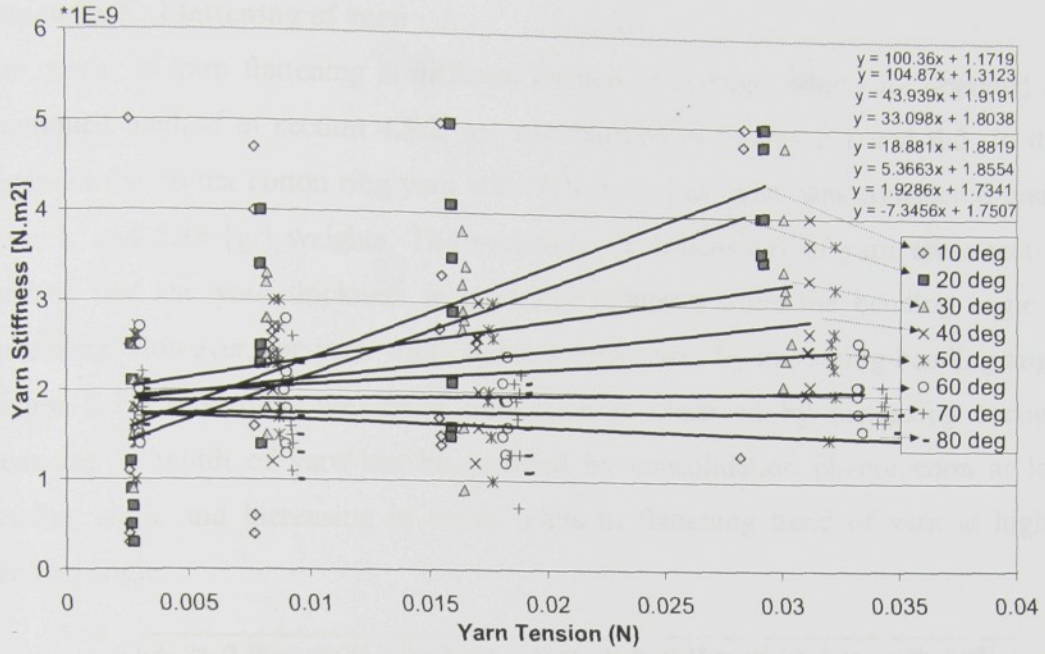

Figure D.3- Yarn stiffness as a function of yarn tension in different bending angle (30 tex)

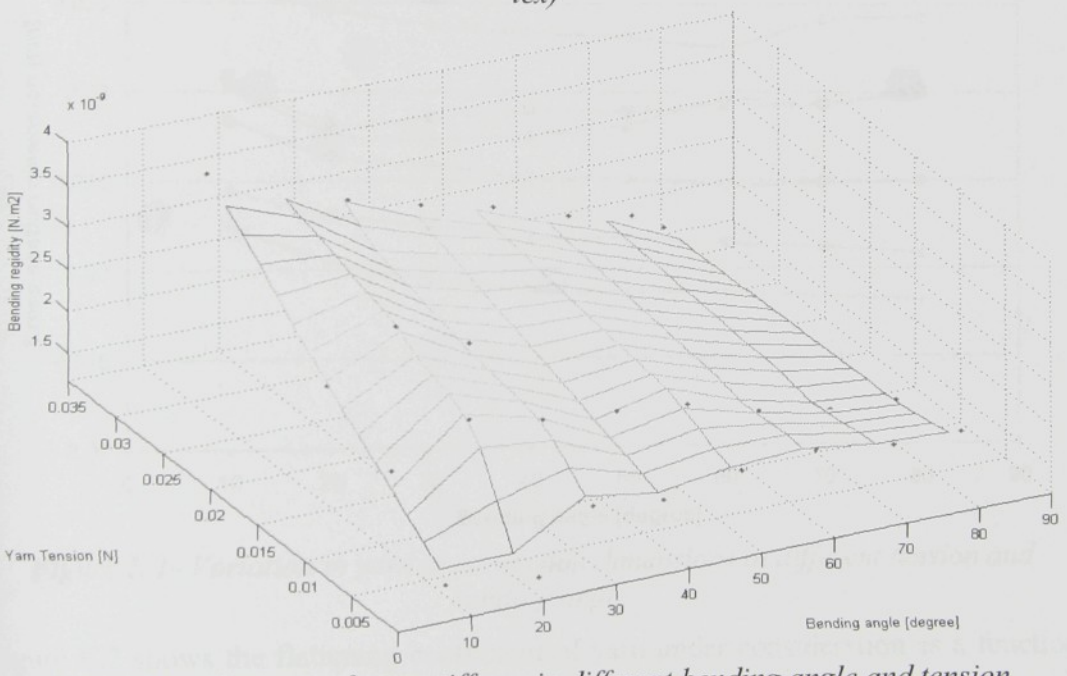

Figure D.4- Average of yarn stiffness in different bending angle and tension.

Appendix E: Flattening of yarn

The results of yarn flattening at different tension in average, which are obtained by mentioned method in section **4.1.2**, are summarized in figures E.1 and E.2. In this appendix the 30 tex cotton ring yarn with 710 [t.p.m] as twist, was considered under 0.36, 1, and 5.36 [gr] weights. The variations in dimensions of yarn cross-section indicate that the yarn thickness is generally reducing when the bending angle is increasing. However, the yarn width reduces then arises by increasing bending angle (figure E.1). Evidently, the lower dimension is observed by increasing tension. Reducing in width of yarn can be justified by consolidation phenomenon at low bending angle and increasing in width refers to flattening trend of yarn at higher bending angle.

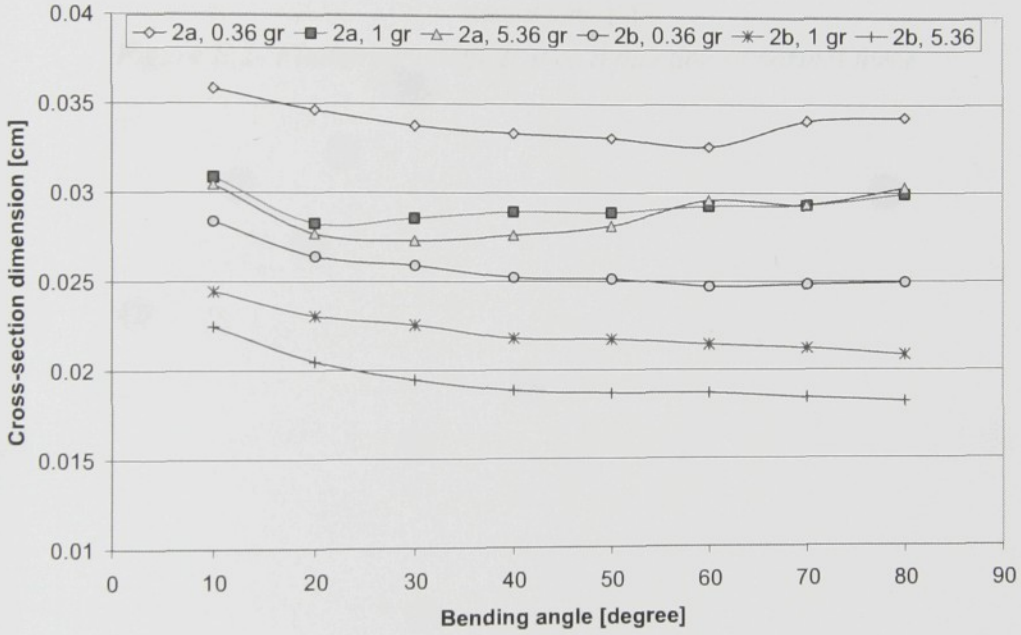

Figure E.1- Variation in yarn cross-section dimensions at different tension and bending angle

Figure E.2 shows the flattening coefficient of yarn under consideration as a function of normal force. The response of tensioned yarn under normal force is fitted by an exponential function. The obtained exponential function was utilized in this study as a known behavior of tensioned yarn under different normal force. Apparently, the deformation in thickness is limited by maximum possibility of yarn packing density.

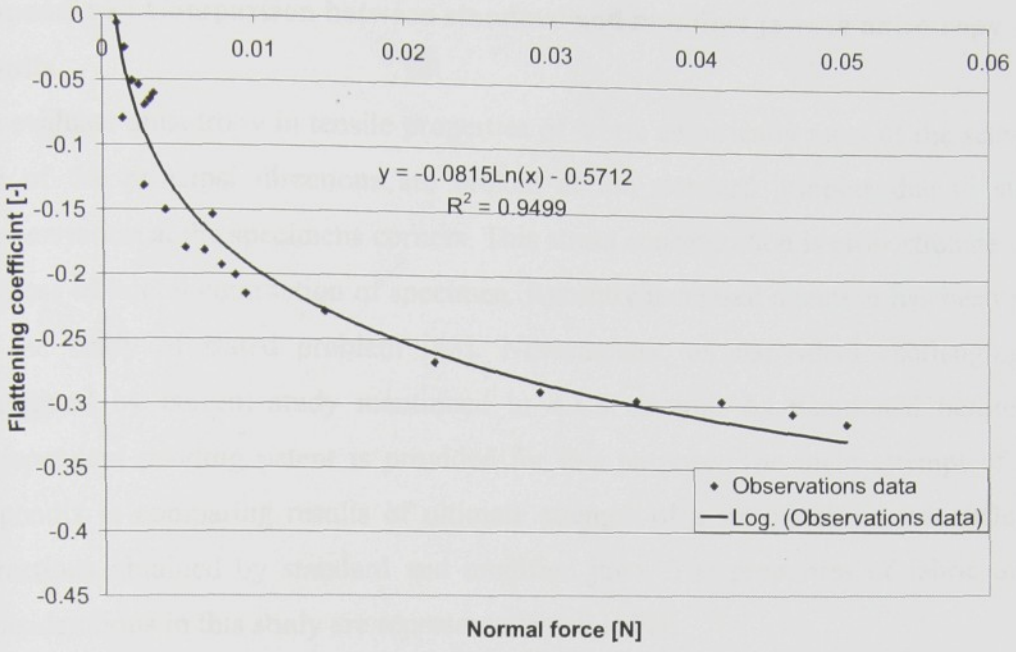

Figure E.2- Flattening coefficient as a function of normal force

Appendix F: Comparison between standard and modified jaws in anisotropy results

To evaluate anisotropy in tensile properties of fabric empirically most of the samples out of the principal directions are broken at the standard grippers due to stress concentration at the specimens corners. This stress concentration is proportionate with bigness of lateral contraction of specimen. Recently increased attention has been paid to the study of stated problem [48]. Nevertheless, an individual challenging is suggested by current study mentioned in **4.1.3** section. As mentioned before an independent pending patent is provided for this purpose. The main attempt of this appendix is comparing results of ultimate strength of a set of fabrics test different directions obtained by standard and modified jaws. The properties of fabric under considerations in this study are represented in table F.1.

Table F.1- Specifications of fabrics under consideration

Fabric code	Material	Warp sett	Weft sett	Yarn tex
C1	Cotton 100%	2600	2500	35.5
C2	Pop0-co100	2360	2320	29.5
P1	Pop 100%	2360	1860	29.5
PC1	pop65-co35	2360	1860	29.5
PC2	Pop35-co65	2360	1380	29.5
PC3	Pop35-co65	2360	1920	29.5

The stress was imposed on 200×50 mm of samples in different directions between 0° (weft direction)-90° (warp direction) force angle. The summarized results in figures F.1-F.6 reveal that there are significant different between standard jaws and modified jaws. Furthermore, most of the samples are broken at gripper nip of standard jaws in out of the principal directions, while the rupture zone is occurred far from the grippers in modified jaws for these samples. Figure F.1 and F.2 indicate the outcomes of square cotton fabrics C.1 and C.2. It is may be interesting to mention that the maximum strength of these fabrics is recorded in 45° angle by modified jaws which is higher than the principal directions. This phenomenon can be justified by proposed models in this study. The difference between results of both jaws in principal directions is negligible for most of the samples.

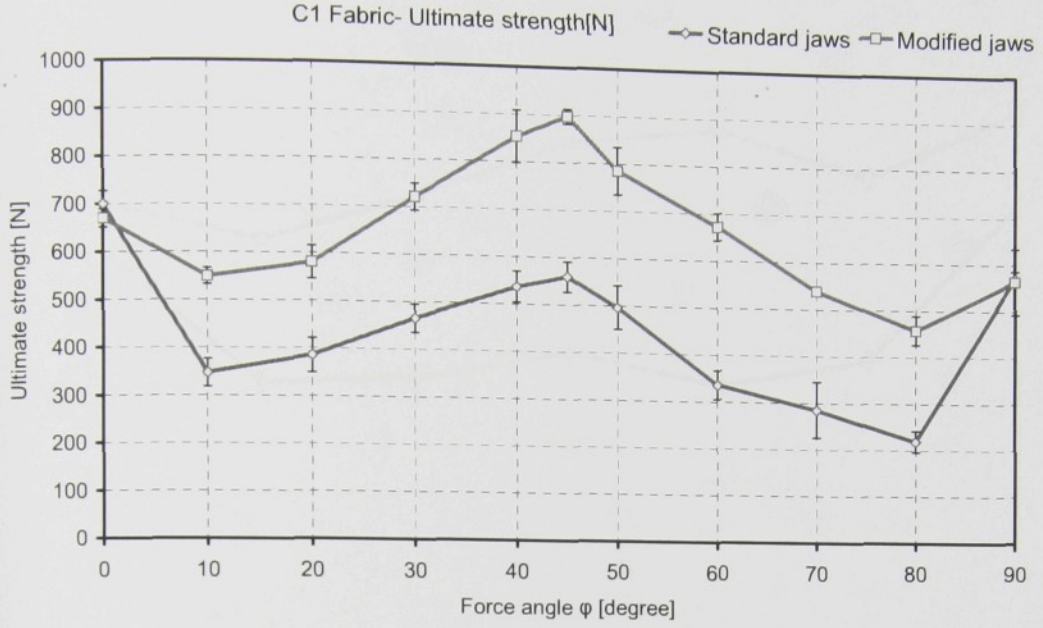

Figure F.1- Anisotropy in ultimate strength of fabric C1; measured by standard & modified jaws

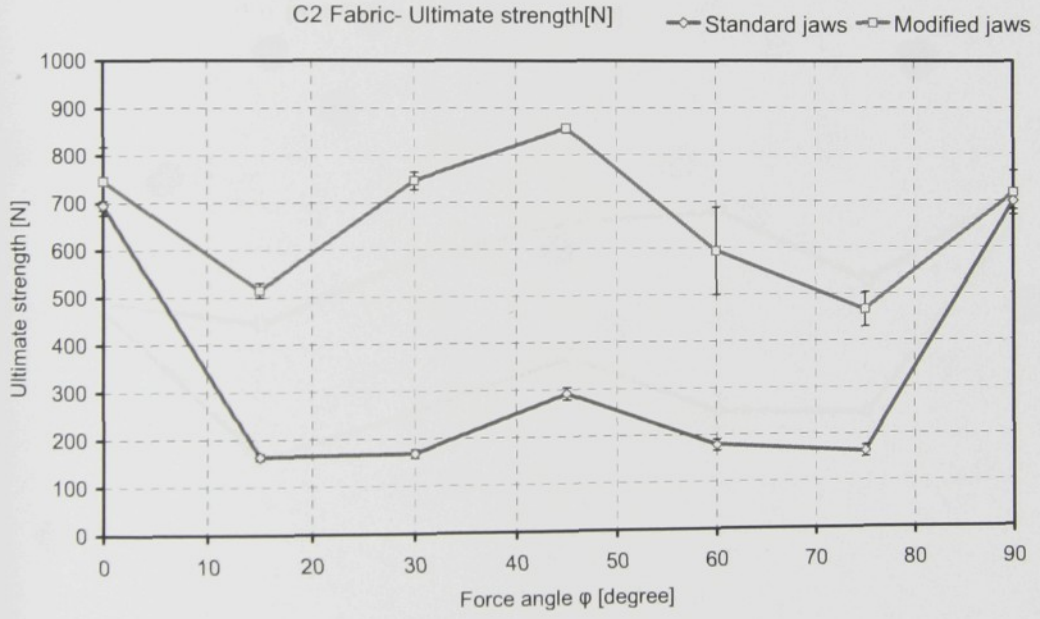

Figure F.2- Anisotropy in ultimate strength of fabric C2; measured by standard & modified jaws

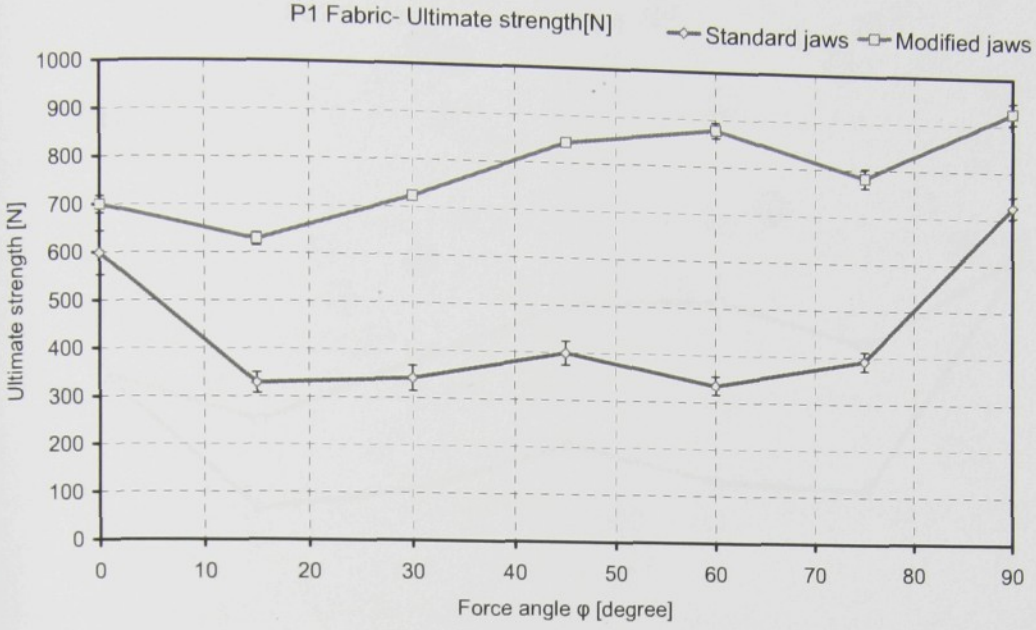

Figure F.3- Anisotropy in ultimate strength of fabric P1; measured by standard & modified jaws

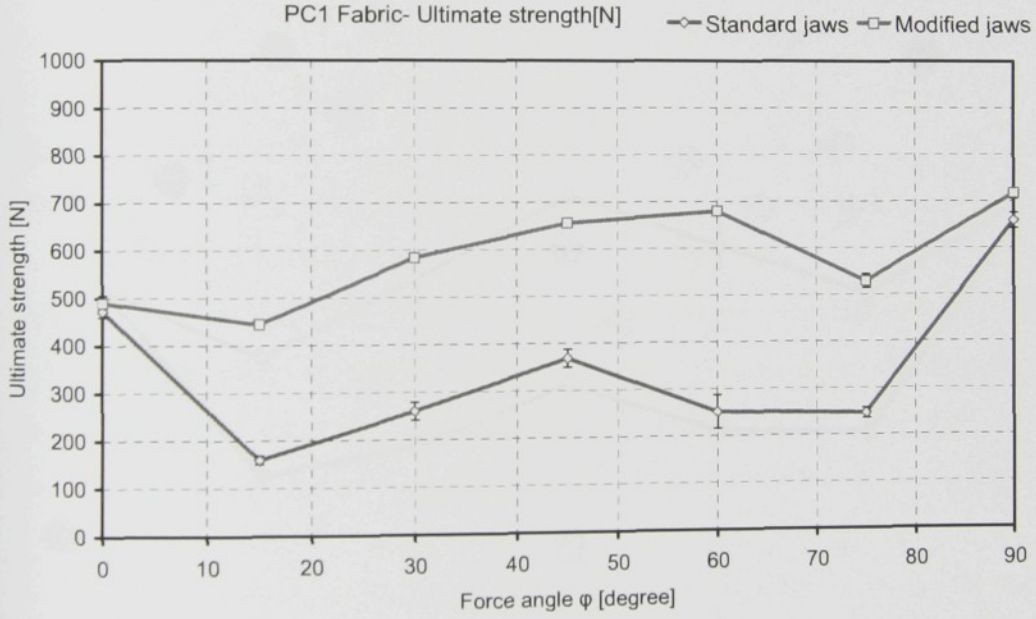

Figure F.4- Anisotropy in ultimate PC1 fabric strength; measured by standard & modified jaws

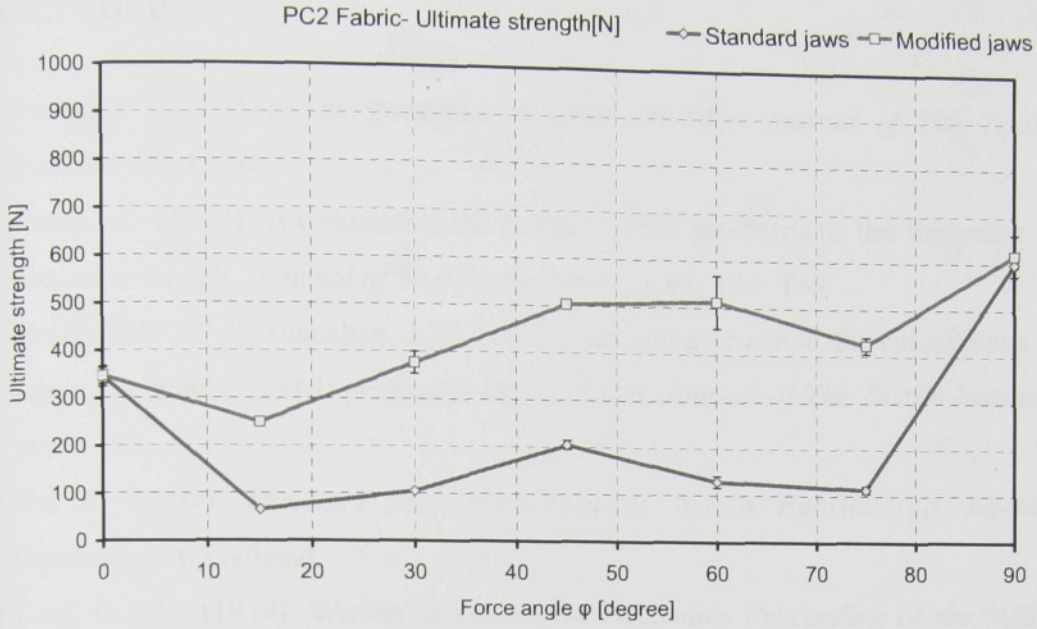

Figure F.5- Anisotropy in ultimate PC2 fabric strength; measured by standard & modified jaws

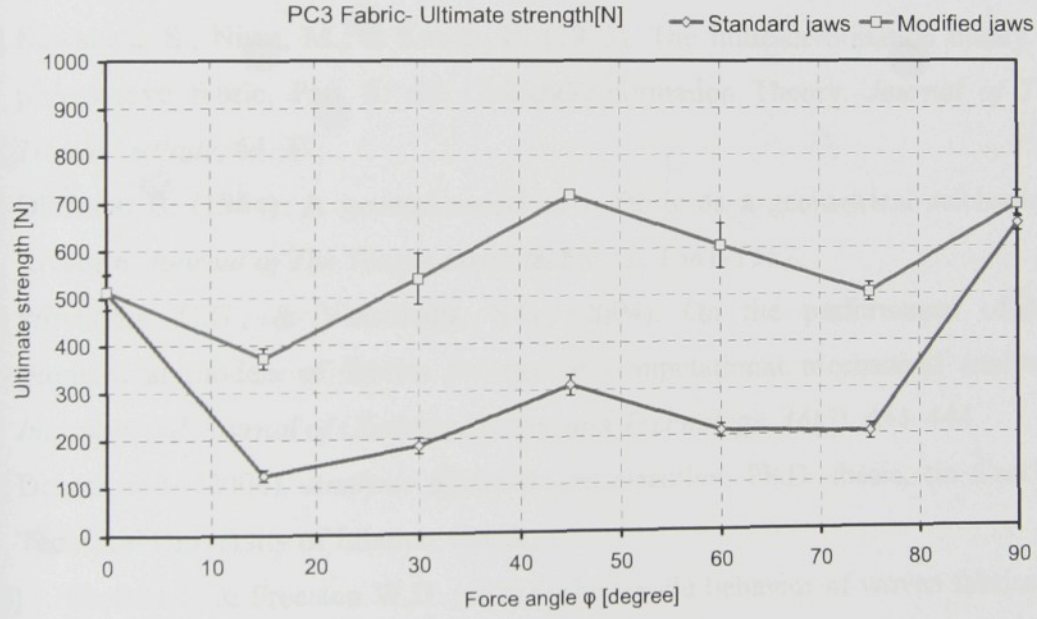

Figure F.6- Anisotropy in ultimate PC3 fabric strength; measured by standard & modified jaws

References

[1] Peirce, F.T. (1937). The geometry of cloth structure. *Journal of The Textile Institute, 28*, 45–96.

[2] Kemp, A. (1958). An extension of Peirce's cloth geometry to the treatment of nonlinear threads. *Journal of The Textile Institute, 49*, T44–T48.

[3] Hearle, J.W.S., & Shanahan, J.W. (1978). An energy method for calculations in fabric mechanics, part I: principles of the model. *Journal of The Textile Institute, 69*, 81–89.

[4] Hu, J. (2004). *Structure and Mechanics of Woven Fabrics* (pp. 61–66). Cambridge: Woodhead.

[5] Leaf, G.A.V. (1979). Woven fabric tensile mechanics *Proceeding of the NATO Advanced Study Institute on Mechanics of Flexible Fiber Assemblies*, Killini, Greece, pp. 143–157.

[6] Kawabata, S., Niwa, M., & Kawai, H. (1973). The finite-deformation theory of plain-weave fabric, Part II: the Uniaxial-deformation Theory. *Journal of The Textile Institute,* 64, 47.

[7] Olofsson B. (1964). A general model of a fabric as a geometrical-mechanical structure. *Journal of The Textile Institute,* 55, 11, T541-T557.

[8] Provatidis, C.G., & Vassiliadis, S.G. (2004). On the performance of the geometrical models of fabrics for use in computational mechanical analysis. *International Journal of Clothing Science and Technology, 16*(5), 434–444.

[9] Drasrova, J. (2004). *Analysis of fabric cross-section.* Ph.D. thesis, (in Czech), Technical University of Liberec, Czech.

[10] Skelton J., & Freeston W.D. (1971). The tensile behavior of woven fabrics at low and high strain rates. *Textile Research Journal,* 41, 3.

[11] Seo M. H., Realff M. L., Pan N., Boyce M., Schwartz P., & Backer S. (1993). Mechanical properties of fabric woven from yarns produced by different spinning technology: Yarn failure in woven fabric. *Textile Research Journal,* 63 (3).

[12] Realff M. L. (1994). Identifying local deformation phenomena during woven fabric Uniaxial tensile loading. *Textile Research Journal,* 64(3).

[13] Realff M.L. (1997).A micromechanical model of the tensile behavior of woven fabric. *Textile Research Journal,* 67(6).

[14] Pan N. (1996). Analysis of woven fabric strength: prediction of fabric strength under uniaxial and biaxial extensions, *Composite Science and Technology*, 56, 311-327.

[15] Rajesh D., Anandjiwala, & Leaf A.V. (1991). Large-scale extension and recovery of plain woven fabrics Part II: experimental and discussion, *Textile Research Journal,* (61) 12,743-755.

[16] Sagar T.V., P. Potluri, & Hearle J. W. S. (2003). Mesoscale modeling of interlaced fiber assemblies using energy method, *Computational Materials Science,* 28, 49-62.

[17] Neckar B., Kovar R., & Kamali D. M. (2008). Theory of fabric deformation in principal directions. *8th AUTEX International conference, Biella, Italy.*

[18] Weissenberg K. (1949). The use of a trellis model in the mechanics of homogeneous materials. *Journal of The Textile Institute,* 40, 89-107.

[19] Weissenberg K., Chadwick G. E., & Shorter S. A. (1949). A trellis model for the application and study of simple pulls in textile materials. *Journal of The Textile Institute,* 40, 108-160.

[20] Lindberg J, Behre B, & Dahlberg B. (1961). Shearing and buckling of various commercial fabrics. *Textile Research Journal,* 99-122.

[21] Kilby W F. (1963). Planar stress-strain relationships in woven fabrics, *Journal of The Textile Institute,* 54, T9.

[22] Treloar, L.R.G. (1965). The effect of test-piece dimensions on the behavior of fabrics in shear. *Journal of Textile Institute, 56,* T533–T550.

[23] Grosberg P, & Park BJ. (1966). The mechanical properties of woven fabrics, part V: The initial modulus and the frictional restraint in shearing of plain weave fabrics. *Textile Research Journal*, 420-431.

[24] Grosberg P, & Park BJ. (1968). The mechanical properties of woven fabrics, part VI: the elastic shear modulus of plain weave fabrics. *Textile Research Journal*, 1085-1100.

[25] Spivak, S.M. & Treloar, L.RG. (1968). The behavior of fabrics in shear, part III: The relationship between bias extension and simple shear. *Textile Research Journal, 38*(9), 963–971.

[26] Skelton J. (1976). Fundamental of fabric shear. *Textile Research Journal*, 862-869.

[27] Leaf GAV., & Sheta M F. (1984). The initial shear modulus of plain-woven fabric. *Journal of The Textile Institute,* 75, 157.

[28] Postle R., Carnaby GA., & Jong Sde. (1988). *The mechanics of wool structures*. EllisHorwood.

[29] Sinoimeri A., & Drean JY. (1996). A study of the mechanical behavior of the plain-weave structure by using energy methods: fabric shear. *Journal of The Textile Institute,* 87(1),121-128.

[30] Ning P., & Mee-Young Y. (1996). Structural anisotropy, failure criterion, and shear strength of woven fabrics, *Textile research Journal*, 66(4), 238-244.

[31] Buckenham P. (1997). Bias-Extension /measurements on Woven Fabrics. *Journal of The Textile Institute,* 88. Part 1, No 1: 33-41.

[32] Prodromou, A.G. & Chen, J. (1997). On the relationship between shear angle and wrinkling of textile composite performs. *Compo. Pt. A, 28A*, 491–503.

[33] McBride, T.M., & Chen, J. (1997). Unit cell geometry in plain weave fabrics during shear deformations. *Computer Science and Technology, 57*, 345–351.

[34] Wang, J., Page, J.R., & Paton, R. (1998). Experimental investigation of the draping properties of reinforcement fabrics. *Component Science Technology, 58*, 229–237.

[35] Page J., & Wang J. (2000). Prediction of shear force and an analysis of yarn slippage for a plain-weave carbon fabric in a bias extension state. *Journal of Composite Science and Technology*, 60:977-986.

[36] Zhang Y.T., & Fu. Y. B. (2000). A micromechanical model of woven fabric and its application to the analysis of buckling under uniaxial tension. Part 1: The micromechanical model. *International Journal of Engineering Science*, 1895-1906.

[37] Zhang Y.T., & Fu. Y. B. (2001). A micromechanical model of woven fabric and its application to the analysis of buckling under uniaxial tension. Part 2: Buckling analysis. *International Journal of Engineering Science*, 39, 1-13.

[38] Zhang Y. T., & Xu J. F. (2002). Buckling analysis of woven fabric under simple shear along arbitrary directions. *Textile Research Journal,* 72, 2, p147.

[39] Page J., & Wang J. (2002). Prediction of shear force using 3D non-linear FEM analyses for a plain weave carbon fabric in a bias extension state, *Finite elements in analysis and design*, 38, 755-764.

[40] Lo W. M., & Hu J. L. (2002). Shear properties of woven fabrics in various directions. *Textile Research Journal,* May, 72, 5.

[41] Lomov S. V., Parnas R. S., Ghosh S. B., & Verpoest I. (2002). Experimental and theoretical characterization of the geometry of two dimensional braided fabrics. *Textile Research Journal,* Aug., 72, 8.

[42] Lomov S. V., Willems A., Vandepitte D., & Verpoest I. Simulation of shear and tension of glass/pp woven fabrics, Downloaded from:
http://www.mtm.kuleuven.ac.be/ Research/C2/poly/index.htm

[43] Lomov S. V., Barburski M., Truong Chi T., & Verpoest I. Deformability and internal geometry of textile reinforcements and laminates, Downloaded from:
http://www.mtm.kuleuven.ac.be/ Research/C2/poly/index.htm

[44] Lomov S. V., Bernal E., Ivanov D.S., Kondrative S.V., & Verpoest I. Homogenization of a sheared unit cell of textile composites: FEA and approximate inclusion model. Downloaded from:
http://www.mtm.kuleuven.ac.be/Research/C2/poly/index.htm

[45] Kuwazuru O., & Yoshikawa N. (2004). Theory of elasticity of plain weave fabrics 1st report, New concept of Pesudo-Continuum Model, *JSME international journal*, series A vol. 47 No. 1, 17-25.

[46] Kuwazuru O., & Yoshikawa N. (2004). Theory of elasticity of plain weave fabrics 2nd report, Finite Element Formulation, *JSME international journal*, series A vol. 47 No. 1, 26-34.

[47] Kuwazuru O., & Yoshikawa N. (2006). Strength Anisotropy Estimation of Plain-weave Fabrics by Pseudo-continuum Model. *Key Engineering Materials Vols.* 306-308, pp. 835-840

[48] R. Kovar, S.,Kovar, S., & Pitucha,T. (2004). *Measuring of anisotropy of woven fabric deformation.* 2nd International Textile Clothing and Design Conference, Dubrovnik, Croatia.

[49] Zhu, B., Yu, T.X., & Tao, X.M. (2007). An experimental study of in plane large shear deformation of woven fabric composite. *Component Science Technology, 67*, 252–261.

[50] Zouari, R., Amar, S. B. & Dogui (2008). Experimental and numerical analyses of fabric off-axes tensile test. *Journal of The Textile Institute,* A.

[51] Neckar, B. (1985). *Yarn: Creation, structure and properties* (in Czech), SNTL, Praha, Czech.

[52] Tsai, D.M. & Hsieh, C.Y. (1999). Automated surface inspection for direction textures. *Image Vis. Comput., 18*, 49–62.

[53] Tunak,M. & Linka, A. (2004). *Applying spectral analysis to automatic inspection of weaving density*. 11th International Conference STRUTEX, Liberec.

[54] Tunak, M. & Linka, A. (2005). *Planar anisotropy of fiber systems by using 2D Fourier transform*. 12th International Conference STRUTEX, Liberec.

[55] Zborilova J., & Kovar R. (2003). Uniaxial Woven fabric deformation. *STRUTEX, Conference Liberec*.

[56] Kovar R., & Kamali D. M. (2009). Modifying of jaws to reduce tension concentration at corners of fabric, (Pending Patent in Czech language).

List of related publications

1. Conference Presentations:

- Tensile Properties of Plain Weave Fabric in Arbitrary Direction, Mehdi Kamali Dolatabadi, Radko Kovar, Monika Vysanska, 15th International conference STRUTEX, Liberec, Czech Republic, 2008.
- Contribution to Formulate Bending Rigidity of Tensioned Yarn, Mehdi Kamali Dolatabadi, Radko Kovar, TEXCOMP9 International Conference on Textile Composite, Delaware USA 2008.
- A Micromechanical and Geometrical Model of Tensile - Deformation Behavior of Plain Weave Fabric in Principal Direction, Mehdi Kamali Dolatabadi, Radko Kovar, The Fiber Society Fall Conference, Boucherville, Canada, 2008.
- Yarns tension distribution and rupture mechanism in narrow strip of plain weave fabric under bias stress. M. Kamali Dolatabadi, R. Kovar, Fall International conference and technical meeting of The Fiber Society, University of California at Davis, USA, 2007.
- Verifying a New Model for Geometry of Plain Weave Fabric. M. Kamali Dolatabadi, R. Kovar, J. Drasarova,14th International conference STRUTEX, Liberec, Czech Republic, 2007.
- On the relationship between plain weave fabric geometry and bias extension deformation. Part I: Initial state, 3D model of plain weave fabric before deformation, M. Kamali Dolatabadi, R. Kovar, 6th International Textile Science conference (TEXSCI), Liberec, Czech Republic, 2007.
- On the relationship between plain weave fabric geometry and bias extension deformation. Part II: Shear state, 3D model of plain weave fabric under deformation. M. Kamali Dolatabadi, R. Kovar, 6th International Textile Science conference (TEXSCI), Liberec, Czech Republic, 2007.
- Angular deformation of warp-weft yarns in cut bias plain weave fabric under uniaxial load. M. Kamali Dolatabadi, R. Kovar, A. Linka, 13th International conference STRUTEX, Liberec, Czech Republic, 2006.

2. Patent and Publications in Journals:

- Modifying of jaws to reduce tension concentration at corners of fabric, Radko Kovar, Mehdi Kamali Dolatabadi, Pending Patent.

- Geometry of plain weave fabric under shear deformation Part I: measurement of exterior deformation, M. Kamali Dolatabadi, R. Kovar, A. Linka. *Journal of The Textile institute*. Under press, available at Forthcoming Articles 28 Jul. 2008.
- Geometry of plain weave fabric under shear deformation Part II: 3D model of plain weave fabric before deformation, M. Kamali Dolatabadi, R. Kovar. *Journal of The Textile institute*. Under press, available at Forthcoming Articles 28 Aug. 2008.
- Geometry of plain weave fabric under shear deformation Part III: 3D model of plain weave fabric under shear deformation, M. Kamali Dolatabadi, R. Kovar. *Journal of The Textile institute*. Under press, accepted for Publication 27 Nov. 2007.